THE UNIVERSITY OF CHICAGO

INTESTINAL LYMPHATICS NICHE SPECIFIC PROPERTIES AT HOMEOSTASIS AND UPON HELMINTH INFECTION

A DISSERTATION SUBMITTED TO

THE FACULTY OF THE DIVISION OF THE BIOLOGICAL SCIENCES

AND THE PRITZKER SCHOOL OF MEDICINE

IN CANDIDACY FOR THE DEGREE OF

DOCTOR OF PHILOSOPHY

COMMITTEE ON IMMUNOLOGY

BY

JORDEN ISAIAH LANE

CHICAGO, ILLINOIS

AUGUST 2024

Table of contents

List of Tables

LIST OF FIGURES

Acknowledgements

My time in graduate school has been nothing short of transformative both personally and professionally. I would not have made it this far without my community support system.

I would first like to thank my mentor, Daria Esterházy, for entrusting me with a project initially outside our expertise. Not many people are lucky enough to have a mentor who take the amount of time that you must properly develop their trainee's science acumen and skills, and I am fortunate that you did so. It has been a joy developing this work and listening to the science at every turn it took. The ways in which you have advocated without my knowing and pushed for me to attend conferences to get the most out of my work will never be forgotten as I move forward in my career.

Thank you to my committee, Eric Pamer, De'Broski Herbert, and Melody Swartz for positively pushing the work into a focused story. Furthermore, thank you to Melody to taking the time outside of the committee meetings to discuss the project, its implications, and for your generosity at conferences when I often did not know anyone prior.

To the Esterházy Lab, Aliia, Dean, Elida, Macy and each of the undergrads, thank you for making the lab environment supportive and joyous. Several times throughout my tenure, you all have endured my talks which at times may have seemed abstract but your willingness to provide feedback has helped me to not only better present my work, but also focus on the questions and themes I am attempting to convey. The immunology community at The University of Chicago has been a fantastic environment to learn and gain confidence. The confidence gained from speaking at Journal Club and WIP is truly immeasurable.

To the best friends I've gained in the program, Sean and Riley, I have truly enjoyed getting to better know you and your wives, Megan and Jen, over these last 5 years. Having two people that understand the significance of your hardships and successes will never be something I will

take for granted. To the chosen-family I've gained while living in Chicago, Ellie, Elliott, Nick, Terrin, and Thomas you have all been a wonderful reprieve graduate school. Without all of you I would not have been able to remain as grounded and mentally fit to endure. To the friends I had to leave behind in Maryland, Isabel, Jamie, Justin, Kelly, Michelle, and Taylor thank you for coming to visit and keeping in touch when even at times where I was not the best at it. You lot, have been my biggest cheerleaders and have witnessed this journey from beginning to end.

To my partner, Joshua, thank you for being a ray of sunshine in the times where I needed it most. We met at a time where I needed help the most and you have never disappointed me in our time together. Kindness is a dying trait but I am thankful it is your defining trait.

To my siblings, Briana and Zuriel, and my parents, thank you for your love and encouragement. You all have always taken the time to make sure I have what I need to push forward in the troubled times. I am grateful for your support system, our bond, the playfulness

Abstract

Tissue lymphatics are crucial for fluid homeostasis and immunosurveillance. We asked whether the lymphatics are adapted to the organ in which they reside, such as along the gut. Duodenal lymphatic capillaries (lacteals) displayed the most discontinuous tight junction composition within the gut, resulting in a dependence on duodenal lacteals for rapid dietary lipid uptake. Duodenal helminths abrogated these features. Parallel RNA sequencing of lymphatic endothelial cells (LECs) and mucosa along the intestine revealed that the transcriptomes overlapped in functional profiles. Helminth infection reversed key duodenal signatures like lipid metabolism and immune activation, instead triggering lymphangiogenic and mucosal antimicrobial responses. We identified a putative VEGFR-2/3 signaling gradient that may explain differences in LEC tight junctions along the small intestine at homeostasis. Inflammation-induced lymphangiogenesis likely underlay duodenal lymphatic impermeability upon helminth infection, while microbial depletion acted additively on lymphatic restructuring. Our study provides molecular insights into lymphatic function along the intestine and stages lymphatic permeability as subject to modulation by environmental queues.

1. Introduction

1.1 Discovery of lymphatics

The description of intestinal lymphatics draining “white chyle” (lymph) to the mesenteric lymph nodes by several ancient civilizations establishes the system as the earliest described lymphatic vessel bed (Bernier-Latmani & Petrova, 2017a). In the centuries following, it has been found that each lymphatic vessel bed serves the crucial functions of fluid recuperation and facilitating immune cell trafficking to the draining lymph nodes (LN) (Fig. 1A); however, intestinal lymphatics are unique in that in addition to these aforementioned functions, they are also involved in the uptake of dietary lipids and hydrophobic molecules not taken up by the blood either due to size exclusion or hydrophobicity (Fig. 1A) (Bernier-Latmani & Petrova, 2017a).

1.2 Lymphatic structure and lymph flow

Despite being a continuous vascular system, molecular and morphological differences between the initial lymphatics and the collecting lymphatics also translate to functional differences across the system. Generally, the formation of lymph and initiation of immune cell trafficking begins at the initial lymphatic capillaries regardless of the organ(Baluk et al., 2007). A single layer of lymphatic endothelial cells (LECs) compromising each initial lymphatic capillary bed is loosely inter-locked through discontinuous button-like junctions which facilitate the entry of fluid, cells, and in the case of intestinal lymphatics dietary lipids packaged into chylomicrons into the vasculature (Fig. 1B). The initial lymphatic capillaries in the small intestine, called lacteals, are embedded within the lamina propria of the finger-like structures known as villi. The colon, the major site of fluid reabsorption from the lumen has a unique two-layered lymphatic system that

looks very different from that of the small intestine (Bernier-Latmani & Petrova, 2017a; Esterházy et al., 2019). The lymph and immune cells drain into progressively larger collecting lymphatic vessels which are afferent to the draining LNs. Impermeable LECs inter-locked through continuous zipper-like tight junctions, lymphatic unidirectional valves, and contracting smooth muscle surrounding the lymphatic collecting vessel to prevent cellular/fluid loss and propel lymph unidirectionally to the draining LN (Baluk et al., 2007; Hampton & Chtanova, 2019; Petrova & Koh, 2020). Once the lymph enters the LN, via the subcapsular sinus, much of it exits the LN through the efferent collecting vessel where the lymph will eventually enter the thoracic duct returning the lymph to the bloodstream (Oliver et al., 2020a).

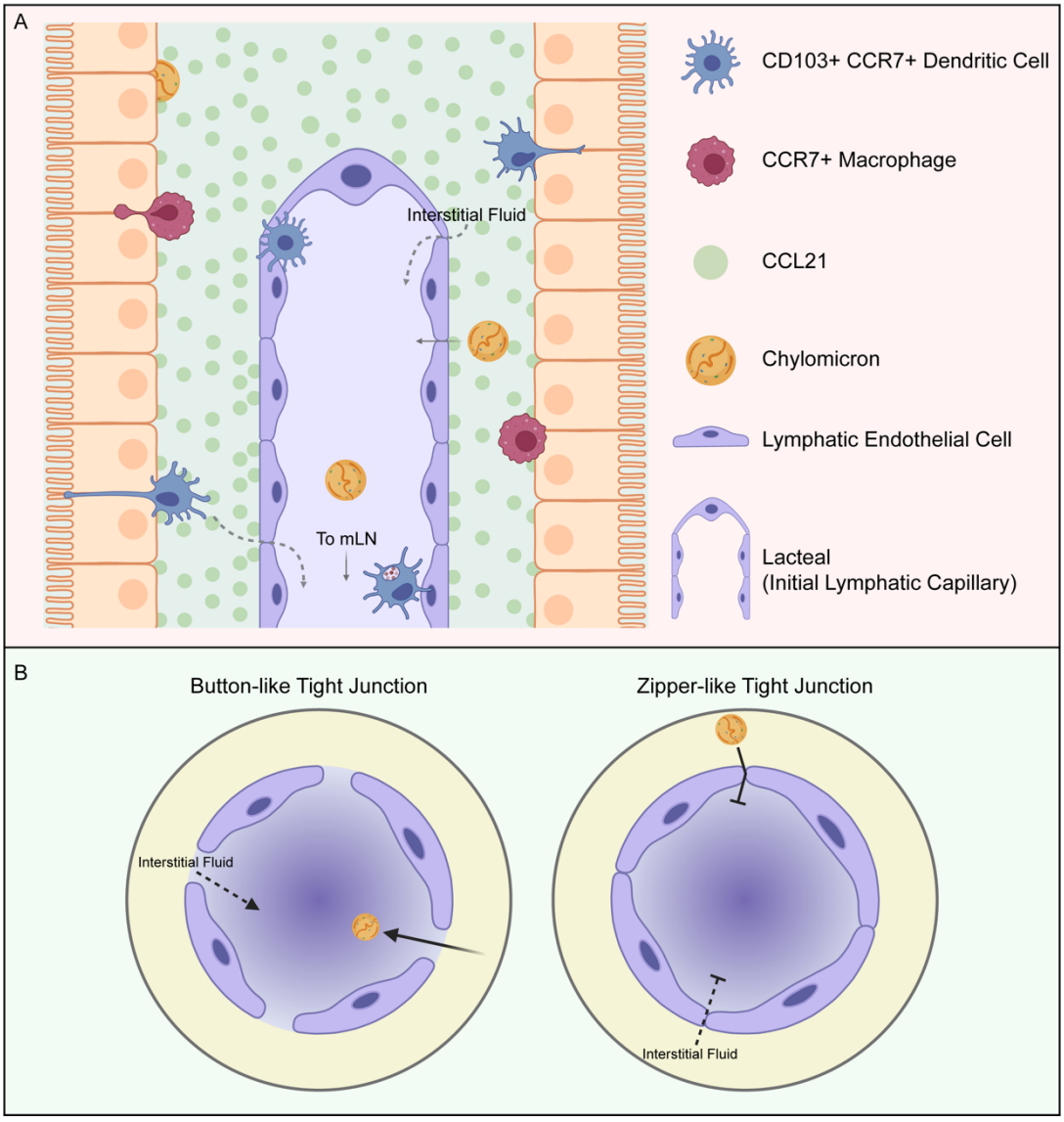

Figure 1. Intestinal lymphatic features and functions
A. Similar to each initial lymphatic capillary bed, the initial intestinal lymphatic capillary within the small intestine (lacteal) is where CCR7+ migrating cells and interstitial fluid within the tissues enters the lymphatic vasculature. Intestinal lymphatics additionally must uptake dietary nutrients and other hydrophobic molecules packaged into chylomicrons. Capillary lymphatic endothelial cells (LEC) produce the chemokine CCL21 in a gradient that traffics CCR7+ migrating cells both towards and into the vasculature. B. Interstitial fluid and chylomicron entry into initial lymphatics have been found to be modulated by LEC tight junction composition. "Button-like" tight junctions allow for fluid and cargo entry into the vasculature. "Zipper-like" tight junctions restrict fluid and cargo entry into the vasculature.

1.3 Lymphatic regulation of migration and immunity

As a conduit for immune cells to traffic to and from tissue draining LNs, the lymphatics facilitate the initiation of adaptive immunity and tissue specific immunity. Migratory immune cells such as CD103+ dendritic cells (DCs) leave the tissue and enter the initial lymphatic capillaries in a CCR7-CCL21 dependent manner (Card et al., 2014; Förster et al., 2012; Hampton & Chtanova, 2019; Schineis et al., 2019; Schwager & Detmar, 2019). A CCL21 gradient maintained and derived from lymphatic endothelial cells (LECs) attracts CCR7+ immune cells to enter the initial lymphatic capillary between open LEC junctions. The immune cells then slowly migrate towards the lymphatic collecting vessel adhering and detaching from the vessel wall in a stochastic manner until an increase in fluid pressure within the collecting vessels leads the cells to move at an increased unidirectional manner. Once the migratory immune cell reaches the LNs subcapsular sinus, it either initiates its effector function to prime and tune adaptive responses or continues to circulation (Esterházy et al., 2019; Jalkanen & Salmi, 2020). The role of the lymphatic vasculature in adaptive immunity does not stop there; it has also been found to have a role in peripheral tolerance through the presentation of MHC restricted peptides and in the maintenance of resting tissue resident memory cells by the expression of IL-7 (Amezcua Vesely et al., 2019; Garnier et al., 2022; Gkountidi et al., 2021). Thus, without lymphatic vasculature to uphold this conduit

system from the tissue to the draining lymph node, tissue specific adaptive immunity is unable to be initiated and to a lesser degree tuned and maintained.

1.4 Tissue versus lymph node lymphatics

As an added layer of complexity, several studies have found differences in LEC function at the tissues versus the LN and even differences in LEC function within the LN. Furthermore, evidence suggesting differences in lymphatic function between organs has emerged primarily from imaging studies of the lymphatics revealing unique architecture and density at sites such as the e.g. skin (Karaman et al., 2015), kidney (Cai et al., 2023), airways (Baluk et al., 2007), gut (Esterházy et al., 2019) and LN (Xiang et al., 2020). These findings largely indicate the existence of tissue specific lymphatic function rather than a generalizable system that similarly responds regardless of the context as many treat it as.

1.5 Lymphatic dysfunction upon disease and infection

The lymphatic system has also been found to be regulated in several non-inflammatory and inflammatory context. In neonatal mice alterations in lymphatic morphology have been linked to exposure to dietary lipids (Zarkada et al., 2023); in adult mice high fat diet regulates lacteal regeneration (Bernier-Latmani et al., 2015). Lymphatic dysfunction has been associated with several disease states such as obesity and most notably lymphedema. In Crohn's Disease, the "leaky gut" and "creeping fat" disease manifestations have been shown to be associated with dysregulated lymphatics (Oliver et al., 2020b). Errant lymphangiogenesis within solid tumors has been linked to metastases of tumor cells to the tumor draining LN and eventually to other tissue sites if not detected in time (Oliver et al., 2020b; Yeo & Angeli, 2017). Additionally, lymphatic MHC presentation and PD-L1 expression at solid tumors has been shown to dampen anti-tumor T

cell immunity further promoting tumor development. Altered lymphatic morphology and function have also been observed at the skin and trachea upon bacterial infection where lymphatic tight junction zippering was shown to limit viral dissemination to the draining lymph node (Churchill et al., 2022a; Yao et al., 2012a). Intestinal bacterial infection has also been shown to impact mesenteric lymphatic collecting vessels integrity leading to compromised immune cell trafficking to the draining lymph node (Fonseca et al., 2015). The microbiome has also been found to regulate intestinal lymphatic vasculature morphology (Suh et al., 2019), setting the stage for potential impact on lymphatics in other disease states where microbial dysbiosis occurs. Despite the immune systems co-evolution with pathogens in a proverbial arms race, the role of the lymphatics in the immune response against pathogens remains poorly understood.

1.6 Type-2 immune response and wound healing upon helminth infection

The co-evolution of vertebrates and helminth parasites is thought to have a beneficial role in promoting the activation of tissue healing and wound repair mechanisms while simultaneously promoting anti-helminth type-2 immune responses (Gieseck et al., 2018). Upon helminth induced tissue damage, alarmins TSLP and IL-33 trigger the initiation of type-2 immunity leading to the recruitment of mast cells and basophils, ILC2s, T_H2 Cells, and pro-inflammatory M2 macrophages(Lloyd & Snelgrove, 2018). Together, these cells release several effector cytokines and growth factors such as IL-13, histamines, and vascular endothelial growth factors (VEGFs) that promote tissue repair at the site of infection while also promoting anti-helminth immunity(Gause et al., 2013). Efficient and rapid tissue repair is critical to constrain inflammation without causing further damage to the tissue and prevention from pathogens breaching the wound site through the establishment of a both physical and bactericidal barrier.

1.7 Uncovering the impact of the tissue microenvironment on lymphatics

Here we sought to uncover whether the lymphatics functionally adapt to the microenvironment they drain at both homeostasis and upon inflammatory perturbation, using the gut as a site of investigation. Despite being a singular organ, differences in microenvironments (pH, O_2 availability, microbiome abundance and diversity, and luminal contents) across the small intestine make it a great model system to uncover the degree to which intestinal lymphatics are dynamically regulated by the tissue the drain. We hypothesized that the tissue lymphatics along the intestine are tuned to the gut segment they drain, and perturbations to the system (e.g. infections) will translate to alterations in the lymphatic vasculature. Using imaging, nutrient uptake assays, genetic based approaches to alter lymphatic properties, transcriptomics and infections with duodenal tropism we uncovered that indeed the lymphatics along the small intestine have niche specific properties and are susceptible to impairment, whereby the duodenal lymphatics being the most permissive of chylomicron uptake and most immunologically active, and these functions are perturbed by helminth infections.

2. Materials and Methods

2.1 Animals

All mouse studies were approved by The University of Chicago Institutional Animal Care and Use Committee. Mice were maintained at the University of Chicago animal facilities under MNV, SFB, *Hpp* free, specific pathogen free (SPF) conditions. B6 (C57BL/6J), TdTomato (B6.Cg-Gt(ROSA)26Sor$^{tm14(CAG-tdTomato)Hze}$/J) and RAG1 knockout (B6.129S7-Rag1tm1Mom/J), were purchased from the Jackson Laboratories and maintained inhouse. Flt4^{creERT2} (Flt4$^{tm2.1(cre/ERT2)Sgo}$) (Gardenier et al., 2016) mice were obtained from Babak J. Mehrara (Memorial Sloan Kettering Cancer Center) with consent of S. Ortega (CINO, Spain) and Vegfr3$^{lox/lox}$ mice were obtained from Melody A. Swartz (University of Chicago) after material transfer agreement with the generating investigator Kari Alitalo (University of Helsinky), Prox1^{creERT2} (Jannaway et al., 2023) mice were gifted by Joshua P. Scallan (University of South Florida), and all maintained inhouse following rederivation into our facility. In general a mix of male and female mice were used for this study, and animals were 7-10 weeks of age. Exclusively male mice (on a C57BL/6J background) were used for all experiments involving helminth infections due to the relative resistance of female mice to helminths. All mice were on the C57BL/6J background and when relevant Cre negative littermates were used as controls.

2.2 VEGFR-2 Blocking antibody

VEGFR-2 blocking antibody (DC101, Bio X Cell, BP0060; 45 μg/g) and isotype control antibody (eBR2a, Thermo Fisher, 16-4321-85; 45 μg/g) were injected i.p. once every 24 hrs for 96 hrs and 48 hrs for the Sv and triglyceride challenge experiments respectively (all diluted in PBS).

2.3 Dietary interventions

To induce Cre activity, mice were placed on a diet containing 500mg/kg tamoxifen (TD.130857, Inotiv) for one week and taken off the diet for one week before further interventions.

To study the impact of loss of fat on lymphatic morphology, 6 weeks old male C57BL/6J mice were placed on a CHOW diet (2020x, Inotiv, 16% of calories from fat) or the same diet without added soy bean oil (TD.180890, Inotiv, 0.5% of calories from fat, which come from the grain shells) and sacrificed 4 weeks later in the morning. For an overnight fast, one group of mice fed diet 2020x for 4 weeks had its food removed and cages exchanged for 16 h prior to sacrifice the following morning. The cages of all mice to be compared were exchanged the late afternoon before sacrifice.

For studying the interaction between helminth infection and increased dietary fat content, 6 week old male B6 mice were placed on either a refined diet with 13% calories from fat (TD.200502, Inotiv) or a diet with 60% calories from fat (TD.200501, Inotiv) that was otherwise isonutritional to the 13% fat content diet. Mice were fed these diets for 2 weeks prior to infecting mice with Sv and then kept on the diet during the infection. Diet was changed every week throughout the experiment. Mice were weighed prior to being put onto the diet and every week subsequently while on the diet.

2.4 Infections

S. venezuelensis and *N. brasiliensis* were maintained in NSG (NOD.Cg-Prkdcscid Il2rgtm1Wjl/SzJ) mice at The University of Chicago by subcutaneous injection of 10,000 larvae

(*S. venezuelensis*) or 2,500 larvae (*N. brasiliensis*). The cycle was started anew every 3 months (*S. venezuelensis*) or month (*N. brasiliensis)*. *H. polygyrus* was maintained in C57BL/6J mice at The University of Chicago by oral gavage of 500 larvae. 2 weeks following infection, feces or caecal contents containing helminth eggs were spread on top of a Whatman paper, which was rolled up and placed into a beaker with 150 ml of water at 28 ºC with the feces-free end standing in the water . The hatching larvae were collected over 2-7 days and the cycle re-initiated. For experiments, mice were subcutaneously injected with 1,000 *S. venezuelensis* larvae and 2,000 *N. brasiliensis* larvae, the height of each of these pathogens is 8 days following injection and B6 mice used in experiments cleared each infection 12-14 days following subcutaneous infection. Mice were administered an oral gavage of 200 *H. polygyrus* larvae, the acute phase of the infection is 14 days following administration after which the infected mice are chronically infected.

Reovirus strain T1L was prepared at the University of Pittsburgh by the Terrence Dermody lab as previously described (Holm et al., 2010). Briefly, T1L was recovered using reverse genetics, plaque-purified, and tittered by plaque assay as described. The genotype of T1L was confirmed by SDS-polyacrylamide gel electrophoresis. Mice were infected with $1x10^9$ PFU T1L diluted in PBS by oral gavage and sacrificed 48 hours following infection.

Y. pseudotuberculosis (strain IP32777) was originally obtained from Igor Brodsky (University of Pennsylvania) and grown in 2XYT media supplemented with 2µg/ml Irgasan overnight at 25 ºC with vigorous shaking. Mice were fasted overnight prior to oral gavage with 1x108 CFU of *Y. pseudotuberculosis* and harvested 48 hours following infection.

2.5 Immunofluorescence Staining

For whole-mount imaging the corresponding small-intestine segment was excised and cut longitudinally to expose the lumen. The intestines were immediately washed with ice-cold PBS then pinned down lumen side-up and fixed in 4% PFA for 2 h at room temperature (RT) followed by two consecutive quick washes with PBS to remove any remaining PFA. Intestines were then embedded in 4% low melt agarose (Goldbio) then sectioned with a vibratome (125 um, 0.8 mm/s, 0.8 mm) for a single row of intestinal villi. Floating tissue sections were washed on a nutator at RT 3 times for 15 minutes each in 0.5% Triton-X 100 (Thermo Fisher) in PBS (PBST) then replaced with block (5% BSA, 5% donkey serum, and 0.002% sodium azide in PBST) and placed back on the nutator for 3 h at RT. Once complete, samples were stained with indicated primary antibody solution made in block nutating for 48 h at 4º C followed by 3 consecutive 15 min washes in PBST then staining in secondary antibody solution made in block nutating for 24 h at 4º C. Upon completion of staining, tissues were washed a final 3 times for 30 minutes each at RT to remove excess unbound secondary antibody then mounted in DAPI fluoromount-G clear mounting media (Thermo Fisher). The following primary antibodies were used for immunofluorescence: goat polyclonal anti-Lyve1 (1:200, Thermo Fisher Scientific, AF2125), rabbit polyclonal anti-Lyve1 (1:200, Abcam, Ab14917), Goat polyclonal anti-VE Cadherin (1:100, R&D Systems, AF1002), rabbit polyclonal anti-Prox1 (1:100, Abcam, Ab101851). Alexa Fluor secondary antibodies, donkey anti-goat 488, donkey anti-goat 568, donkey anti-rabbit 488, and donkey anti-goat 568 (1:500, Thermo Fisher Scientific) were used for visualization. Images shown were captured with a Leica SP5 Tandem Scanner Spectral 2-photon confocal microscope (Leica Microsystems, Inc., Buffalo Grove, IL). Digital image files which the scoring was based off were

created with an Olympus VS200 Research Slide Scanner (Olympus / Evident, Center Valley, PA) with a Hamamatsu ORca-Fusion camera (Hamamatsu Photonics, Skokie, IL). Individual images were created with the OlyVIA Viewer software (Olympus / Evident, Center Valley, PA).

2.6 Fluorescent in situ hybridization

The FISH protocol adapted from the following literature (Salzman et al., 2002; Swidsinski et al., 2005). Briefly, intestinal tissue was harvested with removal of all mesentery attached to the bowel wall. Tissue was immediately fixed in 0.5 mL of Methacarn (60% MetOH, 30% Chloroform, 10% CH_3COOH) for 6 hrs at 25º C in an Eppendorf tube. Tissues were washed 3x in 70% EtOH for 10 minutes each then paraffin embedded with the lumen facing the upright position. 5 µm thick paraffin sections were deparaffinized with serial 10 minute washes with 95% xylene then 90% xylene with brief washes in dH_2O between. Rehydrate sections in successive 10 minute 95% and 90% EtOH washes followed by a 10 minute wash in dH_2O. Add 40 µl of bacterial probe (EUB338) diluted 1:150 in hybridization buffer (0.9 M NaCl, 20 mM Tris-HCl (pH 7.2), 0.1% SDS) warmed to 50º C directly over the paraffin section then covered with a plastic coverslip. Slides were then incubated in a humidifying slide chamber for 3 hrs at 50º C. Following incubation, slides were washed 2X for 10 minutes each in wash buffer (0.9 M NaCl, 20 mM Tris-HCl (pH 7.2)) with excess wash removed after the final wash with a kimwipe. Slides were mounted in DAPI fluoromount-G clear mounting media (Thermo Fisher) and covered with a glass coverslip for imaging.

2.7 Histological analysis/scoring

Digital image .vsi files of whole-mount z-stacks were imported and analyzed with QuPath and ImageJ software's (Bankhead et al., 2017; Schneider et al., 2012). Tissue ID was blinded to

the analyzer. Villus length was measured from the base of the crypt to the tip of the villus. Villus width was measured at the center of the villus. Lacteal length and surface area was measured from the base of the lacteal to its tip. Prox1+ nuclei were co-stained with DAPI and were within the LYVE-1+ lacteal. Lacteal tight junction organization was categorized based on the following VE-cadherin staining patterns previously established by other groups (Baluk et al., 2007; Bernier-Latmani et al., 2015; Yao et al., 2012b): Button-like junctions (discontinuous puncta), Zipper-like junctions (continuous lines), and Mixed/both (combination of discontinuous and continuous staining along the lacteal). For villus/lacteal length, villus width, and lacteal surface area at least 100-200 non-consecutive villi were scored per group. 10 non-consecutive lacteals per mouse were used to enumerate Prox1+ nuclei enumeration and analyze tight junction composition. Tight junction lengths were measured using the *Analyze particles* function in ImageJ as follows: individual VE-Cadherin channel was converted to an 8-bit image then adjusted to threshold. The region of interest (ROI) was defined with the freehand selection tool then then particles within the ROI were analyzed with the size limits set to 1 to infinity to minimize the contribution of background staining.

2.8 Lipid uptake test

Following overnight fast, 150 µl of olive oil (Millipore Sigma) was delivered via oral gavage for plasma and lymph node triglyceride measurements and Oil Red O staining. If indicated, 100 µl of 1% poloxamer 407 (Sigma-Aldrich) was administered via IP injection 15 min prior olive oil gavage. 90 µl of blood was taken via cheek bleed into a tube containing 10 µl 0.5 mM EDTA at the following time intervals: 0, 30, 60, and 180 min after oil gavage (depending on the experiment). Lymph nodes were harvested and weighed into pre-weighed 1.5 mL tubes on ice with 25 µl of the Triglyceride assay kits (Cayman Chemical Company) diluted NP40 substitute and

further processed according to manufacturer's instructions and snap frozen over dry ice and kept at -80ºC until use. Plasma and lymph node triglyceride concentrations were measured using the Triglyceride assay kit according to instructions and absorbance was measured at 540 nm. Fresh un-fixed small intestine floating vibratome sections were stained with Oil red O 3 h after olive oil gavage following the manufacturer's protocol of the Oil Red Staining Kit (Sigma-Aldrich).

2.9 APC Isolation from lymph nodes

Lymph nodes were dissected into RPMI containing 2% FCS and 1% Hepes. Lymph nodes were finely chopped and digested with 2.5 mg/ml Collagenase D for 30 minutes at 37º C. The digestion was then quenched on ice and by adding RPMI to the isolation. Cells were then used for staining immediately.

2.10 Flow Cytometry and flow antibodies

Fluorescent-dye-conjugated primary antibodies were purchased from Fisher: anti-CD11b (365-0112-82), Live/Dead Fix Aqua (50-112-1525), anti-MHC Class II (I-A/I-E) (46532182), BD Biosciences: anti-CD45 (564225), anti-CD103 (562771), and BioLegend: anti-CD8a (100744), anti-CD11c (117324), anti-CD19 (115555), anti-TCR**b (**109243**).** Following cell surface staining, cells were fixed according to the manufacturers protocol (BD 554714). Flow cytometry was performed on an LSRII (BD Biosciences) and analyzed using FlowJo Software (Tree Star).

2.11 Mucosal Scrape (RNAseq)

The small intestine was removed from the mesentery, and Peyers patches were removed. The small intestine was divided into four quarters and the proximal ¼ was taken as the duodenum, ¼ of the middle of the small intestine was taken as the jejunum and the terminal ¼ was taken as

the ileum. The tissue were cut longitudinally and gently washed with ice-cold PBS to remove any luminal contents. The tissue segments were immobilized and the straight edge of a blade was then used to scrape away the intestinal mucosa and submucosa from the muscularis. The muscularis was discarded and the mucosa layers were then snap frozen on dry ice in 1.5mL Eppendorf Tubes with 0.5 mL of RNAlater and kept at -80º C until processing. Samples were defrosted on ice and mucosal scrapes were transferred into 2mL Bead Mill Tubes pre-filled with ceramic beads and 1mL cold TRIzol™ Reagent (Thermo Fisher). Samples were lysed with a bead beater then transferred to a new Tube and processed according to manufacturer's instructions. Briefly, the samples were incubated at RT then spun down at 4º C and the supernatant was transferred to a new tube with chloroform to extract the RNA and spin down again. The RNA was precipitated by adding equal volumes of 70% EtOH and continuing the RNA purification process with the PicoPure RNA Isolation Kit (Thermo Fisher) according to manufacturers instructions and eluting in 20 uL of the elution buffer and RNA concentration was measured with a nanodrop.

2.12 Mucosal scrape RNAseq library prep

RNA samples were normalized to 200 ng/µl with ddH_2O. 1000 ng of RNA was then used as the starting material for cDNA synthesis and tagmentation using the NEBNext Poly A kit per the manufacturer's instructions. The concentration of the eluted samples was calculated by Qubit and the average fragment length of 300-400 bp was measured with the bioanalyzer. Samples were pooled at 10 nM and handed off to the Univerity of Chicago Genomics Core for sequencing using paired end 50 bp reads on a Novaseq S2 flowcell.

2.13 BEC/LEC Isolation from small intestine

Flt4^{creERT2}tdTomato mice were administered dietary tamoxifen for one week and harvested two weeks after the tamoxifen regime had been terminated. Their small intestine was removed from the mesentery and Peyers patches were removed. The small intestine was divided into four quarters and the proximal ¼ was taken as the duodenum, ¼ of the middle of the small intestine was taken as the jejunum and the terminal ¼ was taken as the ileum. The tissue were cut longitudinally and gently washed with ice-cold PBS to remove any luminal contents. The tissue was cut into 1 cm pieces and incubated in PBS with 1mM DTT for 15 min at RT at 80 rpm to remove the mucus from the tissues. Tissues were then washed in PBS with 30 mM EDTA for 10 min at 37º C at 230 rpm with vigorous shaking after the incubation then washed in fresh PBS and incubated for 5 min at 37º C at 230 rpm. Tissues were washed again with PBS on a metal sieve and placed into a 6 well plate where they were finely chopped and digested in RPMI containing 2% FCS, 1% HEPES, and 2 mg/ml Collagenase VIII, 200 mg/ml DNase I for 35 min at 37º C at 80 rpm. Tissues were physically disrupted by passing them ten times through a 18G needle using a 3 mL syringe every 10 min, then 20 times at the completion of the digestion, as monitored for the appearance of single red cells under a benchtop fluorescent microscope. Digests were filtered and quenched in cold RPMI with 2% FCS.

2.14 BEC-LEC Sorting

250 BECs (live CD45-TER119-LIN-Podplanin-CD31+) and 250 LECs (live CD45-TER119-Podplanin+CD31+) were sorted from the duodenum, jejunum, ileum, and colon of uninfected and Sv infected Flt4cre^{ERT2} ROSA26^{tdTomato} mice. Live cells were sorted into 25 µL TCL buffer containing 1% 2-mercaptoethenol, immediately spun down and snap frozen on dry ice.

Samples were kept at -80ºC until further processing. All sorts were conducted at the University of Chicago Flow Cytometry core using a BD FACSAria Fusion Cell Sorter.

2.15 BEC-LEC RNAseq Library Prep

Cells were sorted into TCL buffer containing 1% 2-mercaptoethanol. RNA was isolated using RNA Clean XP beads (Agentcourt) on a magnetic stand. Reverse transcription primers were: P1-RNA-TSO: Biot-rArArUrGrArUrArCrGrGrCrGrArCrCrArCrCrGrArUrNrNrNrNrNrNrGrGrG, P1-T31: Biot-AATGATACGGCGACCACCGATCG31T, P1-PCR: Biot-GAATGATACGGCGACCACCGAT. RNA was eluted for 1 min in RT-cDNA synthesis mix 1 (0.5 µl P1-T31 (20µM), 0.3 ml RNasinplus (Promega), 1.5µl 10µM dNTP, 3.5 µl 10µM Tris pH 7.5-0.5% IGEPAL CA-630 (Sigma) and 1.7 µl RNase free ddH_2O) and pipetted up and down to mix. The eluted sample was then incubated for 3 min at 72ºC, followed by 1 min on ice, then 7.5 µl of mix 2 was added (3µl 5X RT Buffer, 0.375 µl 100 mM DTT, 0.375 µl RNasin plus, 0.5 µl P1-RNA-TSO (40 µM), 0.75 µl Maxima RT Minus H (Thermo Scientific), 1.8 µl 5M Betaine (Sigma), 0.9 µl 50 mM $MgCl_2$ and 0.175 µl RNase free ddH_2O and mixed well. Samples were placed in a thermocycler and subjected to the following protocol: 42ºC for 90 s, (50ºC for 2 min, 42ºC for 2 min) x10 cycles, 70ºC for 15 min. The cDNA was then amplified using 13.5 µl cDNA, 20 µl KAPA HiFi 2x Mix, 1.5µl P1-PCR, and 5 µl H_2O. Samples were subjected to the following protocol: 98ºC for 3 min, (98ºC for 15 s, 67ºC for 20 s, 72ºC for 6 min) x12 cycles, 72ºC for 5 min. cDNA was cleaned up using RNA Clean XP beads and eluted in water. The concentration was calculated using a Qubit fluorometer and the average fragment length of 1500-1800 was determined by Bioanalyzer. Samples were normalized to 0.1 ng/µL using ddH_2O, and 2.5 µl cDNA were tagmented using Nextera XT Index Kit according to the manufacturer's protocol, except that all volumes were used at 0.5x of the indicated volumes.

The concentration of the eluted samples was calculated by Qubit. Samples were pooled at 10 nM and handed off to the UChicago Genomics Core for sequencing using paired end 50 bp reads on a Novaseq S2 flowcell.

2.16 RNAseq Analysis

Raw fastq files were pseudo-aligned to the mouse reference transcriptome M26 (GRCm39) using Kallisto(REF). The gene counts were input to R and transcripts per million (tpm) was scaled by gene length. Initial filtering removed genes with expression under 2 counts per million (cpm). The un-normalized filtered gene counts were then used as input for the R package DEQeq2 using the default paramerters (Wald test) to compare genes differentially expressed across conditions or segments, correcting for replicates. The *apeglm* method was used for log fold change shrinkage to better visualize effect sizes. Genes with $\log_2$ fold changes greater than 1.5 or less than -1.5 and an adjusted p value (padj) ≤ 0.05 were considered significant for downstream studies. To generate segment or condition specific gene sets, the significant genes for both pairwise comparisons (i.e. Ileum LEC vs Duodenum LEC, Sv 8 dpi Duodenum LEC vs Non-infected Duodenum LEC) were acquired using the R package DESEQ2. To perform and plot gene set enrichment analysis (GSEA) comparing two different segments or conditions the R packages *fgsea* and *dplyr* were used with the following parameters: Log_2 fold change greater than 1.5 and less than -1.5, 10 genes per pathway minimum, 500 genes per pathway maximum, 10,000 permutations. Gene Ontology Biological Process pathway (m5.go.bp.v2023.1.Mm.symbols.gmt) was used as a reference for the analysis. GSEA plots shown were curated with removal of redundant or non-applicable pathways, pathways with the highest number of genes were kept over those with fewer genes. Heatmaps were generated using total DEG list or from list of genes within collapsed GOBP pathways using the R

package pheatmap. Venn diagrams comparing differentially expressed gene (DEG) list between data sets were generated using the R package Venn Diagram.

Transcription factor (TF) network and associated analysis was performed by in putting all DEGs into the ChEA3 search database (Keenan et al., 2019). Key TF's identified were confirmed to be expressed in sorted LECs as to having expression levels over 2 cpm.

Overrepresentation Gene Ontology (GO) pathway analysis was performed by entering DEG list into several independent data bases (Aleksander et al., 2023; Ashburner et al., 2000; Ge et al., 2020). For pie charts, pathways were collapsed into general like-categories. In several instances, genes were found to contribute to more than one pathway, to avoid biasing data these genes were accounted for in each of the general pathways. Venn diagram comparing the DEGs regulated by each pathways were generated using the Venn diagram R package.

2.17 Tissue RNA extraction and Quantitative PCR

Whole intestinal tissue was harvested and any attached mesentery was removed, the gut was then longitudinally cut to expose the lumen. The luminal contents were removed by washing the tissue in ice cold PBS. Excess PBS was removed by briefly dabbing the tissue with kimwipes then the tissue was placed into a 1.5mL Eppendorf Tubes with 0.5 mL of RNAlater and frozen over dry-ice and kept at -80 °C until processsing. Samples were defrosted on ice and tissue was transferred into 2mL Bead Mill Tubes pre-filled with ceramic beads and 1mL cold TRIzol™ Reagent (Thermo Fisher) and RNA was isolated via TRIzol protocol. Briefly, samples were lysed with a bead beater then transferred to a new Tube and processed according to manufacturer's instructions. Briefly, the samples were incubated at RT then spun down at 4ºC and the supernatant was transferred to a new tube with 200 µl chloroform to extract the RNA and incubate on spin

down again for 15 minutes. The RNA was precipitated by adding equal volumes of isopropanol to the volume of the chloroform aqueous layer then incubated at -80ºC for at least 1 hour. Samples were centrifuged for 20 minutes at 4ºC, then the pellet was washed with 75% EtOH. After the RNA pellet was dried it was resuspended in RNase-free water. cDNA was prepared with the SuperScript™ IV Reverse Transcriptase system and protocol using 1 ng RNA as input, cDNA was diluted with RNase free-water (1:10) upon completion. qPCR master mixes were prepared using Power Sybr Green (Invitrogen) containing 1 ng cDNA sample, 7.5 µl Sybr, 0.15 µl 10 µM forward and reverse primer mix, and water up to 14 µl. Samples were multichanneled into 384 well plates in duplicate and run on a Applied Biosystems QuantStudio 6 Flex machine. Delta Ct was calculated by subtracting the average of duplicate values for each gene from the average duplicate values for the housekeeping gene *36B4* for each sample. Relative expression values were then calculated by the equation: $2^{-\Delta CT}$x10,000.

2.18 qPCR Primer Sequence Table:

Gene	Primer sequence	Reference
36b4	Fwd: 5'-GCCGTGATGCCCAGGGAAGAC-3'	(Moest et al., 2013)
	Rev: 5'-CATCTGCTTGGAGCCCACGTT-3'	
Gata3	Fwd: 5'-CAACCTCTACCCCACTGTG-3'	IDT
	Rev: 5'-GATGTCCCTGCTCTCCTTG-3'	
Gata1	Fwd: 5'-CCCAATGCACTAACTGTCAAAC-3'	IDT
	Rev: 5'-ATCTTTCCTCATGGTCAGTGG-3'	

Mcp1	Fwd: 5'-GACCCGTAAATCTGAAGCTAATGC-3'	IDT
	Rev: 5'- AATTAAGGCATCACAGTCCGAGTC -3'	
F480	Fwd: 5'- TTGTACGTGCAACTCAGGACT -3'	PrimerBank
	Rev: 5'- GATCCCAGAGTGTTGATGCAA -3'	
Muc2	Fwd: 5'- ACAAAAACCCCAGCAACAAG -3'	(Pedicord et al., 2016)
	Rev: 5'- GAGCAAGGGACTCTGGTCTG -3'	
Il33	Fwd: 5'- ACTCCAAGATTTCGCCG -3'	PrimerBank
	Rev: 5'- CATGCAGTAGACATGGCAGAA -3'	
Cd36	Fwd: 5'- GATGACGTGGCAAAGAACAG -3'	(Cifarelli et al., 2021)
	Rev: 5'- CAGTGAAGGCTCAAAGATGG -3'	
Ctgf	Fwd: 5'- GTGCCAGAACGCACACTG -3'	(Hong et al., 2020)
	Rev: 5'- CCCCGGTTACACTCCAAA -3'	
Itgav	Fwd: 5'-CTTCAACCTAGACGCGGAG -3'	(R. Li et al., 2023)
	Rev: 5'- CGGTAAAACTCCACGGAGAAG-3'	
Cxcr2	Fwd: 5'-TCCTAACACTAGACCCCAAACACTC -3'	(Kawagoe et al., 2020)
	Rev: 5'- TTTCTCTCCTCCACCTCTTCCTT-3'	
Emilin2	Fwd: 5'-CCCTGGTGTATCGGGTAAAC -3'	(Da Ros et al., 2022)

	Rev: 5’- ATGTGGTCTTTGGGACCTTCT-3’	
Il1b	Fwd: 5’-GCCCATCCTCTGTGACTCAT -3’	IDT
	Rev: 5’-AGGCCACAGGTATTTTGTCG -3’	
Reg3a	Fwd: 5’- ATTGGGCTCCATGATCCA -3’	(Kurashima et al., 2021)
	Rev: 5’- AGATAATTCAGCACATCGGAGTT -3’	
Reg3b	Fwd: 5’- ACTCCCTGAAGAATATACCCTCC -3’	(Kurashima et al., 2021)
	Rev: 5’- CGCTATTGAGCACAGATACGAG -3’	
Reg3g	Fwd: 5’- TCCACCTCTGTTGGGTTCAT -3’	(REF)
	Rev: 5’- AAGCTTCCTTCCTGTCCTCC-3’	
Defa20	Fwd: 5’- CTTGGCCTCCAAAGGAGATAG -3’	(Yue et al., 2021)
	Rev: 5’- AGACACTTGTCCTCCTCTCT -3’	
Vegfc	Fwd: 5’- CAGGACAGGGGACAGTGTAAAATTTGC -3’	(Hong et al., 2020)
	Rev: 5’- TGGCATGCATTGAGTCTTTCTCCAC -3’	
Prox1	Fwd: 5’- TTCTTTTACACCCGCTACCC -3’	(REF)
	Rev: 5’- TTGACGCGCATACTTCTCC -3’	

2.19 Luminal content 16s Sequencing

Small and large intestines were harvested and cut longitudinally. Luminal contents were gently removed, weighed then snap frozen in 1.5 mL Eppendorf tubes with liquid nitrogen. Samples were submitted to the University of Chicago, Duchossis Family Institute Microbiome Metagenomic Facility for library preparation, sequencing, and data analysis as previously described (Odenwald et al., 2023) . Briefly, DNA was extracted using the QIAamp PowerFecal Pro DNA kit and quantified using Qubit. TheV4–V5 region within 16S rRNA gene was amplified using universal bacterial primers—563F (5′-nnnnnnnn-NNNNNNNNNNNN-AYTGGGYDTAAA-GNG-3′) and 926R (5′-nnnnnnnn-NNNNNNNNNNNN-CCGTCAATTYHT-TTRAGT-3′), where 'N' represents the barcodes and 'n' are additional nucleotides added to offset primer sequencing. The samples were sequenced on the Illumina MiSeq platform.

2.20 Microbial DNA extraction from tissue and 16S qPCR to enumerate CFU from gene copy number

The protocol is described in detail and adapted from (Barlow et al., 2020; Bogatyrev et al., 2020). Briefly, intestinal tissues were harvested and longitudinally opened. The luminal contents were gently removed, then the mucosa was scraped from the intestine and snap frozen in 1 mL of DNA/RNA Shield solution (R1100-250, Zymo Research) over dry-ice and kept at -80º C until use. Bacterial DNA was isolated from the mucosal scrapes using ZymoBIOMICS DNA Miniprep Kit (D4300, Zymo Research) per the manufacturers instructions. qPCR reaction was set up in triplicate

using 1.5 µl of template DNA , Power Sybr Green qPCR master mix (Invitrogen), 500nM forward (UN00F2, 5'- CAGCMGCCGCGGTAA-3') and 500nM reverse (UN00R0, 5'-GGACTACHVGGGTWTCTAAT-3') primers (Integrated DNA Technologies) with the reaction volume brought up to 15 µL with dH_2O. Thermocycling program: initial denature (95º C for 15 min) and amplification (40 cycles, denature at 95º C for 15 seconds, annealing at 53º C for 10 seconds, and extension at 68º C for 45 seconds). To calculate the CFU per copy number, *L. plantarum* was serially diluted 1:10, 10X then split to be plated on MRS plates (69964-500G, Sigma-Aldrich) and have the DNA extracted as described above. Plate CFUs were paired with their respective CT values to generate a standard curve to extrapolate CFU from the copy number of the test samples.

2.21 Broad spectrum antibiotic treatment

The day before, day of, and day after S. venezuelensis infection, mice were gavaged with 200 µL of antibiotics solution containing10 mg/mL Vancomycin, 10 mg/mL Metronidazole, 20 mg/mL Ampicillin and 20 mg/mL Neomycin ("ABX", each obtained from Sigma), dissolved in drinking water and filter-sterilized. Gavage was used to achieve immediate and synchronized microbial depletion between mice. From 2 days after infection low microbial load was maintained by placing mice on drinking water containing ABX (1g/L of Ampicillin and Neomycin, 0.5g/L Vancomycin and Metronidazole, 2g/L non-caloric sweetener Truvia to overcome avoidance of bitter taste), made available as sole and ad libitum liquid source in cages. Mice were harvested on day 9 post infection. To confirm microbial depletion fecal microbiome was extracted using the QIAamp Fast DNA Stool Mini Kit (Qiagen 51604) and following the manufacturer's protocol. Universal bacterial 16S primers used for QPCR were Universal 16S primers: UNIF340: Fwd: 5'-ACTCCTACGGGAGGCAGCAGT-3' and UNIR514: REV: 5'-ATTACCGCGGCTGCTGGC-3'.

2.22 Quantification and statistical analysis

For lacteal scoring, investigators were blinded to condition allocation during data analysis. RNA sequencing data were analyzed in R, including statistical analysis. All other data were analyzed with Prism software (GraphPad). Data is presented as average ± SD. Multivariate data between segments in a single condition was analyzed by applying one-way ANOVA with Šídák's multiple comparisons test, comparison between two conditions by two-tailed unpaired Student's t-test assuming a Gaussian distribution, and comparison of single variable between conditions was analyzed by applying two-way ANOVA with Turkey's multiples comparisons test. P-values or representative symbols are noted when differences are less than or equal to 0.1; all other differences were not found to be significant (n.s., $p > 0.1$). $*p < 0.05$, $**p < 0.01$, $*** p < 0.001$, $****p < 0.0001$).

Data access

RNAseq data are available at GEO under access codes GSE271711 (mucosal scrape) and GSE271712 (LEC and BEC RNAseq)

3. Results

3.1 Tissue lymphatics are structurally distinct along the small intestine and differ in their absorptive capacity

We first determined whether the lymphatic absorptive properties change along the small intestine. The ultra-architecture of the lymphatic system along the intestine has been examined previously, and notably the lacteals, like the villi, shorten along the small intestine, can appear branched in duodenum and jejunum, yet reach further into the villus tip in the ileum ((Bernier-Latmani et al., 2015), Fig. 2 A,B). Unsurprisingly, the lacteal (LYVE-1+) surface area was also largest in duodenal villi and smallest in the ileum (Fig. 2 B). Since lymphatic absorptive capacity is primarily dictated by permeability, we assessed LEC tight junction organization using tight junction VE-Cadherin staining (Fig. 2 C). As established by others (Baluk et al., 2007; Bernier-Latmani et al., 2015; Yao et al., 2012b; Zhang et al., 2018), we categorized lacteals as containing primarily impermeable "zipper-like" junctions, permeable "button-like" junctions or a mix of both (Fig. S1 A) and found that lacteals were mostly button-like in the duodenum and became increasingly more zipper-like toward the ileum (Fig.2 D). We sought to confirm this with an independent, automated method measuring the length of VE-Cadherin+ junctions (ferets) within LYVE-1+ area. This analysis revealed that while the sum tight junction length per lacteal was not significantly different, the average tight junction length increased from proximal to distal small intestine (Fig. 2 E, F; Fig. S1 B, C). These results suggested a lacteal permeability gradient along the small intestine.

To determine if this tight junction gradient impacts lipid uptake, we gavaged mice with a bolus of olive oil, and measured plasma and gut-draining LN (gLN) triglyceride content over and after 3 hours, respectively. High dose olive oil reaches all gut segments, but since chylomicron

formation efficiency along the small intestine may also differ we coupled this analysis to a comparison to mice in which we induced the loss of *Vegfr3* expression in LECs using the Prox1Cre^{ERT2} driver (Vegfr3$^{\Delta Prox1}$) (Jannaway et al., 2023), which we confirmed to lead to a more zipper-like LEC tight junction organization in the duodenum (Jannaway et al., 2023; Suh et al., 2019) (Fig. S1 D,E). Conversely, we also coupled this study to mice treated with a VEGFR-2 blocking antibody (Churchill et al., 2022b), which as predicted (Churchill et al., 2022b) led to a more button-like LEC tight junction organization in the ileum (Fig. S1 G-L). Lipids accumulated in the gLNs in a decreasing proximal to distal gradient in wildtype *(*Vegfr3^{WT}) littermate and isotype control antibody treated mice (Fig. 2 G, J). Upon tamoxifen treatment, this gradient diminished in Vegfr3$^{\Delta Prox1}$mice, whereby the duodenal LNs accumulated less and the ileal LN more lipid. Correspondingly, there was also a decrease in the plasma triglyceride content early post gavage in Vegfr3$^{\Delta Prox1}$ compared to Vegfr3^{WT} littermate control mice (Fig. 1K). Oil-red-O staining of the gut also confirmed lipid stalling in the duodenum but more effective ileal clearance in the Vegfr3$^{\Delta Prox1}$ mice (Fig. 2 I). This Oil Red O staining phenotype is similar to what has been observed when deletion of the HIPPO pathway in lamina propria stromal cells leads to a zippering of lacteals and lipid stalling at the mucosa (Hong et al., 2020). By contrast, altering tight junctions to a more button like conformation using VEGFR-2 blocking antibody led to a slight increase in jejunal LN lipid levels (Fig. 2 J), but the triglyceride content and lipid uptake kinetics (Fig. 2 K) or villus lipid accumulation (Fig. 2 L) were not impacted, likely because the primary site of lipid absorption, the duodenum, was not disturbed by this intervention. Despite being able to regulate the degree at which lipids are taken up by modulating lymphatic tight junction composition, lipid uptake remains the highest at the proximal small intestine draining lymph nodes. This suggest that in

addition to lymphatic tight junction composition, spatial proximity to the stomach also plays a role into establishing the decreasing lipid uptake gradient we have observed along the small intestine.

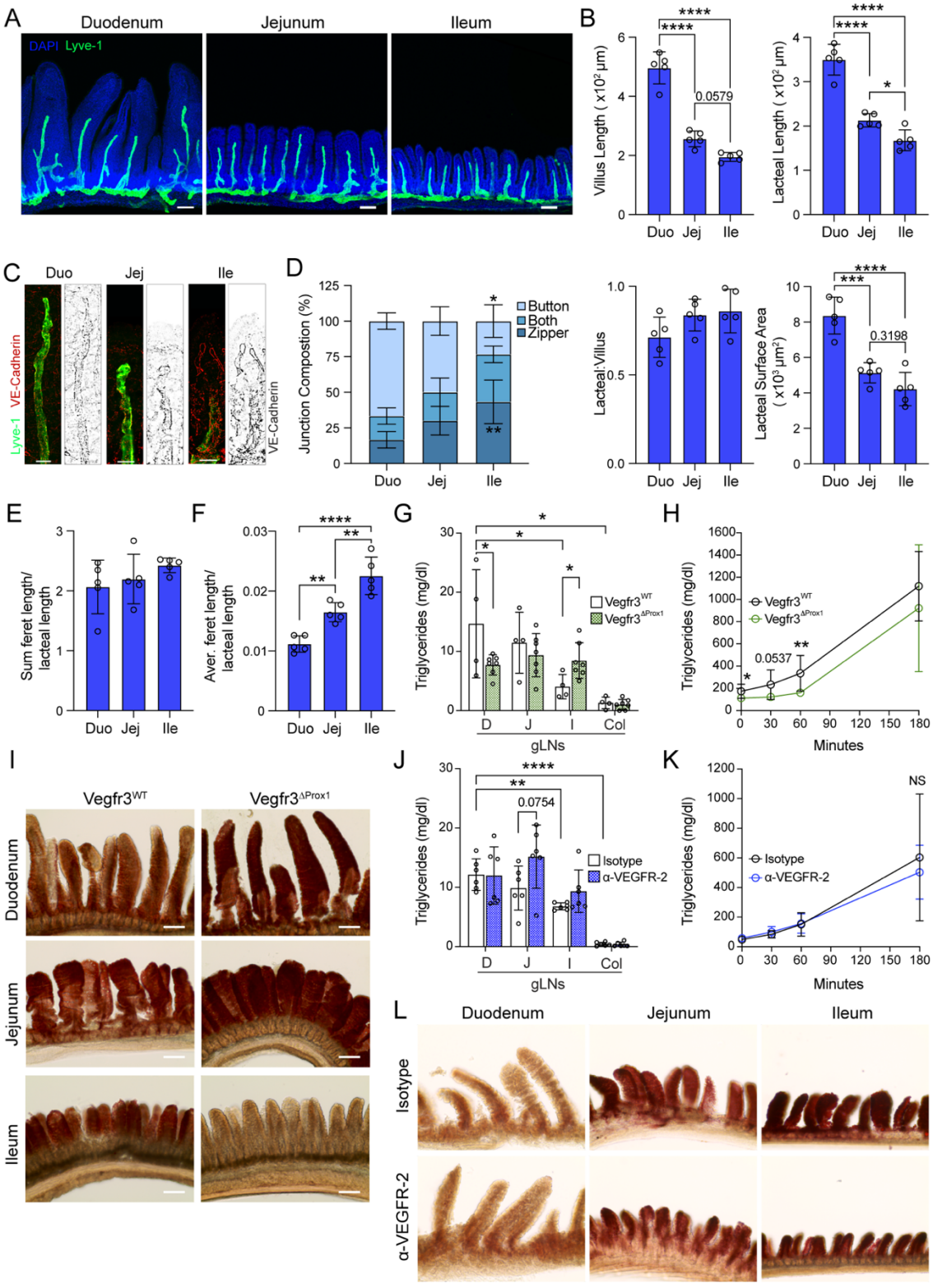

Figure 2. Tissue lymphatics are structurally and functionally different along the gut.
(A and B) Immunofluorescence images (A) and comparisons of villi and LYVE-1+ lacteals along the small intestine (SI) (B): villus length, lacteal length, lacteal to villus length ratio, and lacteal surface area along the small intestine in wild-type (WT) C57BL/6 mice (n = 5). Scale bar: 100 μm. Data representative of two independent experiments. (C-F) Representative images (C) and characterization of VE-cadherin+ LEC junctions of LYVE-1+ lacteals along the SI in C57BL/6 mice. Quantification of SI lacteal tight-junction organization with primarily button-like, zipper-like, or a combination of both tight-junction formations throughout the length of the lacteal (D), sum of VE-Cadherin+ junction (feret) lengths of LYVE-1+ lacteals normalized to the length of the lacteal (E), mean VE-Cadherin+ feret length of LYVE-1+ lacteals normalized to the length of the lacteal (F) (n = 5). Scale bar: 25 μm. Data representative of two independent experiments. (G-I) Intestinal draining lymph node (LN) (G), plasma triglyceride concentration over time (H), and representative images of Oil red O staining (I) of intestinal villi 3 hours after olive oil challenge of $Vegfr3^{\Delta Prox1}$ and $Vegfr3^{WT}$ littermates (n = 4-7). Data pooled from two independent experiments. Scale bar: 125 μm (J-L) Intestinal LNs (J), plasma triglyceride concentration over time (K), and representative images of Oil red O staining (L) of intestinal villi 3 h after olive oil challenge of mice treated with anti-VEGFR-2 or IgG2a isotype control antibody. (n = 6), data pooled from two independent experiments. Scale bar: 125 μm. Abbreviations: duodenum (D), jejunum (J), ileum (I), and Cecal-colonic (Col). Error bars indicate mean ± SD and *P<0.05, **P<0.01, *** P< 0.001, **** P< 0.001 by one-way ANOVA with Šídák's multiple comparisons test (B, D-G, J) or two-tailed student's t-test (comparison between genotypes (G, H) or treatments (J,K) at single locations or time points. Data are represented as mean ± SD. D/Duo=duodenum, J/Jej=Jejunum, I/Ile=ileum.

Finally, we interrogated if in adult mice lipid substrate availability is responsible for the more button-like conformation in duodenal lacteals by either placing mice on a CHOW diet with no added fats (0.5% calories from fat remaining from grain) or subjecting them to an overnight fast (16 h) and comparing the lacteal morphology to fed mice placed on a regular CHOW diet (18% calories from fat). Of note, both interventions would result in luminal lipid levels lower than the ileum receives under fed CHOW conditions. Neither very low fat nor the overnight fast changed lacteal morphology or tight junction length (Fig. S1L, M), suggesting that maintenance of baseline duodenal lacteal architecture in adult mice does not require acute or chronic lipid exposure.

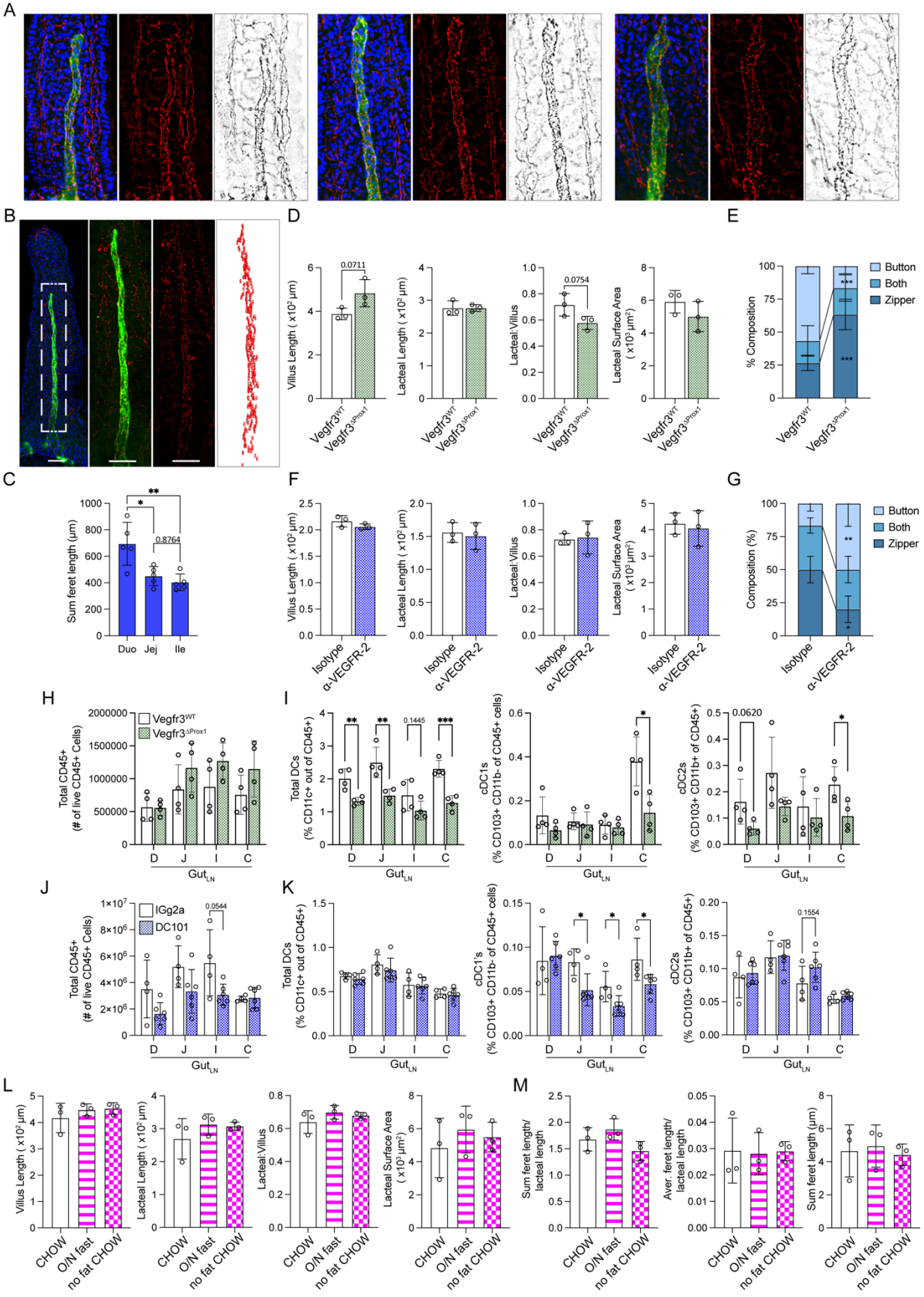
A
B
C
D
E
F
G
H
I
J
K
L
M
Villus Length (x10² µm)
Lacteal Length (x10² µm)
Lacteal:Villus
Lacteal Surface Area (x10³ µm²)
0.0711
0.0754
Vegfr3WT
Vegfr3ΔProx1
% Composition
Button
Both
Zipper
Sum feret length (µm)
0.8764
Duo
Jej
Ile
Isotype
α-VEGFR-2
Composition (%)
Total CD45+ (# of live CD45+ Cells)
Total DCs (% CD11c+ out of CD45+)
cDC1s (% CD103+ CD11b- of CD45+ cells)
cDC2s (% CD103+ CD11b+ of CD45+)
0.0620
0.1445
IGg2a
DC101
0.0544
0.1554
GutLN
D
J
I
C
CHOW
O/N fast
no fat CHOW
Sum feret length/ lacteal length
Aver. feret length/ lacteal length
Sum feret length (µm)

Figure S1. Tissue lymphatics are structurally and functionally different along the gut.
(**A, B**) Immunofluorescent images of villi stained for LYVE-1 (green) and VE-Cadherin (red or grey) and counterstained with DAPI and representative of lacteal classified as displaying zipper-like tight junctions (left), a mix of zippers and buttons ("both", center) and mostly button-like junctions (right) (A) or representative of a lacteal of which VE-Cadherin staining within LYVE-1+ area was subjected to automated feret assignment (B). (**C**) Sum feret length per lacteal along small intestine. (*n*=5). (**D**) Duodenal villus length, lacteal length, lacteal to villus length ratio, and lacteal surface area of $Vegfr3^{\Delta Prox1}$ and $Vegfr3^{WT}$ mice (*n* = 3). (**E**) Quantification of duodenal lacteal tight-junction organization with primarily button-like, zipper-like, or a combination of both tight junction formations throughout the length of the duodenal lacteal of $Vegfr3^{\Delta Prox1}$ and $Vegfr3^{WT}$ mice (*n* = 3). **(F**) Ileal villus length, lacteal length, lacteal to villus length ratio, and lacteal surface area of mice treated with anti-VEGFR-2 or IgG2a isotype control antibody (*n* = 3). (**G**) Quantification of duodenal lacteal tight-junction organization with primarily button-like, zipper-like, or a combination of both tight junction formations throughout the length of the duodenal lacteal of mice treated with anti-VEGFR-2 or IgG2a isotype control antibody (*n* = 3). (**H**, **I**) Total CD45+ cell count (H) and frequency of CD11c+ DCs, CD11b- CD103+ cDC1's, and CD11b+ CD103+ cDC2's from $Vegfr3^{\Delta Prox1}$ mice and littermate controls. (n = 4, Data representative of one experiment). (**J**, **K**) Total CD45+ cell count (H) and frequency of CD11c+ DCs, CD11b- CD103+ cDC1's, and CD11b+ CD103+ cDC2's from mice given anti-Vegfr2 or IgG2a isotype control antibody. (n = 4-6, Data representative of one experiment). (**L**, **M**) Duodenal villus length, lacteal length, lacteal to villus length ratio, and lacteal surface area (L) and sum of VE-Cadherin+ junction (feret) lengths of LYVE-1+ lacteals normalized to the length of the lacteal, mean VE-Cadherin+ feret length of LYVE-1+ lacteals normalized to the length of the lacteal and total feret length (M) in mice fed a CHOW diet, fasted overnight, or fed a diet without added fats (*n* = 3). Error bars indicate mean ± SD and *P<0.05, **P<0.01, *** P< 0.001, **** P< 0.001 by two-tailed student's t-test (D, E, F, G, H, I, J, K) or two-way ANOVA with Šídák's multiple comparisons test (C, L, M).

These results reveal the existence of a stable permeability and lipid uptake capacity gradient of the lymphatics along the small intestine that mirrors the absorptive function of the gut segment they drain.

3.2 Impact of lacteal tight junction composition on immune cell trafficking

We observed this inverse correlation between lacteal tight junction composition and lipid uptake gradient along the intestine and considering tight junction composition has previously been shown to regulate immune cell trafficking from the tissue to the draining lymph node (Churchill

et al., 2022b; Zuo et al., 2020), we next asked whether tight junction composition also impacts dendritic cell trafficking from the intestine to the gLN. 5 week old Vegfr3$^{\Delta Prox1}$ mice, where lymphatic tight junctions become more "zipper-like" were placed on a tamoxifen diet for 5 days, then the gLNs were harvested 14 days following the start of the diet. Lymphatic zippering resulted in a slight increase in the total number of CD45+ cells within the distal draining gLNs (Fig. S1H). Of the CD45+ cells within the gLNs, there was a significant decrease in CD11c+ DCs at each gLN, with trending non-significant decreases in migratory cDC1's and cDC2's at the duodenal and cecal-colonic draining LNs (Fig. S1I). We next asked whether increasing lymphatic tight junction buttoning influences immune cell trafficking to the gLNs from the intestines. To test this, we administered either VEGFR-2 blocking antibody (DC101) or isotype control every 24 hours for 72 hours, then harvested the gLNs. Inverse to what was observed when the lymphatic tight junctions were more zipper-like, shifting the lymphatic tight junctions to be more button-like lead to a slight decrease in total CD45+ cells within the small intestinal draining lymph nodes (Fig. S1J). Additionally, lymphatic buttoning had the most significant impact on cDC1's migrating to the distal gLNs, while total CD11c+ DC's and cDC2's remained unaffected (Fig. S1K). However, since our approaches likely affected the lymphatics of the entire body, including the ones in the LNs, and the VEGFR-2 antibody in addition also affected the blood endothelial junctions our results cannot definitively prove that lacteal tight junction composition dictates migratory immune cell population numbers in the draining LNs.

Taken together, these data suggest that lymphatic tight junction composition has the potential to modulate dendritic cell populations in gLNs, even if the main site responsible was not dissected in this thesis.

3.3 Helminth infections impact duodenum lacteal morphology and absorptive function

Since the duodenum and its associated lymphatics possess the highest lipid uptake potential, we asked if infections at this site might impair this lymphatic function. Infections have previously been observed to modify lymphatic function, where an acute viral skin infection induced rapid dermal lymphatic zippering (Churchill et al., 2022b) or bacterial lung infection led to lymphangiogenesis-associated zippering (Yao et al., 2012b). In the gastrointestinal tract the bacterium *Y. pseudotuberculosis* infectS and kill LECs, leading to leakage of migratory cells into the mesentery (Fonseca et al., 2015). We therefore infected adult mice with pathogens that possess either exclusive or also duodenal tropism and elicit strong immune responses in the draining LNs. These include helminths (*S. venezuelensis*, *N. brasiliensis*, *H. polygyrus*), a reovirus (T1L) and a bacterium *Y. pseudotuberculosis*. At the respective heights of infection, we first analyzed the duodenum lacteal morphology and tight junction organization. Each helminth infection led to an increase in the duodenal lacteal to villus length ratio and lacteal surface area compared to non-infected controls (Fig. 3 A-F). Lacteal LEC tight junctions switched to a mixed/zipper-like conformation (Fig. 3 G-I). By contrast, T1L and *Y. pseudotuberculosis* did not change any of these parameters (Fig. S2 A-J).

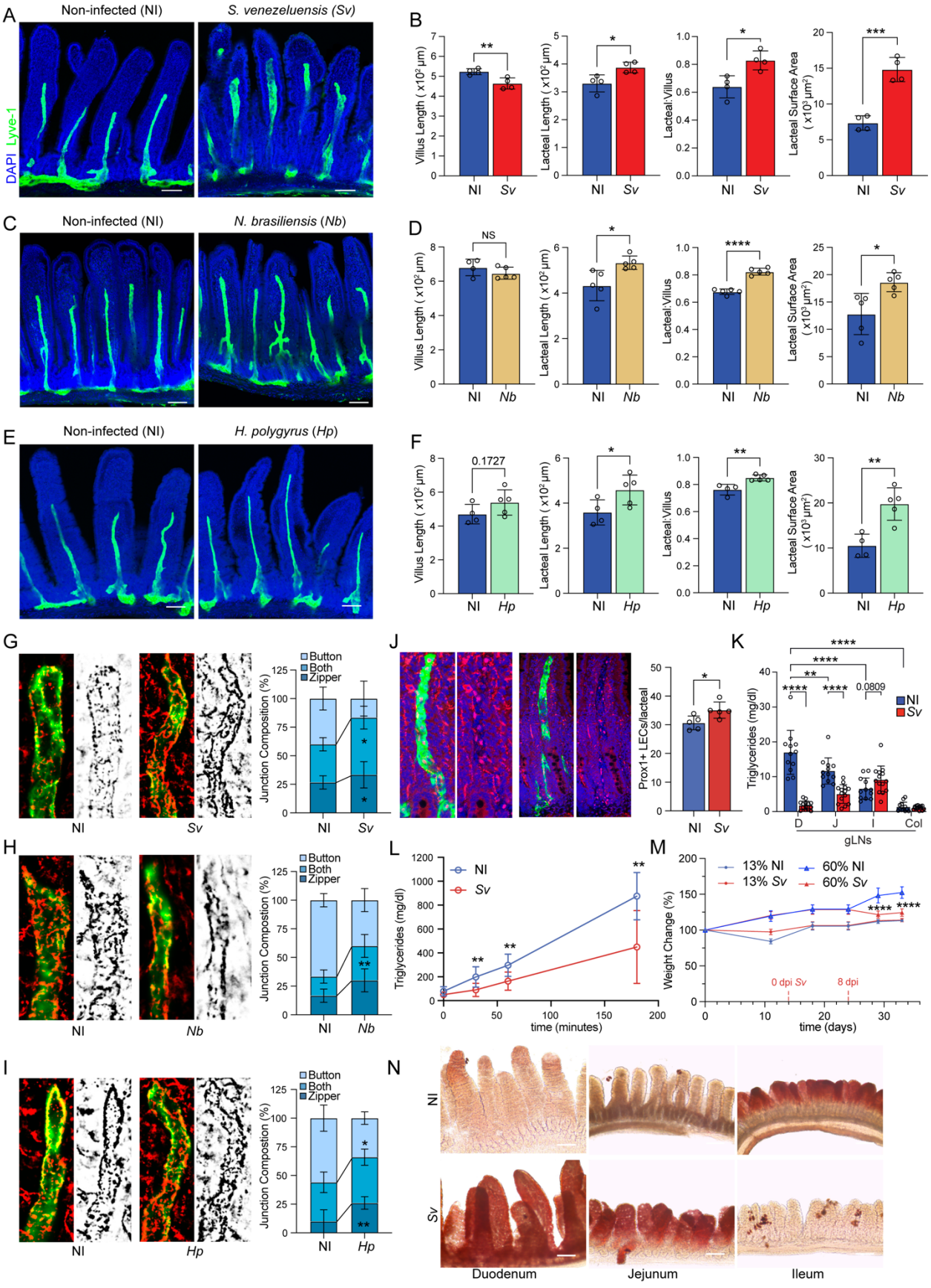
A
Non-infected (NI)
S. venezeluensis (Sv)
DAPI Lyve-1
B
Villus Length (x10² µm)
Lacteal Length (x10² µm)
Lacteal:Villus
Lacteal Surface Area (x10³ µm²)
NI Sv
C
Non-infected (NI)
N. brasiliensis (Nb)
D
NS
NI Nb
E
Non-infected (NI)
H. polygyrus (Hp)
F
0.1727
NI Hp
G
Button
Both
Zipper
Junction Composition (%)
NI Sv
H
NI Nb
I
NI Hp
J
Prox1+ LECs/lacteal
NI Sv
K
Triglycerides (mg/dl)
NI
Sv
D J I Col
gLNs
L
Triglycerides (mg/dl)
NI
Sv
time (minutes)
M
13% NI
13% Sv
60% NI
60% Sv
Weight Change (%)
0 dpi Sv
8 dpi
time (days)
N
NI
Sv
Duodenum
Jejunum
Ileum

Figure 3. Helminth infections impact duodenum lacteal morphology and function.
(A-F) Immunofluorescence images (A, C, and E) and comparisons of duodenum villi and LYVE-1+ lacteals in Non-infected (NI) versus helminth infected mice: villus length, lacteal length, lacteal to villus length ratio, and lacteal surface area 8 days post infection (dpi) with *S. venezeluensis* (Sv) (B), 8 dpi with *N. brasiliensis* (Nb) (D), and 14 dpi with *H. polgyrus* (Hp) (F) (*n* = 3-4). Data representative of one to two independent experiments. **(G-I)** Representative images and characterization of VE-cadherin+ LEC junctions of LYVE-1+ lacteals in NI versus helminth infected mice. Quantification of SI lacteal tight-junction organization with primarily button-like, zipper-like, or a combination of both tight junction formations throughout the length of the duodenal lacteal in NI mice versus mice infected with Sv 8 days (G), Nb 8 days (H), and Hp 14 days (I) earlier. (*n* = 3-4), data representative of two independent experiments (B), data representative of one experiment (D,F). **(J)** Immunofluorescence images and quantification of DAPI+ Prox1+ nuclei within LYVE-1+ duodenum lacteals in NI versus mice infected with *Sv* 8 dpi. (*n* = 5) Data representative of one experiment. **(K and L)** Gut draining lymph node (K) and plasma triglyceride concentration over time (L) of NI mice versus mice infected with *Sv* 8 dpi. (*n* = 5 mice per group), data pooled from two independent experiments. **(M)** Representative images of Oil red O staining of intestinal villi 3 hours after olive oil challenge of NI mice versus mice infected with Sv 8 dpi. (N) Growth curves of NI mice versus mice infected with Sv 2 weeks after starting a 60% high-fat diet or a 13% normal chow diet. (*n* = 5), data representative of one experiment. D/Duo=duodenum, J/Jej=Jejunum, I/Ile=ileum, C/Col=colon. *Sv=S. venezuelensis*, *Nb=N. brasilienesis*, *Hp=H. polygyrus*. Error bars indicate mean ± SD and *P<0.05, **P<0.01, *** P< 0.001, **** P< 0.001 by two-tailed student's t-test (comparison between conditions (B, D, F, J, K, L, and N) at single locations or time points, two-way ANOVA (multiple comparisons between conditions within groups) (G-I). Scale bar: 100 μm (A, C, and E), 25 μm (G-H), 125 μm (M).

To further investigate the impact of helminth infections on lymphatics, we chose *S. venezuelensis* for further analyses as it clears after 12-14 days, allowing for studying post-infection impacts, and maintains a strict trophism to the duodenum. The increase in zipper-like duodenal lacteal tight junctions was independently confirmed with the automated tight junction measurements, showing that the helminth infection led to an increase in the sum of tight junction length (Fig. S2K-M). Prox1 staining of the duodenum showed an increase in the number of counted Prox1+ nuclei per LYVE-1+ lacteal upon *S. venezuelensis* (Fig. 3J), suggesting that lymphangiogenesis rather than an increase in cell spread underlie the increase in lacteal length and surface area upon helminth infection. When examining the whole gut, *S. venezuelensis* infection grossly impacted the duodenal tissue, whereby a slight elongation of the duodenum, significant

increase in circumference of the intestinal ring and a decrease in the number of villi per intestinal ring compared to non-infected control mice was observed (Fig. S2N). Lacteal scoring of the jejunum and ileum of *S. venezuelensis* infected mice indicated the impacts of the helminth infection on the lymphatics were largely confined to the duodenum, the site of infection (Fig. S2O-T).

Based on the altered tight junction composition upon *S. venezuelensis* infection, we speculated that dietary lipid uptake by the lacteals might be compromised consequently. To test this, we orally challenged mice with a bolus of olive oil at the height of infection. Following *S. venezuelensis* infection, triglyceride content in the duodenal draining LNs was drastically decreased, it additionally decreased in the jejunal draining LN but slightly elevated in the ileal draining LN compared to non-infected mice (Fig. 3K). We attribute the jejunal LN effect to the proximal jejunum which may be impacted by local *S. venezuelensis* infection, despite a lack of active helminth infection at the site. Correspondingly, plasma triglyceride content was decreased in *S. venezuelensis* infected mice in the 3 hours ensuing the oil gavage (Fig. 3L). Lipids accumulated in the duodenum but were more cleared in the ileum compared to non-infected mice (Fig. 3N). The middle jejunal tissue 3 hours post-gavage also retained more lipids in infected mice, possibly due to saturation of lipid uptake in the duodenum but unlikely due to an impact of the worm on the lymphatics here (Fig. S2O-T). These results phenocopy observations made in Vegfr3$^{\Delta Prox1}$ mice, further supporting a relationship between tight junction organization and lipid uptake upon helminth infection. We next asked what the long-term consequence of decreased lymphatic lipid uptake capacity is on body weight by placing mice on a high fat diet or nutritionally matched low fat diet (60% vs 13% calories from fat) and infecting them with *S. venezuelensis* two weeks after the start on these diets. No difference in weight gain was observed in mice on the 13% diet, but on the 60% diet, mice infected with *S.venezuelensis* gained less weight day 8-18 post

infection compared to the non-infected control animals (Fig. 3M). We did not monitor the weight beyond this time window as *S.venezuelensis* is cleared from the intestine day 12-14 post infection and lacteal morphology and serum lipid uptake started to normalize around day 16 post infection (Fig. S2U, V).

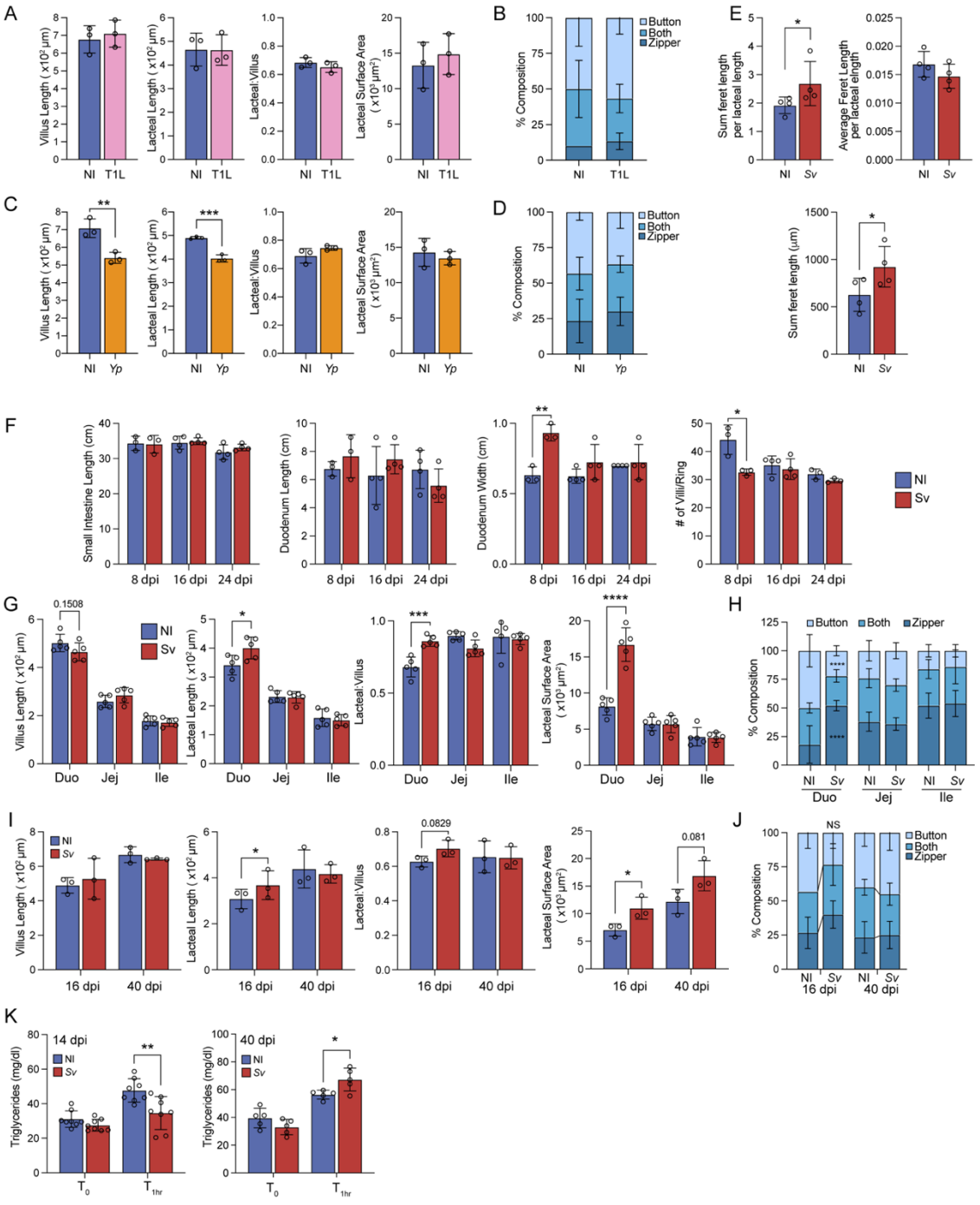

Figure S2. Helminth infections impact duodenum lacteal morphology and function.
A-D. Duodenal villus length, lacteal length, lacteal to villus length ratio, and lacteal surface area (A, C) or quantification of duodenal lacteal tight-junction organization with primarily button-like, zipper-like, or a combination of both tight junction formations throughout the length of the duodenal lacteal (B, D) of mice infected with *Y. pseudotuberculosis* (*Yp*, A, B) or reovirus T1L (C, D) 48h prior to sacrifice (n = 3). (**E**) Sum feret/lacteal length, average feret length/lacteal length and sum feret length per lacteal of mice infected with *S. venezuelensis* (*Sv*) or not (NI) 8 days earlier (n = 4). (**F**) Small intestinal length and duodenal length, circumference, and villi per diameter of mice *S. venezuelensis* (*Sv*) or not (NI) 8,16 or 24 days earlier (n = 4). (**G, H**) Villus length, lacteal length, lacteal to villus length ratio, and lacteal surface area (G) and quantification of SI lacteal tight-junction organization (H) with primarily button-like, zipper-like, or a combination of both tight-junction formations throughout the length of the lacteal along the small intestine of mice infected with *S. venezuelensis* (*Sv*) or not (NI) 8 days earlier (n = 5). (**I**, **J**) Duodenal villus length, lacteal length, lacteal to villus length ratio, and lacteal surface area (I) and quantification of duodenal lacteal tight-junction organization (J) with primarily button-like, zipper-like, or a combination of both tight-junction formations throughout the length of the lacteal along the small intestine of mice infected with *S. venezuelensis* (*Sv*) or not (NI) 16 or 40 days earlier (n = 3). (**K**) Serum triglyceride concentration of mice infected with *S. venezuelensis* (*Sv*) or not (NI) 14 or 40 days earlier before and 1h after gavage with olive oil (n = 7 at 14 days, n = 4 at 40 days). Error bars indicate mean ± SD and *P<0.05, **P<0.01, *** P< 0.001, **** P< 0.001 by two-tailed student's t-test. D/Duo=duodenum, J/Jej=Jejunum, I/Ile=ileum, C/Col=colon.

Taken together, these observations demonstrate that helminth infections alter the structure of duodenal lacteals and compromise lymphatic lipid uptake.

3.4 LECs along the intestine are transcriptionally distinct and duodenal LECs change their transcriptional profile in response to helminth infection

To gain more comprehensive insights into both the regional differences of lymphatics along the intestine and the impact of helminth infection, we performed bulk RNA sequencing (RNAseq) of LECs isolated from the duodenum, jejunum, ileum and colon from non-infected mice or mice infected with *S.venezuelensis* 8 days earlier. In order to understand which helminth-induced impacts are specific to LECs we expanded this comparison to blood endothelial cells (BECs). $Flt4^{CreERT2}$ x $Rosa26^{-lsl\text{-}Tomato}$ mice (Gardenier et al., 2016; Madisen et al., 2010), in which upon

tamoxifen treatment LECs and off-target BECs express red fluorescent tdTomato and enabled us to monitor our digestion under a benchtop fluorescent microscope and quench the reaction the moment we obtained a single cell suspension of red cells (Fig. S3A, B), which we then sorted as BECs and LECs (Fig. S3C). BECs and LECs segregated on principle component (PC) analysis of all samples by PC1, while PC2 accounted for the duodenal BECs and LECs upon *S.venezuelensis* (Fig. 4A). We verified our BECs and LECs had minimal contamination by analysis of marker genes, which showed the expected enrichment of *Prox1* and *Pdpn* in LECs and *Cd34* and *Flt1* in BECs Fig. S3D-G); contamination from gut epithelial cells was also minimal determined by *Vil1* expression (Fig. S3H).

We started by analyzing the LECs from non-infected mice, to determine whether LECs are transcriptionally distinct dependent on the segment they drain. As expected, the colonic LECs separated from the small intestinal LECs by PCA (Fig. 4B). Within the small intestinal LECs, the duodenum was the most distinct from the segment LECs based on the number and nature of differentially expressed genes (DEGs). Focusing on the comparison of DEGs between LECs from non-infected duodenum versus ileum revealed that more genes were enriched in the ileum than duodenum (Fig. 4C). Further, by both gene set enrichment analysis (GSEA) (Fig. 4C) and overrepresentation Gene ontology pathway analysis (Fig. 4D) these genes fell into five major biological pathway categories: Duodenal LECs had a signature indicative of *immune involvement*, including antigen presentation, *lipid metabolism*, and *cell adhesion and motility* mechanisms, ileal LECs one of *active transcription, cell division,* ***and*** *bile acid handling*, and LECs in duodenum and ileum where involved in *environmental sensing*, albeit different pathways (Fig. 4C, D, Fig. S3I). Additionally, ileal LECs also featured a bile acid response program (Fig. 4D), correlating with the bile acid re-uptake function of the ileum. Target-based analysis of the transcription factors

potentially responsible for this DEG list revealed an intertwined network (Fig. 4E), of which two groups, the SOX9-VDR-MYB and FLI1-MAFK-IRF3-JUN-SREBF1-CREB1 networks accounted for more than two thirds of the DEGs (Fig. S3J, K). Finally, when comparing the LECs across all segments and conditions collected based on the DEGs between non-infected duodenum and ileum on a heat map (Fig. 4F) it became apparent that these DEGs show an intermediate level of expression in the jejunum, suggesting a regulation gradient along the small intestine, while the colon started to resemble the ileum.

Intriguingly, upon *S.venezuelensis* infection, some gene clusters in the duodenal LECs looked more similar to the ileal patterns (bracketed in Fig. 4F). We then more closely analyzed the DEGs between duodenal LECs from mice infected with *S.venezuelensis* or not. Indeed, of the roughly 3300 genes upregulated in LECs from infected mice, about 500 overlapped with the genes found enriched in ileal LECs compared to duodenal LECs from non-infected mice (Fig. 4G). These primarily included genes enriched in the proliferation and development pathways, suggesting that duodenal LECs acquired the ileal "regenerative" LEC program upon *S.venezuelensis*. Plotting the DEGs on a heatmap showed that these were not impacted by *S.venezuelensis* in any other gut segment (Fig. 4H), and a comparison of the DEGs enriched in duodenal LECs and BECs upon *S.venezuelensis* showed that although a third of all LEC genes were also regulated in BECs, LECs were more affected by the worm than BECs (Fig. 4I). Jejunal LECs were also somewhat affected by SV (400 DEGs (Fig. 4J), of which about half made the jejunal LECs resemble duodenal LECs (Fig. 4J), predominantly in their immunity-related nature. Ileal LEC gene expression was not affected by SV. Many DEGs between duodenal LECs from non-infected control versus *S.venezuelensis* infected mice fell into similar pathways as those when characterizing duodenal versus ileal LECs (Fig. 4K, L, Fig. S3I). Notably cell adhesion and cell division were major

categories into which DEG upregulated in duodenal LECs upon *S.venezuelensis* fell, while immune signatures and lipid metabolism were de-enriched under this condition. The transcription factor network (Fig. 4M, Fig. S3K) predicted to regulate the DEGs was dominated by TFs described to be involved in activating transcription and cell division, and also included TFs known to promote lymphangiogenesis such as *Sox18* and *Jun* (François et al., 2008; Fu et al., 2023).

In sum, LECs along the intestine differ transcriptionally, with the major duodenal signatures being an enrichment for immune regulation and lipid sensing; *S.venezuelensis* infection compromises these duodenal LEC functions and instead imposes a proliferative program similar to that of ileal LECs.

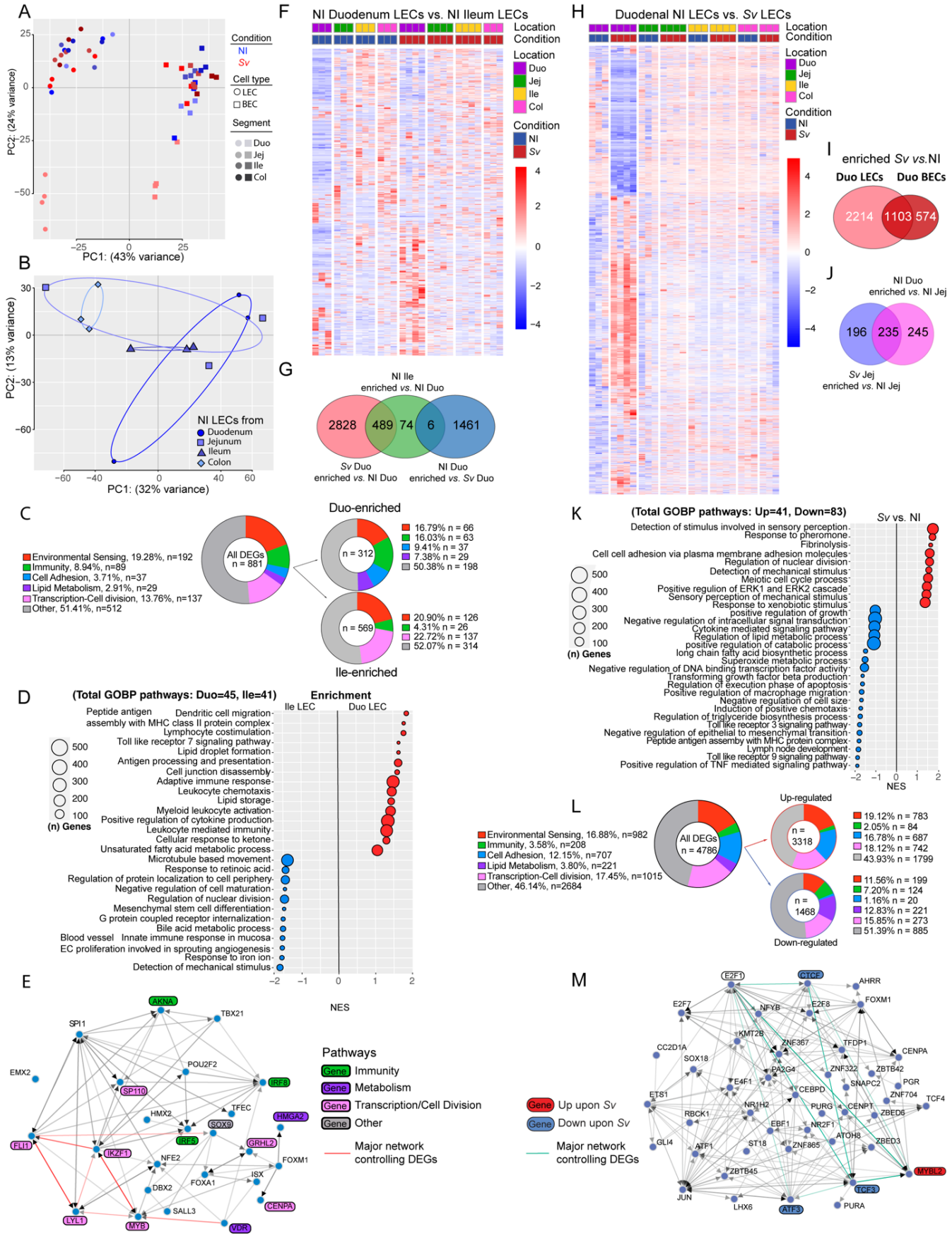
A
PC2: (24% variance)
PC1: (43% variance)
Condition
NI
Sv
Cell type
LEC
BEC
Segment
Duo
Jej
Ile
Col
B
PC2: (13% variance)
PC1: (32% variance)
NI LECs from
Duodenum
Jejunum
Ileum
Colon
C
Environmental Sensing, 19.28%, n=192
Immunity, 8.94%, n=89
Cell Adhesion, 3.71%, n=37
Lipid Metabolism, 2.91%, n=29
Transcription-Cell division, 13.76%, n=137
Other, 51.41%, n=512
All DEGs
n = 881
Duo-enriched
n = 312
16.79% n = 66
16.03% n = 63
9.41% n = 37
7.38% n = 29
50.38% n = 198
n = 569
20.90% n = 126
4.31% n = 26
22.72% n = 137
52.07% n = 314
Ile-enriched
D
(Total GOBP pathways: Duo=45, Ile=41)
Enrichment
Ile LEC
Duo LEC
Peptide antigen assembly with MHC class II protein complex
Dendritic cell migration
Lymphocyte costimulation
Toll like receptor 7 signaling pathway
Lipid droplet formation
Antigen processing and presentation
Cell junction disassembly
Adaptive immune response
Leukocyte chemotaxis
Lipid storage
Myeloid leukocyte activation
Positive regulation of cytokine production
Leukocyte mediated immunity
Cellular response to ketone
Unsaturated fatty acid metabolic process
Microtubule based movement
Response to retinoic acid
Regulation of protein localization to cell periphery
Negative regulation of cell maturation
Regulation of nuclear division
Mesenchymal stem cell differentiation
G protein coupled receptor internalization
Bile acid metabolic process
Blood vessel Innate immune response in mucosa
EC proliferation involved in sprouting angiogenesis
Response to iron ion
Detection of mechanical stimulus
(n) Genes
NES
E
AKNA
TBX21
SPI1
EMX2
POU2F2
IRF8
SP110
TFEC
HMX2
HMGA2
SOX6
IRF5
GRHL2
FLI1
IKZF1
NFE2
FOXM1
ISX
FOXA1
DBX2
CENPA
SALL3
LYL1
MYB
VDR
Pathways
Gene Immunity
Gene Metabolism
Gene Transcription/Cell Division
Gene Other
Major network controlling DEGs
F
NI Duodenum LECs vs. NI Ileum LECs
Location
Condition
Duo
Jej
Ile
Col
NI
Sv
G
NI Ile enriched vs. NI Duo
2828
489
74
6
1461
Sv Duo enriched vs. NI Duo
NI Duo enriched vs. Sv Duo
H
Duodenal NI LECs vs. Sv LECs
I
enriched Sv vs.NI
Duo LECs
Duo BECs
2214
1103
574
J
NI Duo enriched vs. NI Jej
196
235
245
Sv Jej enriched vs. NI Jej
K
(Total GOBP pathways: Up=41, Down=83)
Sv vs. NI
Detection of stimulus involved in sensory perception
Response to pheromone
Fibrinolysis
Cell cell adhesion via plasma membrane adhesion molecules
Regulation of nuclear division
Detection of mechanical stimulus
Meiotic cell cycle process
Positive regulon of ERK1 and ERK2 cascade
Sensory perception of mechanical stimulus
Response to xenobiotic stimulus
positive regulation of growth
Negative regulation of intracellular signal transduction
Cytokine mediated signaling pathway
Regulation of lipid metabolic process
positive regulation of catabolic process
long chain fatty acid biosynthetic process
Superoxide metabolic process
Negative regulation of DNA binding transcription factor activity
Transforming growth factor beta production
Regulation of execution phase of apoptosis
Positive regulation of macrophage migration
Negative regulation of cell size
Induction of positive chemotaxis
Regulation of triglyceride biosynthesis process
Toll like receptor 3 signaling pathway
Negative regulation of epithelial to mesenchymal transition
Peptide antigen assembly with MHC protein complex
Lymph node development
Toll like receptor 9 signaling pathway
Positive regulation of TNF mediated signaling pathway
(n) Genes
NES
L
Environmental Sensing, 16.88%, n=982
Immunity, 3.58%, n=208
Cell Adhesion, 12.15%, n=707
Lipid Metabolism, 3.80%, n=221
Transcription-Cell division, 17.45%, n=1015
Other, 46.14%, n=2684
All DEGs
n = 4786
Up-regulated
n = 3318
19.12% n = 783
2.05% n = 84
16.78% n = 687
18.12% n = 742
43.93% n = 1799
n = 1468
11.56% n = 199
7.20% n = 124
1.16% n = 20
12.83% n = 221
15.85% n = 273
51.39% n = 885
Down-regulated
M
E2F1
CTCF
AHRR
E2F7
NFYB
E2F8
FOXM1
KMT2B
ZNF367
TFDP1
CENPA
CC2D1A
SOX18
PA2G4
ZNF322
ZBTB42
E4F1
SNAPC2
PGR
CEBPD
ZNF704
TCF4
ETS1
PURG
CENPT
ZBED6
RBCK1
NR1H2
EBF1
NR2F1
ATOH8
ZBED3
GLI4
ATF1
ST18
ZNF865
ZBTB45
MYBL2
TCF3
JUN
LHX6
ATF3
PURA
Gene Up upon Sv
Gene Down upon Sv
Major network controlling DEGs

Figure 4. Duodenum lymphatics are transcriptionally distinct and respond to helminth infection.

(A, B) Unsupervised principle component analysis of Bulk RNA sequencing (RNAseq) of sorted lymphatic endothelial cells (LECs) and blood endothelial cells (BECs) along the small intestine and proximal colon from NI mice and mice infected with *S. venezuelensis* (*Sv*) 8 days prior (A), or sorted LECs from NI mice (B). **(C-E)** Pie charts depicting the number of genes contributing to general pathways within Gene ontology biological process (GOBP) pathways of DEGs (C), curated list of gene ontology biological pathway (GOBP) identified by gene set enrichment analysis (GSEA) of DEGs (D), and predicted transcription factor network governing DEGs (E) enriched in LECs from non-infected ileum or duodenum. TF pathway involvement is color coded in accordance with (C). Major transcription factor interactions regulating DEGs are highlighted. (**F**) Heat map of DEGs between LECs from non-infected duodenum and ileum, shown along the intestine and versus upon infection with *Sv* 8 days prior. (**G**) Venn diagram comparing genes upregulated in duodenal LECs upon *Sv* versus LECs from non-infected mice, genes enriched in ileal LECs compared to duodenal LECs of non-infected mice, and genes enriched in duodenal LECs from non-infected mice compared to from mice *Sv* 8 days prior. **(H)** Heat map of DEGs between duodenal LECs from non-infected mice versus mice infected with *Sv* 8 days prior, shown along the intestine. (**I**) Venn diagram comparing DEGs in LECs versus BECs sorted from *Sv* - infected duodenum. (**J**) Venn diagram between genes upregulated in jejunal LECs upon *Sv* infection compared to non-infected mice, and genes enriched in duodenal compared to jejunal LECs in non-infected mice. (**K-M**) Curated list of GSEA of GOBP into which DEGs (K) and pie charts depicting the number of genes contributing to general pathways within GOBP pathways (L), and predicted transcription factor network governing DEGs (M) between LECs from non-infected mice and mice infected with *Sv* 8 days prior. TF pathway involvement is color coded in accordance with (L). Major transcription factor interactions regulating DEGs are highlighted. Duo=duodenum, Jej=Jejunum, Ile=ileum, Col=colon.

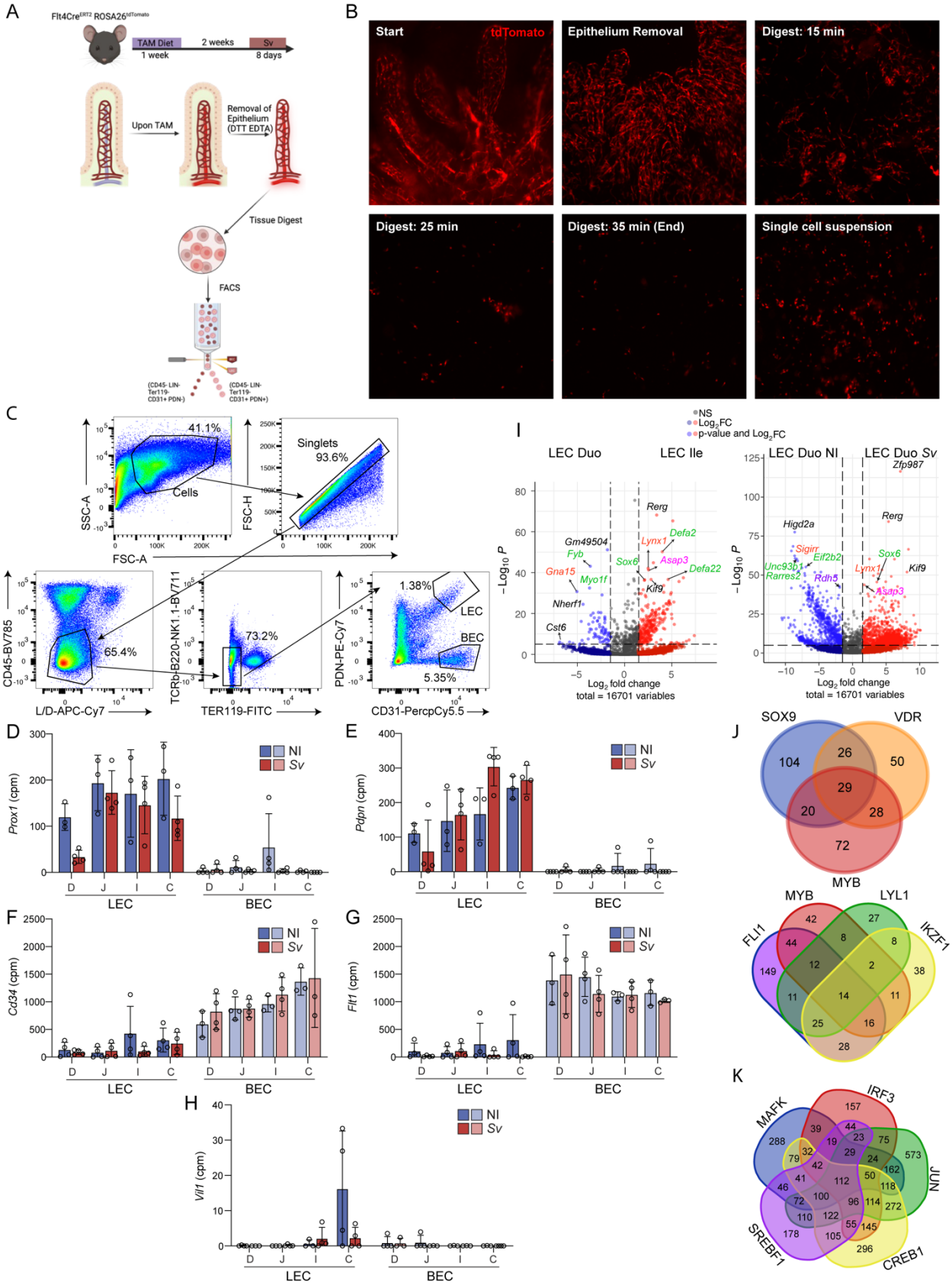
A
Flt4Cre^ERT2 ROSA26^tdTomato
TAM Diet
1 week
2 weeks
Sv
8 days
Upon TAM
Removal of Epithelium (DTT EDTA)
Tissue Digest
FACS
(CD45- LIN- Ter119- CD31+ PDN-)
(CD45- LIN- Ter119- CD31+ PDN+)
B
Start
tdTomato
Epithelium Removal
Digest: 15 min
Digest: 25 min
Digest: 35 min (End)
Single cell suspension
C
41.1%
Cells
SSC-A
FSC-A
Singlets
93.6%
FSC-H
CD45-BV785
65.4%
L/D-APC-Cy7
TCRb-B220-NK1.1-BV711
73.2%
TER119-FITC
PDN-PE-Cy7
1.38%
LEC
BEC
5.35%
CD31-PercpCy5.5
I
NS
Log2FC
p-value and Log2FC
LEC Duo
LEC IIe
LEC Duo NI
LEC Duo Sv
Rerg
Defa2
Lynx1
Asap3
Defa22
Sox6
Gm49504
Fyb
Gna15
Myo1f
Kif9
Nherf1
Cst6
Higd2a
Sigirr
Eif2b2
Unc93b1
Rarres2
Rdh5
Zfp987
−Log10 P
Log2 fold change
total = 16701 variables
D
Prox1 (cpm)
NI
Sv
LEC
BEC
E
Pdpn (cpm)
F
Cd34 (cpm)
G
Flt1 (cpm)
H
Vil1 (cpm)
J
SOX9
VDR
MYB
104
26
50
29
20
28
72
LYL1
FLI1
IKZF1
42
27
44
8
8
149
12
2
38
11
14
11
25
16
28
K
MAFK
IRF3
JUN
SREBF1
CREB1
157
39
44
288
19
23
75
573
79
32
29
24
42
162
41
50
112
118
46
100
72
96
114
272
110
122
55
145
178
105
296

Figure S3. Duodenal lymphatics are transcriptionally distinct from other gut segments at homeostasis and respond to helminth infection.
(**A**) Schematic of LEC and BEC sorting strategy based on *Vegfr3*(FLT-4)-Cre mediated expression of Tomato. (**B**) Immunofluorescent images of digestion state time course of intestine based on Tomato+ cells. At start Tomato+ cells form a lymphatic vessel at center of each villus and a submucosal blood vessel network. At 15 min some vessels are still intact, by 35 minutes a single Tomato+ cell suspension is obtained. (**C**) Gating scheme for sorting BECs and LECs. (**D-H**) CPM for *Prox1* (D), *Pdpn* (E), *Cd34* (F), *Flt1*(G) and *Vil* (H) in sorted LECs and BECs (n = 4). (**I**) Volcano plots of DEGs comparing LECs from non-infected Duo and ILE (left) or non-infected or *S. venezuelensis*-infected (right). Most highly regulated genes called out by gene symbol. Gene symbols in green=immunity-related, orange=environmental sensing, magenta=cell cycle/transcription, purple=metabolism. (**J**) Venn diagrams of number of genes regulated by indicated transcription factors accounting for DEGs between non-infected Duo and ILE. (**K**) Venn diagram of number of genes regulated by indicated transcription factors accounting for DEGs between non-infected or *S. venezuelensis*-infected DUO. D/Duo=duodenum, J=Jejunum, I/Ile=ileum, C=colon.

3.5 The mucosal signatures along the small intestine match the functional profiles of LECs and helminth infection selectively impacts the duodenal mucosa

The various regional properties of the lymphatics we uncovered could in theory be due to cell intrinsic regional patterning or a response to the environment in which they reside. To gauge the extent to which the LEC profiles we observed reflected an adaptation to the local milieu both at homeostasis and upon *S. venezuelensis* infection we performed RNA sequencing of the duodenal, jejunal and ileal mucosa. We reasoned that, to the extent that the regulation was reflected on the transcriptional level, this approach would allow us to holistically capture the environment in which LECs sit. We performed this experiment at 8 days but also 5 days post infection, to investigate the potentially direct regulation of LECs by recently matured worms (Maeda et al., 2019) at a time point at which the host has yet to mount an anti-helminth type-2 immune response in the gut. Unbiased clustering of all samples (Fig. 5A) showed that the duodenal, jejunal and ileal mucosa at homeostasis were distinct (PC1), with the genes falling into similar pathways as found

enriched in the LECs from the corresponding regions, with vascular development, lipid metabolism, immune responses, cell adhesion enriched in the duodenum, and cell cycling in the ileum (Fig. S4A). These signatures were unlikely to originate from LECs or BECs, which are part of the mucosa, as their contribution to the RNAseq reads was marginal compared to e.g. that of the epithelium, based on cpm (Fig. S4B). Rather, this parallel suggests that the LECs are transcriptionally tuned to the local mucosal milieu. The duodenal samples upon *S.venezuelensis* separated day 8 but not day 5 post infection from the non-infected mucosa along PC2 (Fig. 5A), suggesting the change in duodenal LECs upon helminth infection is not mediated directly by worm-derived molecules. As expected, the ileum was unaffected by *S.venezuelensis*. The jejunum on day 8 became more closely related to the non-infected duodenal mucosa (Fig. 5A), and this was due a new similarity in immune-related genes, akin to the observation in the LECs, as well as cell cycle genes. These observations were also evident in the heatmap based on the DEGs of non-infected versus *S.venezuelensis* infected duodenal mucosa 8 days post infection (Fig. 5B, see column 6 resembling columns 1 and 2, and column 7-9 being similar). GSEA and an analysis of the number of DEGs within the GO biological processes pathways into which these DEGs fell (Fig. 5 C, D) showed that the expected pathways part of the classical type 2 response against helminths (inflammatory pathways (Fig. S4 C, D), antimicrobial responses and wound healing) were enriched, as were pathways related to vascular development, while lipid/retinoic acid metabolic process pathways were downregulated (Fig. S4E). When comparing the pathway analyses between the duodenal infected mucosa and LECs from the infected tissue, several signatures in the GSEA were congruent, notably cell migration, cell proliferation and lipid metabolism (compare Fig. 4K and Fig. 5C).

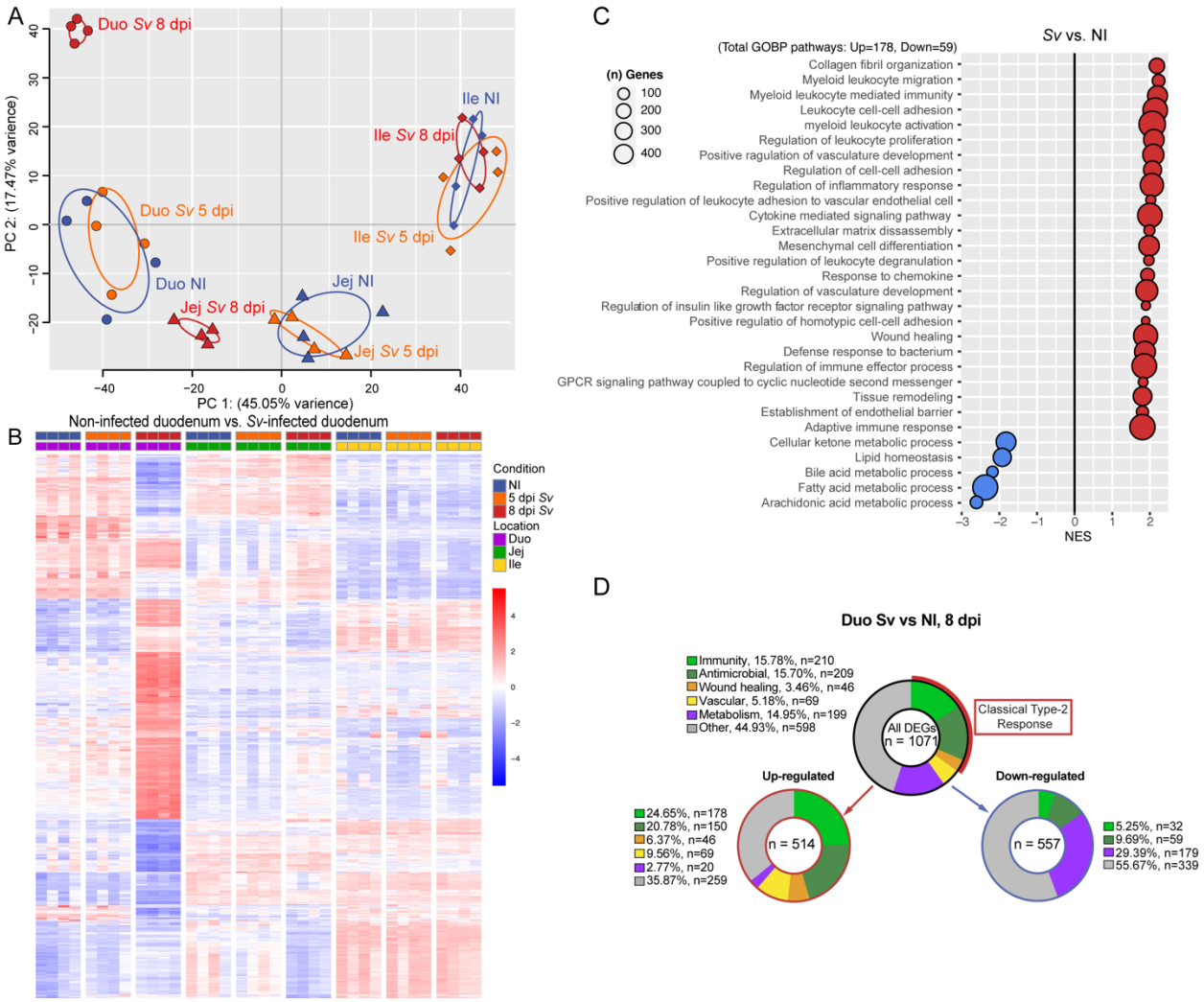

Figure 5. The mucosal signatures along the small intestine match the functional profiles of LECs and helminth infection selectively impacts the duodenal mucosa in its metabolic, vascular, antimicrobial, and type 2 immune responses.

(A-D) Bulk RNA sequencing (RNAseq) of mucosal scrapes (without the serosa) along the small intestine from NI mice versus mice infected with *S. venezuelensis* (*Sv*), 5 and 8 days post infection (dpi). (A) Unsupervised principle component analysis of NI mice and mice infected with *Sv*, 5 and 8 dpi based on counts per million (cpm). (B) Expression of differentially expressed genes comparing the duodenum of mice infected with *Sv* 8 dpi versus the NI duodenum. (C) Curated list of gene ontology biological pathway (GOBP) identified by Gene set enrichment analysis (GSEA) of DEGs between Duodenum infected with *Sv* 8 dpi versus NI duodenum. (D) Pie charts depicting the number of genes contributing to general pathways within GOBP pathways: All DEGs, upregulated-DEGs, and downregulated-DEG. Data representative of one experiment (16, 24 dpi). Data representative of two experiments (8 dpi). Error bars indicate mean ± SD and *P<0.05, **P<0.01, *** P< 0.001, **** P< 0.001 by two-tailed student's t-test. D/Duo=duodenum, J/Jej=Jejunum, I/Ile=ileum, C/Col=colon.

Overall, these data strongly support the notion that the LEC profiles in the small intestine are imprinted by the immunological, metabolic and mitogenic milieu and locally adapt as the environment changes both along the gastrointestinal tract at homeostasis and upon worm infection.

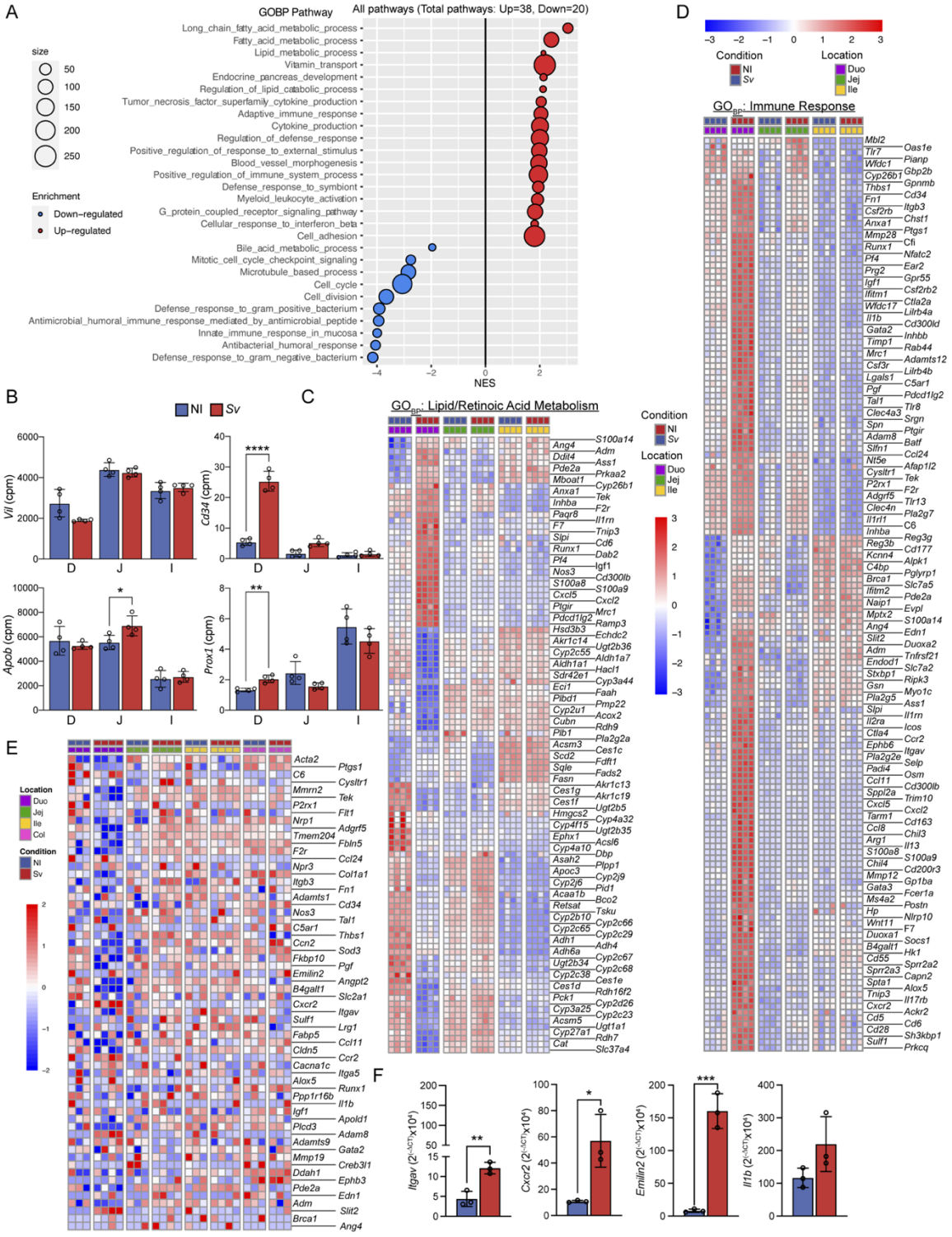

Figure S4. The mucosal signatures along the small intestine match the functional profiles of LECs and helminth infection selectively impacts the duodenal mucosa in its metabolic, vascular, antimicrobial, and type 2 immune responses.
(**A**) Curated list of gene ontology biological pathway (GOBP) identified by gene set enrichment analysis (GSEA) of DEGs between mucosal scrape of duodenum versus ileum of non-infected mice. (**B**) Cpm of epithelial genes (*Vil*, *Apob*), a LEC marker (*Prox1*) and BEC marker (*Cd34*) in mucosal scrapes along the small intestine of non-infected mice or mice infected with *S. venezuelensis* (*Sv*) 8 days earlier. (**C**, **D**) Heat maps of DEGs between duodenal mucosal scrapes of non-infected mice or mice infected with *Sv* 8 days earlier belonging to the lipid/retinol metabolism (C) or immunity-related (D) Gene Ontology biological processes (GOBP) as measured by RNAseq of the mucosal scrapes along the small intestine. (**E**) Heat map of DEGs between duodenal mucosal scrapes of non-infected mice or mice infected with *Sv* 8 days prior, belonging to vascular development-regulatory pathway genes as identified by GOBP pathway analysis as measured by RNAseq of the LECS and BECs along the intestine. (**F**) QPCR of some vascular development genes identified as DEGs in mucosal scrapes in whole duodenum of non-infected mice or mice infected with *Sv* 8 days earlier (n = 3). D/Duo=duodenum, J/Jej=Jejunum, I/Ile=ileum, C=colon. Error bars indicate mean ± SD and *P<0.05, **P<0.01, *** P< 0.001, **** P< 0.001 by two-tailed student's t-test. D/Duo=duodenum, J/Jej=Jejunum, I/Ile=ileum, C/Col=colon.

3.6 LEC & BEC VEGFR signaling pathway expression correlates with increased lacteal zippering along the small intestine but not *S. venezuelensis* infection

We sought to elucidate the molecular mechanisms that may underlie the lymphatic permeability and putative regeneration gradient along the small intestine and how *S.venezuelensis* infection reverses them. Of note, lymphatic tight junction organization and regeneration partially intersect on the VEGF receptor signaling pathways, and lymphangiogenesis is associated with a zipper-like tight junction conformation that is then reconfigured by the local milieu (Suh et al., 2019; Tammela et al., 2007; Yao et al., 2012b). While tight junction organization can be influenced indirectly through other molecules mediators that influence VEGFs and their receptors, it is thought that ultimately all converge onto modulating VEGF signaling ((Olsson et al., 2006; Simons et al., 2016)). Lymphangiogenesis inducing signals also often modulate the VEGF pathway, but independent pathways exist (Tammela & Alitalo, 2010; Zheng et al., 2014a). The VEGF ligand

family consists of four members, VEGF-A,B,C, and D. They bind the receptors VEGFR-1,2,3 (products of the genes *Flt1*, *Kdr* and *Flt4*, respectively) with varying affinity, which can lead to crosstalk and modulate the signal strength. Adding further to complexity, expression of receptors on nearby BECs can lead to competition for the ligands (Zhang et al., 2020). On LECs, zipper-like tight junctions are thought to be primarily governed by the net availability of VEGF-A for binding to VEGFR-2 on LECs, while VEGF-mediated lymphangiogenesis is mediated by VEGF-C/VEGFR-3 activity (Olsson et al., 2006; Simons et al., 2016)).

We thus asked whether the expression pattern of ligands, receptors and co-receptors could potentially explain our LEC tight junction configurations and proliferative signature both along the gut and upon *S. venezuelensis*. Analysis of the mucosal scrapes and the sorted LEC and BEC from each gut segment for their expression of genes involved in VEGF signaling alongside LEC marker genes (Fig. 6A, B) showed that expression gradients exist along the intestine. Most notably, mucosal *Kdr* (VEGFR-2) and *Nrp1*, encoding a VEGFR2-stabilizing co-receptor, decreased in a proximal to distal gradient, in part due to decreased expression per cell by BECs, while LECs maintained equatable per cell expression (Fig. 6C, D). Mucosal *Flt4* (VEGFR-3) and *Nrp2* also decreased along the small intestine, but their per cell expression, while strongly enriched in LECs, remained constant (Fig. 6A-D); similarly *Flt1* (VEGFR-1) decreased in a proximal to distal gradient but remained the same on a per cell basis and was enriched in BECs, suggesting these gradients were due to a total endothelial cell number gradients. With regard to VEGFR ligand expression, *Vegfa* was the dominant VEGF expressed in the gut (Fig. 6E, highest cpm), but displayed no transcriptional gradient; however *Vegfc* and *Vegfb* expression were twice as high in the jejunal and ileal mucosa compared to that of the duodenum (Fig. 6E). The inferred net effect of these expression gradients at homeostasis is that as sequestration of VEGF-A by VEGFR-2 on

BEC decreases along the small intestine, more VEGF-A is available for LEC VEGFR-2, thus permitting more VEGFR-2 activity on LECs, leading to increased lacteal zippering. Increased expression of VEGF-C in the ileum, while potentially contributing to zipper-like structures through VEGFR-2 binding more likely engages more VEGFR-3, thus promoting lymphangiogenesis (Fig. 6F). Alterations in VEGFR signaling was not reflected on the transcriptional level upon *S. venezuelensis* infection; while each VEGFR expression increased in the duodenal mucosa (Fig. 6A, C) this seemed to largely reflect the increase in LEC and BEC numbers following infection, as on a per cell basis the receptors on LECs decreased (Fig. 6B, D). However, *Vegfa* was slightly lower in the duodenal scrape of *S. venezuelensis*-infected mice and *Vegfc* trended to be lower (Fig. 6A, C), thus clearly not correlating with increased tight junction formation or lymphangiogenesis.

Overall, these analyses revealed a putative VEGFR signaling gradient that may underlie the ascending lymphatic tight junction and LEC cell cycle gradient from the proximal to distal end of the small intestine under homeostatic conditions.

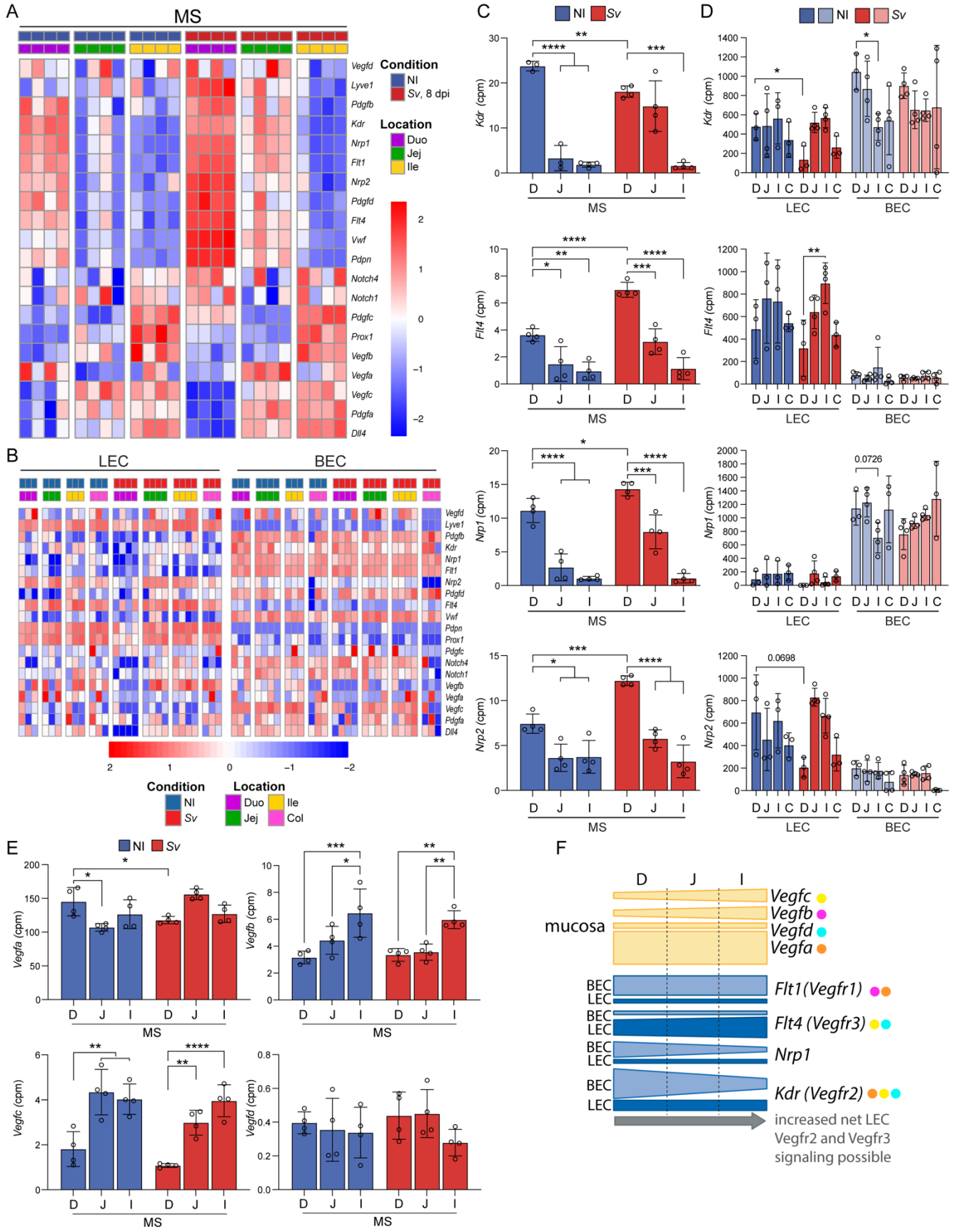
A
MS
Vegfd
Lyve1
Pdgfb
Kdr
Nrp1
Flt1
Nrp2
Pdgfd
Flt4
Vwf
Pdpn
Notch4
Notch1
Pdgfc
Prox1
Vegfb
Vegfa
Vegfc
Pdgfa
Dll4
Condition
NI
Sv, 8 dpi
Location
Duo
Jej
Ile
2
1
0
−1
−2
B
LEC
BEC
Col
C
NI
Sv
Kdr (cpm)
Flt4 (cpm)
Nrp1 (cpm)
Nrp2 (cpm)
D J I D J I
MS
D
NI
Sv
D J I C D J I C
LEC
BEC
0.0726
0.0698
E
Vegfa (cpm)
Vegfb (cpm)
Vegfc (cpm)
Vegfd (cpm)
F
D J I
mucosa
Vegfc
Vegfb
Vegfd
Vegfa
BEC
LEC
Flt1(Vegfr1)
Flt4 (Vegfr3)
Nrp1
Kdr (Vegfr2)
increased net LEC
Vegfr2 and Vegfr3
signaling possible

Figure 6. Canonical BEC and LEC VEGF signaling pathway gene expression correlates with increased lacteal zippering along the small intestine.
(A and B) Expression heatmaps of canonical vascular signaling ligand and receptor signaling pathway molecules relevant to LEC maintenance and remodeling. Mucosal scrape RNAseq (A) and sorted LEC and BEC RNAseq (B). **(C and D)** Expression in counts per million (cpm) from RNAseq of Vascular endothelial growth factor receptors known to be expressed on LECs along the gut from the mucosal scrape RNAseq (C) and the sorted LEC and BEC RNAseq (D). **(E)** Expression in cpm of vascular endothelial growth factors (*Vegf*) along the gut known to influence LEC behavior from RNAseq on mucosal scrape tissue from NI and *S. venezuelensis* (*Sv)* infected mice 8(dpi). (F) Graphical schematic summarizing VEGF, VEGFR, and VEGFR co-receptor expression gradients on both LECs and BECs along the small intestine at homeostasis. (A-F) Abbreviations: Duodenum (Duo) (D), Jejunum (Jeju) (J), Ileum (Ile) (I), and Colon (Col) (C). Error bars indicate mean ± SD and *P<0.05, **P<0.01, *** P< 0.001, **** P< 0.001by two-tailed students t-test (comparison between conditions (C-E)) or one-way ANOVA with Šídák's multiple comparisons test between single locations (C-E). D/Duo=duodenum, J/Jej=Jejunum, I/Ile=ileum, C/Col=colon.

3.7 B and T lymphocytes are not required to alter lacteal structure upon helminth infection

T_H2 cells and their cytokines IL-4/IL-13 have been found to regulate LEC proliferation when cocultured with LECs in-vitro and in-vivo in the context of the lung upon allergen-induced asthma (Shin et al., 2015). We thus asked if changes in duodenal lymphatics were more likely to be imposed by type 2 effector immune cells, such as T_H2 cells, or other factors derived from non-hematopoietic cells. Given the lymphatic phenotype starts to return to the non-infected state ~16 days post infection (Fig. S2U, V) we reasoned that the responsible cell compartment had to display similar infection-resolution kinetics. *Gata3*, *Gata1*, *Mcp1* and *F480* expression were measured by qPCR as proxies for Th2 cells/ILC2s, eosinophils, mast cells and macrophages, respectively. In the duodenum of mice infected with *S.venezuelensis* or not 8,16 or 24 days before, *Gata3* and *Gata1* still displayed similar elevation at day 16 as day 8 (Fig. 7A); *Mcp1* expression returned to non-infected levels by that time point, and *F480* expression increased upon resolution, likely reflecting the recruitment of tissue repair-associated macrophages. By contrast, genes associated with the epithelial type 2 response (*Muc2* and *Il33*) (Hammad & Lambrecht, 2015), fatty acid

signaling (*Cd36*) (Hammad & Lambrecht, 2015) and tissue fibrosis and wound repair (*Ctgf*) (Gieseck et al., 2018; Hong et al., 2020) were all upregulated day 8 but returned to non-infected expression levels by day 16 post infection (Fig. 7B). These results imply that changes in lymphatic morphology upon infection with *S.venezuelensis* are not directly driven by T_H2 cells/ILC2 or eosinophils and rather it is potentially regulated by signals from more transiently recruited innate immune cells and non-hematopoeitic cells such as the epithelium or lamina propria stromal cells.

To directly test the impact of B and T cell recruitment and effector function during the type-2 response on lacteal structure, we subcutaneously infected B6 RAG1 -/- mice with *S. venezuelensis* and harvested the duodenum 8 days later. Lacteal scoring indicated that the increase in lacteal surface area upon *S. venezulensis* infection persisted despite the lack of B and T cells (Fig. 7C). Furthermore, the duodenal lacteals also retained their predominantly zipper-like tight junction conformation upon *S. venezulensis* infection (Fig. 7D).

Together these data strongly suggest that adaptive immunity (B and T lymphocytes) are not necessary to directly induce structural changes to tissue lymphatics upon helminth infection.

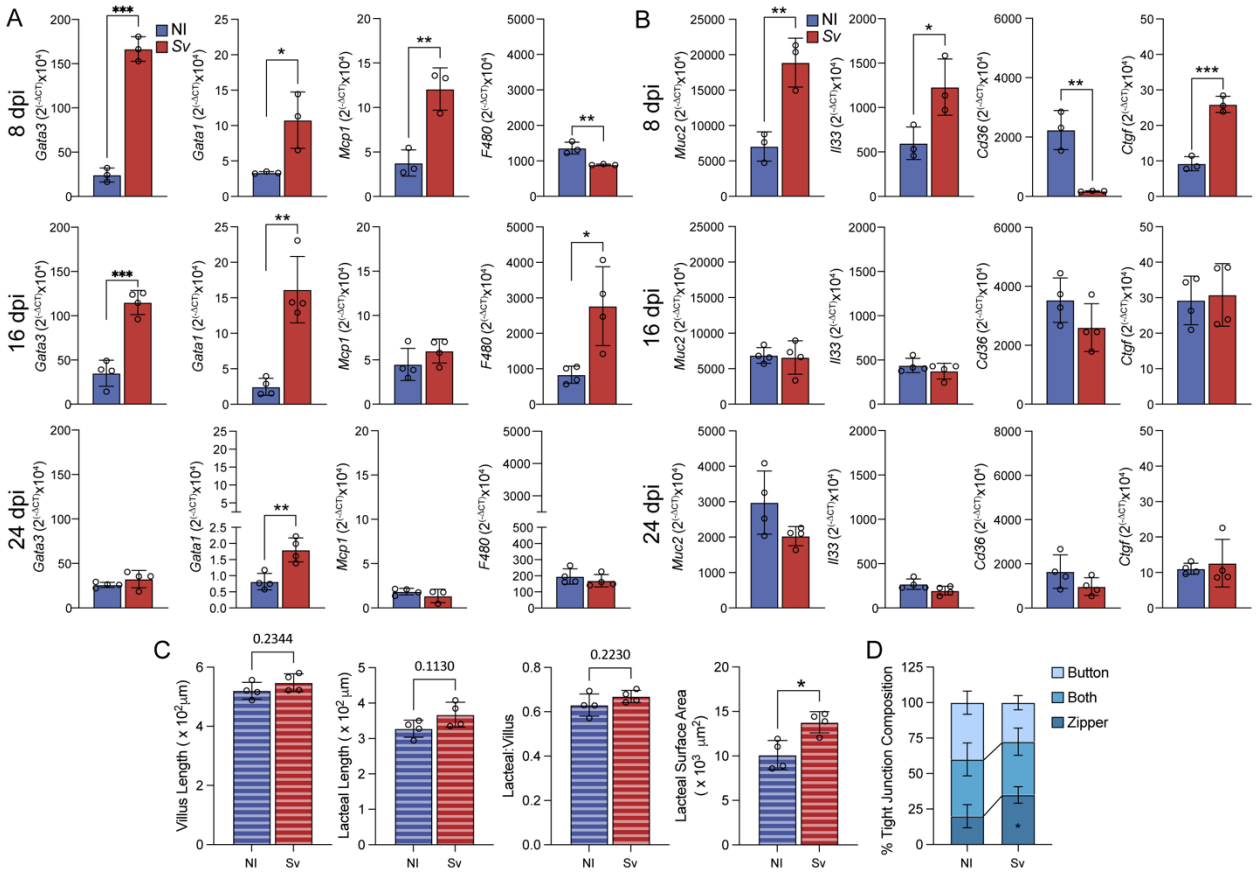

Figure 7. B and T lymphocytes are not required to alter lacteal structure upon helminth infection.

(A and B) QPCR of key immune (A) and non-hematopoietic (B) genes on the whole duodenum of NI mice versus mice infected with *Sv* 8, 16, and 24 dpi. (*n* = 3-4). Data representative of one experiment (16, 24 dpi). Data representative of two experiments (8 dpi). (**C** and **D**) Comparisons of duodenal villi and LYVE1+ lacteals in Non-infected (NI) versus *S. venezuelensis* infected RAG1 deficient B6 mice 8 days following infection. (n = 4, Data representative of one experiment). Error bars indicate mean ± SD and *P<0.05, **P<0.01, *** P< 0.001, **** P< 0.001 by two-tailed student's t-test. D/Duo=duodenum, J/Jej=Jejunum, I/Ile=ileum, C/Col=colon.

3.8 Pro-lymphangiogenic factors regulated upon helminth infection correspond with altered lymphatic morphology

The lack of a transcriptional signature linking altered VEGFR signaling to the changes in lymphatics upon *S. venezuelensis* infection does not rule out these events occurring on a post-transcriptional and secretory level. However, within the mucosal gene signatures of *S.*

venezuelensis infected mice, the strong vasculature and cell-cycling signature led us to speculate about the role of inflammation-induced molecular mediators involved in lymphangiogenesis. Revisiting the genes that contribute to these pathways upon *S. venezuelensis* in the duodenal mucosa (Fig. 8A), we asked whether these genes were also upregulated in isolated LECs. (Fig. S4F). This analysis revealed that three genes, *Slit2*, *Cxcr2* and *Adam8*, displayed a significant upregulation and a few more trended (*Gata2*, *Itgav*, *Ddah1*) in the duodenal LEC of *S. venezuelensis* infected mice. Through literature search we next uncovered additional mucosal genes in our RNAseq data for secreted factors linked to LEC maintenance and development (*Il1b*, *Igf1*, *Angpt2*, *Emilin2*, and *Slit2)* (Baluk et al., 2013; Colombatti et al., 2012; Gale et al., 2002; Z.-J. Li, 2013; Yang et al., 2010; Zheng et al., 2014b). To determine if these factors could directly modulate duodenal LECs upon *S. venezuelensis* infection, we interrogated our LEC RNAseq dataset for the expression of the receptors for these factors. Analysis of the counts per million (cpm) of these ligand-receptor genes in the mucosa and the sorted LECs (Fig. 8B-K), revealed that all receptors were expressed in LECs at minimum upon *S. venezuelensis* infection (≥ 2 cpm). Ligand expression was also verified as ≥ 2 cpm at least after infection. To determine the potential source of the ligands we performed a literature search (Baluk et al., 2013; Colombatti et al., 2012; Gale et al., 2002; Z.-J. Li, 2013; Yang et al., 2010; Zheng et al., 2014b), interrogated Immgen (for immune cell sources), and looked for an enrichment in LECs or BECs compared to mucosal scrapes (for endothelial sources). This analysis suggested that the ligands are expressed primarily by endothelial cells (LECs and BECs), enterocytes, macrophages and mast cells (Fig. 8L). These potential sources are also in line with signals that start to cease from 16 days post *S. venezuelensis* infection, thus no longer promoting lymphangiogenesis then, as we had observed that genes indicative of these cell types had returned to non-infected levels at 16 days (Fig. 8E, F).

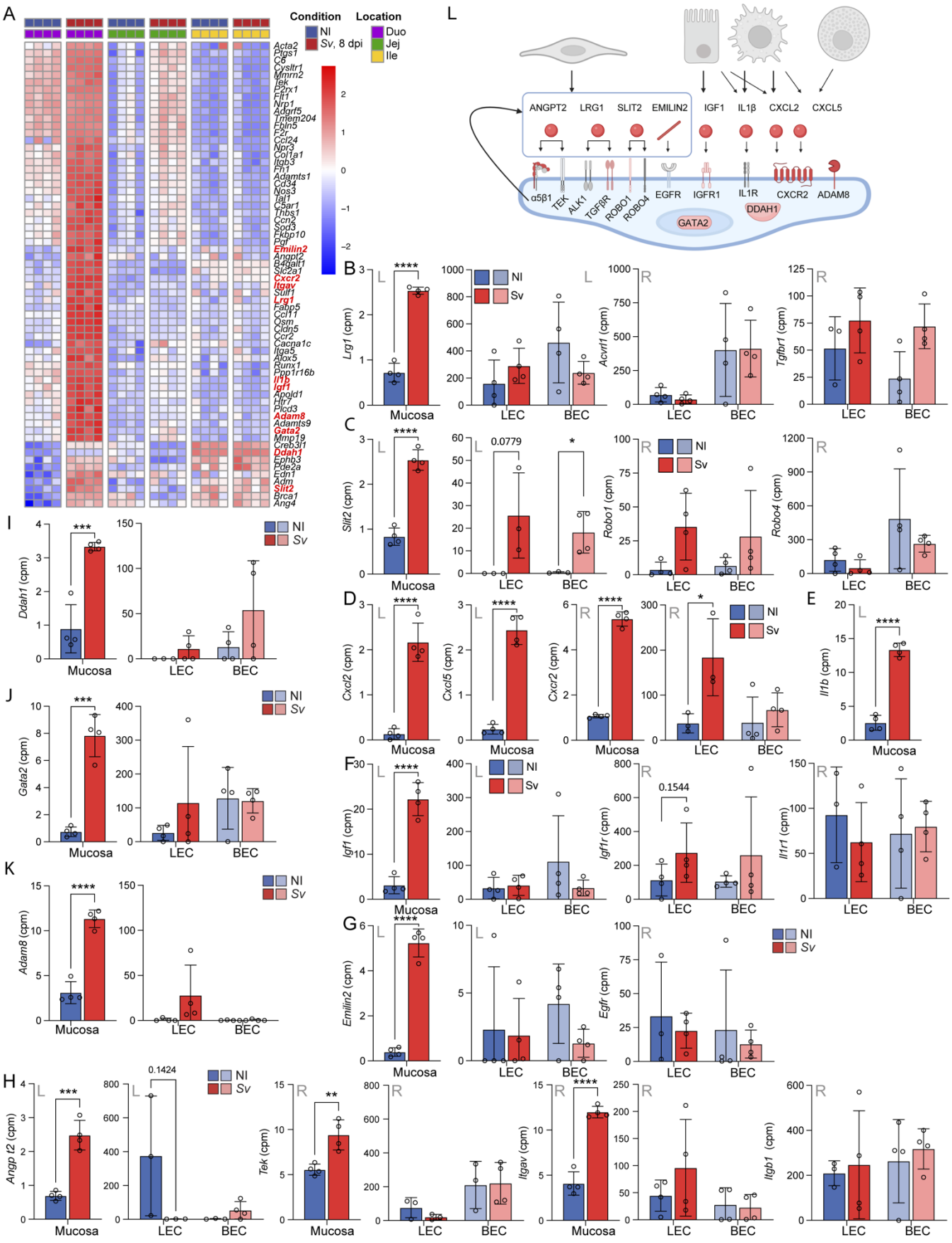
A
Condition
NI
Sv, 8 dpi
Location
Duo
Jej
Ile
Acta2
Ptgs1
C6
Cysltr1
Mmrn2
Tek
F2rl1
Flt1
Nrp1
Adgrf5
Tmem204
Fbln5
F2r
Ccl24
Npr3
Col1a1
Itgb3
Fn1
Adamts1
Cd34
Nos3
Tal1
C5ar1
Thbs1
Con2
Sod3
Fkbp10
Cgnl1
Emilin2
Angpt2
B4galt1
Slc2a1
Cxcr2
Itgav
Stil1
Lrg1
Fabp5
Ccl11
Osm
Cldn5
Ccr2
Cacna1c
Itga5
Alox5
Runx1
Ppp1r16b
Il1b
Igf1
Apold1
Htr7
Plcd3
Adam8
Adamts9
Gata2
Mmp19
Creb3l1
Ddah1
Ephb3
Pde2a
Edn1
Adm
Slit2
Brca1
Ang4
L
ANGPT2
LRG1
SLIT2
EMILIN2
IGF1
IL1β
CXCL2
CXCL5
α5β1
TEK
ALK1
TGFβR
ROBO1
ROBO4
EGFR
IGFR1
IL1R
CXCR2
ADAM8
DDAH1
GATA2
B
Lrg1 (cpm)
Acvrl1 (cpm)
Tgfbr1 (cpm)
C
Slit2 (cpm)
Robo1 (cpm)
Robo4 (cpm)
D
Cxcl2 (cpm)
Cxcl5 (cpm)
Cxcr2 (cpm)
E
Il1b (cpm)
F
Igf1 (cpm)
Igf1r (cpm)
Il1r1 (cpm)
G
Emilin2 (cpm)
Egfr (cpm)
H
Angpt2 (cpm)
Tek (cpm)
Itgav (cpm)
Itgb1 (cpm)
I
Ddah1 (cpm)
J
Gata2 (cpm)
K
Adam8 (cpm)
NI
Sv
Mucosa
LEC
BEC

Figure 8. Pro-lymphangiogenic factors regulated upon helminth infection correspond with altered lymphatic morphology.
(A) Heatmap of expression of vascular development-regulatory pathway genes identified in GOBP pathway analysis in RNAseq of duodenal mucosal scrape of non-infected mice and mice infected with *S. venezuelensis* (*Sv*) 8 days prior. **(B-J)** Counts per million expression of pro-lymphangiogenic ligands and receptors from duodenal mucosal scrape (MS) and sorted LEC/BEC determined by RNAseq, whereby *Lrg1-Acvrl1-Tgfbr1* (B), *Slit2-Robo1-Robo4* (C), *Cxcl2/5-Cxcr2* (D), *Il1b-Il1r1* (E), *Igf1-Igf1r* (F), *Emilin2-Egfr* (G) and *Angpt2-Tek-Itgav-Itgb1*(H) form ligand (grey L)-receptor (grey R) pairs, while *Ddah1* (I), *Gata2* (J), *Adam8* (K) are just enriched in LECs. **(L)** Proposed ligand-receptor interactions between LECs and other cell-types within the duodenal microenvironment. Receptors or ligands in red are DEGs in MS or LECs, in pink are trending, in grey are not regulated. Error bars indicate mean ± SD and *P<0.05, **P<0.01, *** P< 0.001, **** P< 0.001by two-tailed students t-test (comparison between conditions) (B-J). D/Duo=duodenum, J/Jej=Jejunum, I/Ile=ileum, C/Col=colon.

In sum, the *S. venezuelensis* induced lymphangiogenesis is reflected on the transcriptional level and represents an inflammation-induced lymphangiogenic pathway. This lymphangiogenesis peaks at day 8 post infection and could account for the more zipper-like tight junctions between LECs upon helminth infection.

3.9 Mucosal microbial depletion does not account for the lacteal morphology upon helminth infection

Infection with *S. venezuelensis* induces a strong, transient duodenal antimicrobial response (Fig. 5D, Fig. 9A, Fig. S5A). Microbial depletion has previously been reported to impact lacteal morphology, most notably to increase lacteal zippering and blunt lacteal length (Suh et al., 2019). We interrogated if the observed antimicrobial signature at 8 dpi with *S. venezuelensis* correlated with an impact on microbial diversity and abundance in our facility (Afrin et al., 2019) and if so, whether this alone was responsible for the zipper-like tight junction observed upon helminth infection. Luminal microbial composition and load were largely unaffected by helminth infection (Fig. S5B, C). Given the antimicrobial response is spatially localized to the mucosa, we also assessed if the tissue associated microbiota was affected by *S. venezuelensis*. Fluorescent in situ hybridization (FISH) detection of the microbiota with 16S DNA probes on the duodenum upon *S.*

venezuelensis revealed a decrease in probe signal staining at the intestinal crypts (Fig. 9B, C). This decrease in microbial abundance was independently confirmed via a qPCR based method to quantify bacterial colony forming units (CFU) in the mucosa (Fig. 9D), and via a decrease in CFUs from plated infected tissue scrapes to determine if microbial depletion (Fig. S5E). To determine if microbial depletion induces lymphatic changes, we next put mice on broad spectrum antibiotics (Abx) three days prior to *S.venezuelensis* infection and then assessed duodenal lacteal morphology 9 days post infection. Successful microbial depletion was confirmed by 16S QPCR (Fig. S5F). Abx did not compromise worm fecundity and rather led to an increased egg load at 9 days post infection (Fig. S5G). Overall, the effects of antibiotic mediated depletion and *S.venezuelensis* appeared additive: lacteal length and surface area (Fig. 9E, F) as well as duodenal width (Fig. S5 H, I) increased upon either perturbation alone but was further increased when antibiotics treated mice were infected with the helminth. Antibiotic mediated microbial depletion led to an increase in zipper-like duodenal lacteal LEC junctions both in the non-infected and *S. venezuelensis* infected mice (Fig. 9G), but a further enhancement of this phenotype was not observed. In line with observations by others, duodenal *Vegfc* expression was not affected by antibiotics (Fig. S5J), though interestingly antibiotic depletion reversed the decrease in VEGF-C expression by *S. venezuelensis*. qPCR of genes identified to be regulated by *S. venezuelensis* and potentially responsible for the change in LEC morphology and junction composition were either unaffected by antibiotic treatment (Fig. S5 J-M) or behaved additively (Fig. S5 O, P).

In sum, these data exclude *S. venezuelensis* induced mucosal microbial depletion as the primary mechanism through which helminths alter duodenal lymphatics and suggest complete microbial depletion works in tandem with an independent inflammation-induced mechanism to alter tissue lymphatics in a site specific manner.

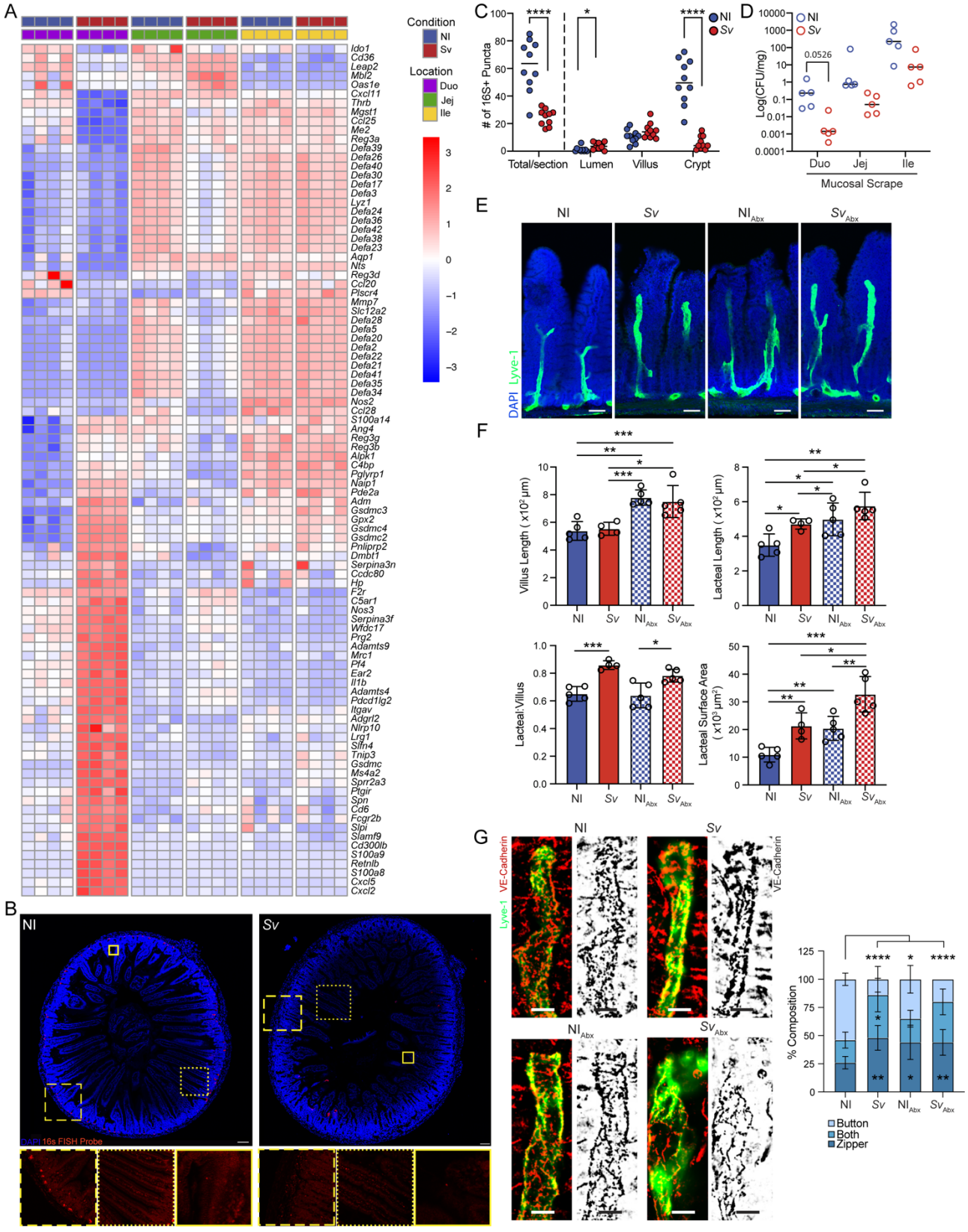
A
Condition
NI
Sv
Location
Duo
Jej
Ile
3
2
1
0
−1
−2
−3
Ido1
Cd36
Leap2
Mbl2
Oas1e
Cxcl11
Thrb
Mgst1
Ccl25
Me2
Reg3a
Defa39
Defa26
Defa40
Defa30
Defa17
Defa3
Lyz1
Defa24
Defa36
Defa42
Defa38
Defa23
Aqp1
Nts
Reg3d
Ccl20
Plscr4
Mmp7
Slc12a2
Defa28
Defa5
Defa20
Defa2
Defa22
Defa21
Defa41
Defa35
Defa34
Nos2
Ccl28
S100a14
Ang4
Reg3g
Reg3b
Alpk1
C4bp
Pglyrp1
Naip1
Pde2a
Adm
Gsdmc3
Gpx2
Gsdmc4
Gsdmc2
Pnliprp2
Dmbt1
Serpina3n
Ccdc80
Hp
F2r
C5ar1
Nos3
Serpina3f
Wfdc17
Prg2
Adamts9
Mrc1
Pf4
Ear2
Il1b
Adamts4
Pdcd1lg2
Itgav
Adgrl2
Nlrp10
Lrg1
Slfn4
Tnip3
Gsdmc
Ms4a2
Sprr2a3
Ptgir
Spn
Cd6
Fcgr2b
Slpi
Slamf9
Cd300lb
S100a9
Retnlb
S100a8
Cxcl5
Cxcl2
B
NI
Sv
DAPI 16s FISH Probe
C
# of 16S+ Puncta
Total/section
Lumen
Villus
Crypt
NI
Sv
D
Log(CFU/mg)
0.0526
Duo
Jej
Ile
Mucosal Scrape
E
NI
Sv
NIAbx
SvAbx
DAPI Lyve-1
F
Villus Length (x10² µm)
Lacteal Length (x10² µm)
Lacteal:Villus
Lacteal Surface Area (x10³ µm²)
G
NI
Sv
NIAbx
SvAbx
Lyve-1
VE-Cadherin
% Composition
Button
Both
Zipper

Figure 9. Microbial depletion along does not alter lacteal morphology upon helminth infection.

A. Heatmap of expression of antimicrobial pathway genes identified in GOBP pathway analysis in RNAseq of duodenal mucosal scrape of non-infected (NI) mice versus 8 days post infection (dpi) with *S. venezuelensis* (*Sv*). **(B and C)** Fluorescence in situ hybridization (FISH) probe (EUB338) detection (B) and enumeration (C) of bacteria in the duodenum of NI mice and mice infected with *Sv*, 8 dpi. (Dots represent count per duodenum section, 2 sections per mouse counted, n = 5 mice per group), representative of one experiment. Scale bar: 100 μm, zoomed in picture 350 μm **(D)** Microbial CFU within the small intestine mucosal scrape of NI mice and mice infected with *Sv*, 8 dpi, as determined by qPCR. Data normalized to the sample input weight. (Dots represent individual mouse, n = 5 mice per group), data representative of two independent experiments. **(E-F)** Immunofluorescence images (E) and comparison (F) of duodenum villi and LYVE-1+ lacteals in NI versus, *Sv* infected 8 dpi, NI antibiotic depleted (NI_{abx}), and Sv infected antibiotic depleted (Sv_{abx}) mice, 8 dpi: villus length, lacteal length, lacteal length to villus length ratio, and lacteal surface area. (n = 5 mice per group), data representative of one experiment. **(G)** Representative images and characterization of VE-cadherin+ LEC junctions of LYVE-1+ lacteals in NI versus *Sv* infected mice, 8 dpi, NI_{abx}, and Sv_{abx} infected mice, 8 dpi. Quantification of duodenal lacteal tight-junction organization with primarily button-like, zipper-like, or a combination of both tight junction formations throughout the length of the lacteal. (n = 5 mice per group), data representative of one experiment. Error bars indicate mean ± SD and *P<0.05, **P<0.01, *** P< 0.001, **** P< 0.001 by two-tailed student's t-test (F), two-way ANOVA with Šídák's multiple comparisons test. Scale bar: 100 um (B and E), 25 um (G). D/Duo=duodenum, J/Jej=Jejunum, I/Ile=ileum, C/Col=colon.

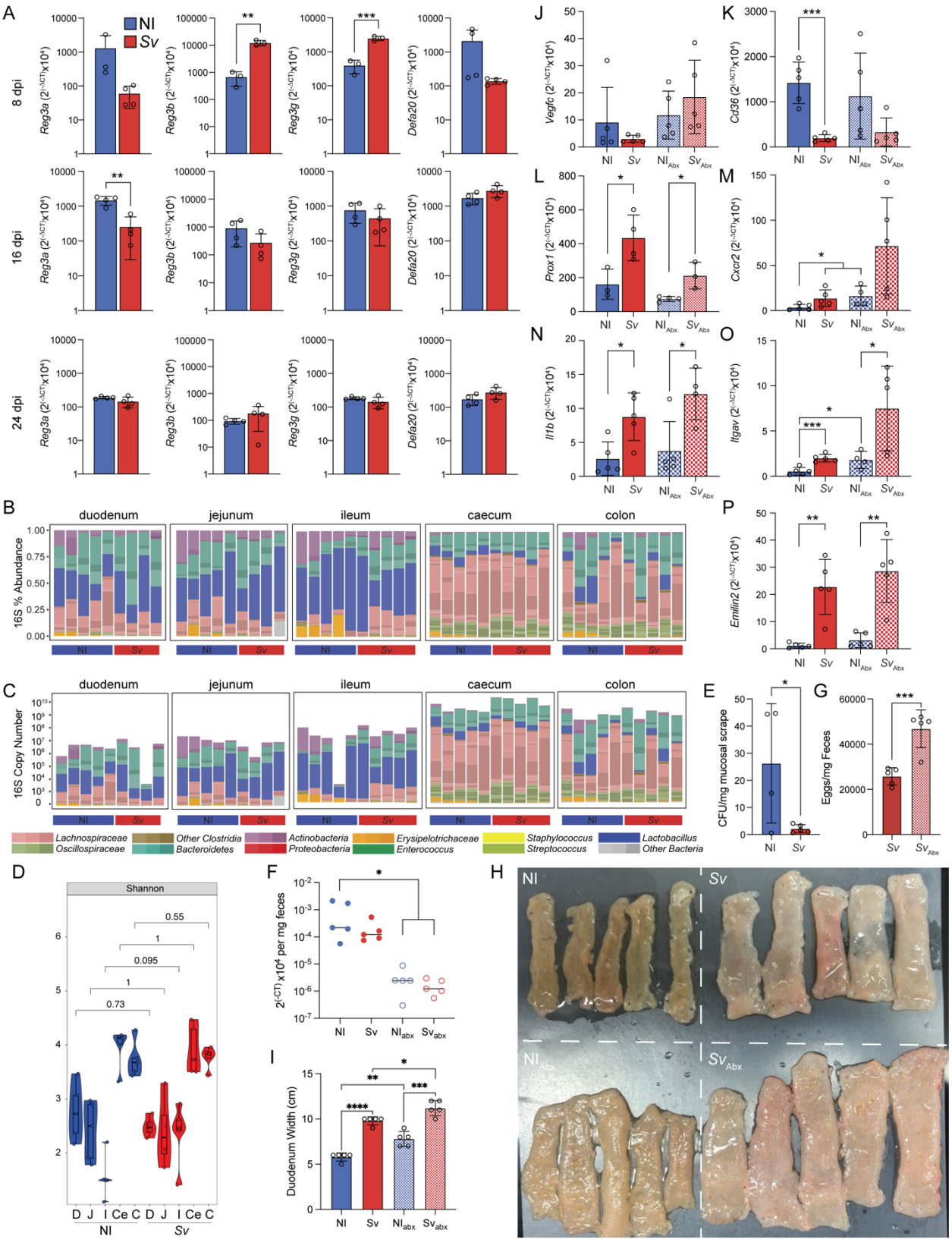
A
NI
Sv
8 dpi
16 dpi
24 dpi
Reg3a (2^-ΔCT)x10^4
Reg3b (2^-ΔCT)x10^4
Reg3g (2^-ΔCT)x10^4
Defa20 (2^-ΔCT)x10^4
B
duodenum
jejunum
ileum
caecum
colon
16S % Abundance
C
16S Copy Number
Lachnospiraceae
Oscillospiraceae
Other Clostridia
Bacteroidetes
Actinobacteria
Proteobacteria
Erysipelotrichaceae
Enterococcus
Staphylococcus
Streptococcus
Lactobacillus
Other Bacteria
D
Shannon
0.55
1
0.095
1
0.73
D J I Ce C D J I Ce C
NI
Sv
E
CFU/mg mucosal scrape
F
2^-CT x10^4 per mg feces
NI
Sv
NIabx
Svabx
G
Eggs/mg Feces
H
NI
Sv
NIAbx
SvAbx
I
Duodenum Width (cm)
J
Vegfc (2^-ΔCT)x10^4
K
Cd36 (2^-ΔCT)x10^4
L
Prox1 (2^-ΔCT)x10^4
M
Cxcr2 (2^-ΔCT)x10^4
N
Il1b (2^-ΔCT)x10^4
O
Itgav (2^-ΔCT)x10^4
P
Emilin2 (2^-ΔCT)x10^4

Figure S5. Microbial depletion along does not alter lacteal morphology upon helminth infection.

(A) QPCR for *Reg3a*, *Reg3b*, *Reg3d*, and *Defa20* in whole duodenum of age and sex matched none-infected mice or 8, 16 or 24 days post *S. venezuelensis* (*Sv*) infection (dpi), (*n*= 3, 4, 4 for 8, 16, 24 days post infection, respectively. (**B-D**) Relative abundance (B), absolute abundance (C) and diversity (D) of bacterial phyla based on 16S Sequencing of luminal contents along gut of non-infected mice or mice infected with *Sv* 8 days earlier. (**E**) Colony forming units (CFU) in duodenal mucosal scrapes of non-infected mice or mice infected with *Sv* 8 days earlier (*n*=5). (**E**) qPCR for pan-bacterial ribosomal 16S gene in feces of mice treated with broad spectrum antibiotics cocktail (Abx) or not, infected with *Sv* 8 days earlier or not (*n* = 5). (**F**) Fecal egg count of mice infected with *Sv* and treated with Abx or not (*n* = 5). (**G, H**) Picture of longitudinally opened duodena and jejuna (G) and duodenal diameter (H) of mice treated with broad spectrum antibiotics cocktail (Abx) or not, infected with *Sv* 8 days earlier or not (*n* = 5). (**I-O**) qPCR of indicated gene in extracts from whole duodenum of mice treated with broad spectrum antibiotics cocktail (Abx) or not, infected with *Sv* 8 days earlier or not (*n* = 5). Error bars indicate mean ± SD and *P<0.05, **P<0.01, *** P< 0.001, **** P< 0.001 by two-tailed student's t-test. D/Duo=duodenum, J/Jej=Jejunum, I/Ile=ileum, C/Col=colon.

4. Discussion

In this thesis, I initially sought to understand how the tissue lymphatic vasculature dynamically regulates immunity within the draining lymph node along the gut. As lymphatic vasculature is often treated as an after-thought in studies that aim to understand how tissue specific immunity is achieved and regulated amidst immune response following inflammatory perturbation, little work has been published on how the lymphatics are altered upon inflammatory perturbation (Bernier-Latmani & Petrova, 2017b). Furthermore, lymphatic vascular beds across the body are often treated as generic, disregarding much of the nuance that potentially underlies efficiently draining different tissues and organs, or how the expression profile of the vessels could modulate the trafficking immune cells. Given these larger open questions, we felt it inappropriate to immediately ask how lymphatics impact immune responses in the context of infection without first knowing how lymphatics adapt to the tissue they drain. In this study we have uncovered regional transcriptional and functional properties of the intestinal lymphatics which match to the mucosal milieu that they drain. We also highlight how they can adapt to an inflammatory insult, such as a helminth infection, but also return to steady state function once the pathogen is cleared.

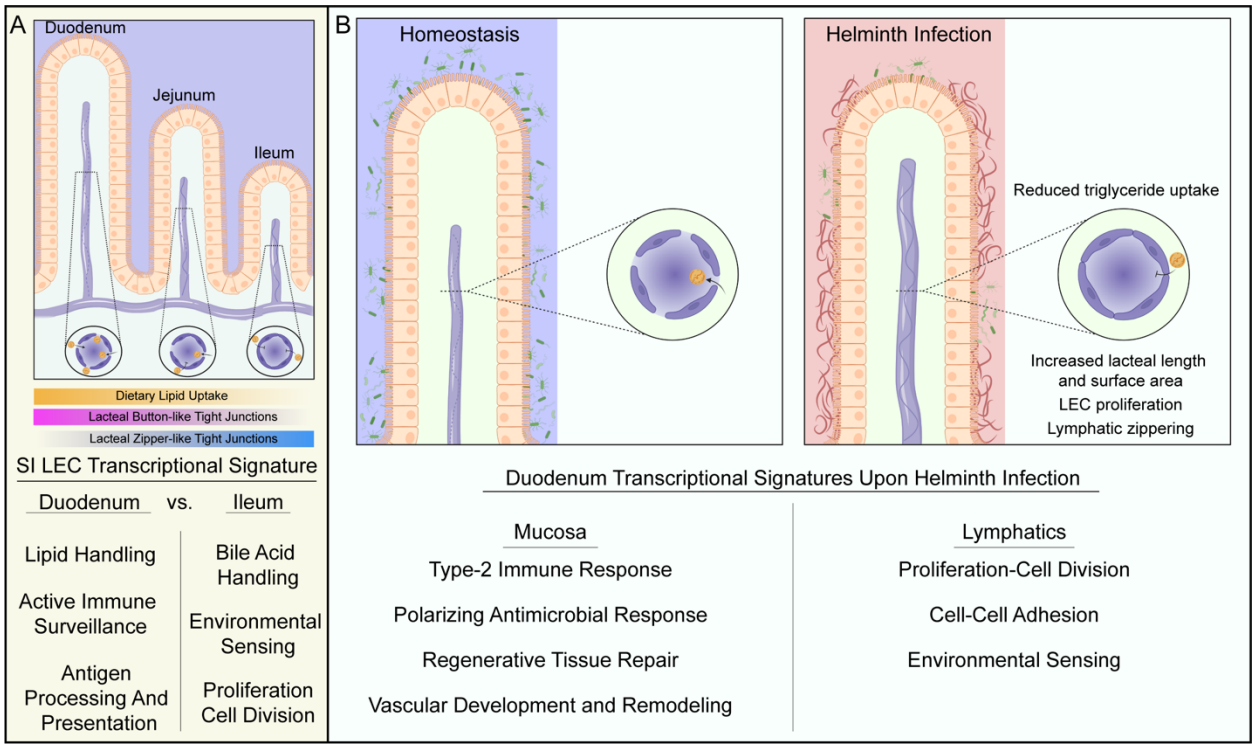

Figure 10. Intestinal lymphatics functionally reflect the gut segment they drain and respond upon helminth infection
A. Lacteal length and tight junction composition is segment specific. The duodenum lacteals have a more permeable tight junction conformation compared to ileal lacteals. This difference in tight junction composition along the small intestine seems to partially drive the functional decreasing lipid uptake gradient. Similar to the morphology, the transcriptional signature of the lymphatics at each site are also segment specific and correlate with the mucosal signature. B. Duodenal helminth infection impacts lymphatic morphology exclusively at the site of infection. The type-2 immune response in association with a vascular remodeling and tissue regeneration response is initiated upon tissue damage elicited by the helminth. As a consequence, the lymphatics ability to uptake lipids is impaired.

4.1 Tissue lymphatics are structurally and transcriptionally distinct along the small intestine and differ in their absorptive capacity

4.1.1 Intestinal lymphatic vasculature is structurally unique between segments

It has been well established that along with the small intestinal villi, the lacteals that are embedded within decrease in length and number per villus distally along the tract (Bernier-Latmani et al., 2015; Bernier-Latmani & Petrova, 2017b); however, potential differences in the lacteal LEC

tight-junction composition along the small intestine have not been assessed until this thesis. Scoring of the duodenum, jejunum, and ileal lacteal LEC tight junctions uncovered that these tight junctions become increasingly zipper-like moving distally along the small intestine (Fig. 10A). To substantiate these claims, with aid from the microscopy core I developed a semi-automated scoring method that measures the lengths of lacteal LEC tight junctions within an area defined by the lymphatic marker (LYVE-1). This method confirmed the manual scoring results showing that the tight junctions significantly increased in length towards the distal intestine.

4.1.2 Differences in lymphatic structure regulate lipid uptake at each segment

Taking into consideration previous works showing that dietary lipids are decreasingly taken along the small intestine (Esterházy et al., 2019) and that lacteal LEC tight junction composition tightly regulates chylomicron uptake by the lymphatics (Zhang et al., 2018, 2020) we asked whether altering the lacteal tight junctions could potentially influence lipid uptake at each segment. In doing so, we found that making the lacteals LECs to have a more zipper-like conformation lead to significant decreases in proximal lipid uptake. This also resulted in a slight compensatory effect in the distal intestine where there was an observed increase in taken up lipids. Shifting the lacteal LECs to have a more button-like conformation on the other-hand did not significantly impact where along the small intestine nor the degree at which lipids were taken up by the lymphatics. Of note, in each of the experiments regardless of the configuration of the lacteal LEC tight junctions, lipid uptake roughly remained the highest at the proximal small intestine where dietary lipids first enter the intestinal lumen. Considering this, lacteal tight junction composition cannot be attributed as the sole driver of the lipid uptake gradient, as spatial proximity to the stomach also seems to influence the degree at which dietary lipids are taken up at a specific segment. That said, in adult

mice at least, the duodenal tight junction conformation seemed stable and not driven by continuous fat exposure, as omitting fat in the diet did not change the duodenal lacteal tight junctions.

With respect to migratory cell trafficking from the tissue to the draining lymph node, additional work needs to be performed to gain a better understanding of how the structural properties of lymphatics impacts this process. Better tools need to be developed to allow the simultaneous perturbation of lymphatic vasculature (without impact on blood vasculature) and track migration of cells from the tissue to the draining lymph nodes. Furthermore, there is a current lack in mouse models that specifically target LECs in a site-specific manner (i.e. exclusively the capillary or LN LECs) to better elucidate the nuances between migration out of the tissue versus within the LN. As it stands, Prox1^{creERT2}-Vegfr3$^{fl/fl}$ and Prox1^{creERT2}-Vegfr2$^{fl/fl}$ mice have been shown to modulate LEC tight junction composition to be either more zipper or button-like respectively (Churchill et al., 2022b; Suh et al., 2019). Lethal irradiation of these mice, followed by reconstitution with bone marrow from Kaede mice would potentially allow you to address this question by tracking the movement of photoconverted cells from the tissue to the draining lymph node. While this system would circumvent the bias of a single cell type being preferentially labeled, invasive surgery will need to be performed to study migration at lymphatic beds other than the skin. Nonetheless, the issue of potentially changing LN LECs using these mouse models remains a challenge.

4.1.3 Intestinal lymphatics are transcriptionally heterogeneous between segments

Many groups have had difficulties sequencing LECs from tissues as the digestion process often kills viable cells. To overcome this, we used Flt4^{creERT2}-ROSA26^{TdTomato} mice where the LECs express RFP which we can use to monitor the digestion process on a benchtop fluorescent

microscope. We then were able to sort the single cell suspension and prepare cDNA libraries for sequencing from the sorted cells. Sequencing of sorted LECs along both the small and large intestine from non-infected mice and mice infected with *S. venezuelensis* granted us the ability to computationally ask how helminth infection impacts duodenal LECs but also whether LECs along the intestines at homeostasis are different depending on the gut segment they drain. Comparing duodenal LECs to ileal LECs revealed that the small intestinal lymphatics are transcriptionally heterogeneous between segments (Fig. 10A). Duodenal LECs are enriched in the expression of genes related to immune modulation and lipid handling while ileal LECs are enriched in genes related to bile acid metabolism and suggest they have increased proliferative potential. Sequencing of the mucosa along the small intestine largely shares the enrichment of these properties and pathways at each segment with the LECs that lie within them: The duodenal mucosa is enriched in genes related to active immune monitoring and lipid handling, while the ileal mucosa was enriched in genes related to cell division and interfacing with the microbiome.

In the duodenum LECs, the enrichment of lipid handling/metabolic genes could plausibly be a direct consequence of the heightened dietary lipid uptake at the segment relative to the other distal segments. In future studies, it would be interesting to determine what would occur if you were to artificially distribute the lipid uptake burden across each of the segments, similar to what was done with the VEGFR-2 blocking antibody, then transcriptionally profile the lymphatics at each site, or perform RNAseq on LECs from mice fed a diet devoid of lipids. Given that the lymphatic vasculature seems sensitive to changes in the tissue environment, one would anticipate that this would lead to the distal segments also acquiring the lipid handling signature. While the lymphatic lipid metabolic signature seems to directly result from increased lipid uptake at the site, the enriched immunity signature within the duodenum LECs may be attributed to the active

immune surveillance against pathogens and opportunistic commensals in an effort to constrain inflammatory responses at the intestinal barrier rather the draining lymph node.

The expression of toll-like receptors (TLRs) by the LECs here may signal that they are also engaged in this immune surveillance for a breach in the barrier, while MHC expression by the lymphatic vasculature may directly regulate lymphocyte maintenance and function as they establish residency at the tissue. To elucidate why LECs present peptides at homeostasis, the peptide processing and presentation machinery needs to be knocked down and the lymphocytes should be profiled to gain a deeper understanding on the role of MHC expression in LECs in the absence of inflammatory insult. One intriguing correlation between MHC expression and the duodenal function is that it is also the main site of dietary antigen uptake, a homeostatic process.

Functionally we focused on the phenomenon of lymphatic permeability and its role in chylomicron uptake. Our data suggest that the molecular basis underlying this process under homeostatic conditions, likely attributable to the balance of VEGF signaling on LECs versus BECs along the small intestine, is not the same as under inflammatory conditions, where lymphangiogenesis-associated zippering transiently dictates permeability. Further work needs to be done to uncover how this balance and gradient in VEGF signaling is established at homeostasis. Given the expression gradient closely mirrors many of the known environmental gradients in the intestine (i.e. microbiome, O_2, pH, etc) (Beumer & Clevers, 2017) it stands to reason that they may play a key role in establishing this VEGF signaling balance on the vasculature directly or through other local mediators. Additionally lymphangiogenesis appears to be governed by different inflammatory triggers and molecular cues compared to the during development or upon homeostatic turnover. We have thus identified a potentially crucial pathway also relevant for chronic inflammatory diseases such as IBD where lymphatic dysfunction has also been observed.

Taken in concert, these data suggest that the lymphatics transcriptionally reflect the tissue that they drain. Duodenal lymphatics appear to be uniquely poised to maximize lipid uptake. This may be initially substrate-driven during early postnatal development (Zarkada et al., 2023), but once established this appeared to be a structurally stable feature at homeostasis (see Fig. S1 I, J). How these permeability and metabolic properties synergize with other unique features of duodenal LECs such as their immunostimulatory profile and properties will be interesting to interrogate in the future. Similarly, since lymphatic lipid uptake also increases lymph flow rate (Turner & Barrowman, 1977), it will be intriguing to study how this duodenal uptake bias translates into a flow rate gradient along the intestine and may influence immune outcomes in the draining LNs. The duodenum's low microbial load, due to active immune surveillance, may also influence the LEC profile. It is likely that the microbiota plays a more direct role in shaping the more distal intestinal LEC transcriptome.

The transcriptional profiling of LECs along the intestine has long been overdue to be reported in the field of mucosal immunology. Our study reveals compelling regional differences even within the small intestine, but likely also only scratches their surfaces, given we had bulk-sorted LECs. The degree at which the LECs between small intestinal segments differed was drastically reduced when comparing LECs between their corresponding draining lymph nodes, further suggesting that the tissue environment that the lymphatics lie within and drain directly influences their behavior. With improved spatial transcriptomics on the horizon, permitting for single cell resolution and high transcriptome coverage, the current hurdles of yield and cell death of endothelial and rare cells in the gut will soon be surmountable, and provide additional insights into the potential regional differences of the stromal cells supporting the lymphatics. Such approach will also more easily expanded to human tissues.

4.2 Helminth infections impact duodenum lymphatic structure, transcriptional state, and absorptive function

4.2.1 Helminth infection induces structural changes to lymphatics directly at the site of infection

It has been well appreciated that vascular remodeling is often associated with lymph node swelling during the immune response(Benahmed et al., 2012; Esterházy et al., 2019); however, when this work was started, little was known on how infections impacted tissue lymphatic vasculature directly at the site of infection. To determine if infections impacted intestinal tissue, we first assessed the impact of the helminth *S. venezuelensis* on duodenal tissue as the draining lymph nodes massively swell at the height of infection. Upon observing significant changes in lacteal length, surface area, and tight junction composition (Fig. 10B) we expanded to other infections to determine if the phenotype was unique to *S. venezuelensis* infection or if it could be recapitulated. Helminths turned out to have the strongest impact on the duodenal lymphatics among the infections tested. This may have been due to timing, but more likely the degree of damage and corresponding response this type of infection elicits compared to the virus and bacteria we used. Whether other type 2 immune response-eliciting pathogens or for example also type 3 immune response inducing pathogens cause a similar lymphatic phenotype in the duodenum remains to be determined.

Without B and T lymphocytes upon helminth infection in RAG1 deficient mice, the increase in duodenum lacteal surface area was moderately increased relative to that of immune competent mice while the length trended towards increasing compared to the non-infected duodenum lacteals. This result may be attributed to sub-prime recruitment of Type-2 effector cells such as M2 macrophages and eosinophils that would otherwise be recruited by T_H2 cells. To

further test this, these innate cells would need to be depleted in a setting where B and T cells are intact. If these innate cells are required to regulate lymphatic morphology upon helminth infection, then there will not be a difference in lacteal properties at the height of infection.

The commensal microbiome has been previously shown to modulate intestinal lacteal length and permeability (Suh et al., 2019), albeit at the jejunum and ileum but not duodenum. To test the role of the microbiome in regulating lymphatic structure upon helminth infection we depleted the microbiome by placing helminth infected and non-infected mice on antibiotics and assessed the change to duodenal lymphatics. While many of our findings are in line with what was previously found to occur upon microbial depletion (Esterházy et al., 2019), our studies also contradict these same works, as microbial depletion alone in their study did not impact duodenal lacteals and resulted in a blunting of lacteal length at the jejunum and ileum while we observed significant increases in both duodenal and jejunal lacteal length and surface area. Other groups have also previously reported there to be an increase in intestinal villus length in germ-free mice (Esterházy et al., 2019); however, phenotypic differences between our studies may simply be attributed to differences in experimental set up or microbiome differences between facilities.

4.2.2 Duodenal lymphatic lipid uptake is severely repressed upon helminth infection

In the duodenum, compromised lymphatic function translates into lipid malabsorption; injury at other sites may have different consequences. Surprisingly, while several groups have reported the resistance to weight gain on high fat diet upon gastrointestinal helminth infection (Kabat et al., 2022, 2023; Su et al., 2018), most have attributed this phenomenon to peripheral metabolic effects such as altered adipose tissue and distal macrophage behavior, rather than studying the gut directly. Our data strongly suggest that helminths already influence efficient fat

absorption in the intestine itself. While we monitored triglycerides because of its ease, this phenomenon likely also means that all sorts of other molecules packaged into chylomicrons, such as fat-soluble vitamins, are also less efficiently absorbed. The focus of our study were the intestinal lymphatics, but we did also observe lipid stalling at the epithelium and lamina propria, likely as consequence of lymphatic dysfunction as preventing button-like junctions genetically, uncoupled from the worm, led to the same phenotype. This is likely to impose stress on epithelial cells. From this standpoint the use of helminths as a weight loss measure or to counter inflammatory bowel diseases should be treated with caution, and particular attention paid to the gut segment that the worm infects. Rather identifying the specific mechanism that elicits lymphatic zippering and bacterial exclusion from the epithelium each upon helminth infection, then developing therapeutic approaches to engage those pathways for weight loss and IBD respectively may prove to be the more advantageous solution. In theory, this approach would reduce the tissue damage and inflammation induced from administering live helminth or helminth products.

4.2.3 Transcriptionally, duodenal lymphatics seem sensitive to the inflammatory environment upon helminth infection

Similar to what was found in the non-infected setting, the mucosa and the lymphatics that drain the tissue are transcriptionally comparable. Upon helminth infection there is a loss in the lipid metabolic signature and an upregulation in the vascular development-cell division signatures within the mucosa and sorted LECs respectively. Additionally, there was a loss in the immunity signature observed to be enriched in non-infected duodenum LECs (Fig. 10B). This signature loss

may be attributed to proliferation of the cells where maturation of the cells would lead to antigen processing and presentation on MHC. Gene ontology biological process pathway analysis of the non-infected versus helminth infected duodenum mucosa and its associated lymphatics revealed the upregulation of several inflammation associated mediators of lymphangiogenesis. Immgen analysis of these molecular mediators suggest potential interactions between the LECs with macrophages and granulocytes.

While we believe lymphangiogenesis associated zippering is behind lacteal LEC zippering upon helminth infection, the promotion of lacteal integrity by the microbiome, and lymphatic zippering upon viral infection at the skin (independent of lymphangiogenesis), strongly suggest the existence of several potentially redundant mechanisms to dynamically alter lymphatic structure and potentially function. Furthermore, the existence of independent mechanisms to impact lymphatic vasculature sets the stage for several questions from an evolutionary perspective: 1. Why do independent mechanisms exist? 2. Under what context are they preferred (Does it come down to type-1 versus type-2 immune response, or the specific biology of host-pathogen interaction, including the host target cell)? and 3. Why are they contextually employed? To achieve this, more work needs to be performed to understand how and why different tissue environments differentially regulate the lymphatic vasculature at homeostasis versus inflammatory perturbation

5. Outlook

In summation, this thesis reveals the intestinal lymphatic intratissue heterogeneity on the transcriptional level both at homeostasis and upon pathogen infection. Interesting further studies building upon this work may seek to understand the degree of immune regulation at the proximal small intestine exerted by the lymphatics already at the tissue, and whether it has a role in regulating immunity downstream at the draining lymph node. On an organismal level, this work suggest that the lymphatic vasculature adapts to the organ it drains, signaling that the tissue lymphatics do not respond in a generic fashion and that caution should be taken when generalizing contextualized observations. While we observed a resolution of the phenotype upon helminth clearance, what occurs to the lacteals in the case of chronic infections, caused by helminths or other triggers, remains to be studied. These studies may potentially have broader implications on human health outcomes upon helminth infection: If lacteal zippering persist upon chronic infection in both mice and humans, chronic helminth infection in tropical climates may be a driving factor of decreased incidences of obesity-but also exacerbate lipid soluble vitamin deficiencies-in these areas.

6. References

Afrin, T., Murase, K., Kounosu, A., Hunt, V. L., Bligh, M., Maeda, Y., Hino, A., Maruyama, H., Tsai, I. J., & Kikuchi, T. (2019). Sequential Changes in the Host Gut Microbiota during Infection with the Intestinal Parasitic Nematode Strongyloides venezuelensis. *Frontiers in Cellular and Infection Microbiology*, *9*(JUN). https://doi.org/10.3389/fcimb.2019.00217

Aleksander, S. A., Balhoff, J., Carbon, S., Cherry, J. M., Drabkin, H. J., Ebert, D., Feuermann, M., Gaudet, P., Harris, N. L., Hill, D. P., Lee, R., Mi, H., Moxon, S., Mungall, C. J., Muruganugan, A., Mushayahama, T., Sternberg, P. W., Thomas, P. D., Van Auken, K., … Westerfield, M. (2023). The Gene Ontology knowledgebase in 2023. *GENETICS*, *224*(1). https://doi.org/10.1093/genetics/iyad031

Amezcua Vesely, M. C., Pallis, P., Bielecki, P., Low, J. S., Zhao, J., Harman, C. C. D., Kroehling, L., Jackson, R., Bailis, W., Licona-Limón, P., Xu, H., Iijima, N., Pillai, P. S., Kaplan, D. H., Weaver, C. T., Kluger, Y., Kowalczyk, M. S., Iwasaki, A., Pereira, J. P., … Flavell, R. A. (2019). Effector TH17 Cells Give Rise to Long-Lived TRM Cells that Are Essential for an Immediate Response against Bacterial Infection. *Cell*, *178*(5), 1176-1188.e15. https://doi.org/10.1016/j.cell.2019.07.032

Ashburner, M., Ball, C. A., Blake, J. A., Botstein, D., Butler, H., Cherry, J. M., Davis, A. P., Dolinski, K., Dwight, S. S., Eppig, J. T., Harris, M. A., Hill, D. P., Issel-Tarver, L., Kasarskis, A., Lewis, S., Matese, J. C., Richardson, J. E., Ringwald, M., Rubin, G. M., & Sherlock, G.

(2000). Gene Ontology: tool for the unification of biology. *Nature Genetics*, *25*(1), 25–29. https://doi.org/10.1038/75556

Baluk, P., Fuxe, J., Hashizume, H., Romano, T., Lashnits, E., Butz, S., Vestweber, D., Corada, M., Molendini, C., Dejana, E., & McDonald, D. M. (2007). Functionally specialized junctions between endothelial cells of lymphatic vessels. *Journal of Experimental Medicine*, *204*(10), 2349–2362. https://doi.org/10.1084/jem.20062596

Baluk, P., Hogmalm, A., Bry, M., Alitalo, K., Bry, K., & McDonald, D. M. (2013). Transgenic Overexpression of Interleukin-1β Induces Persistent Lymphangiogenesis But Not Angiogenesis in Mouse Airways. *The American Journal of Pathology*, *182*(4), 1434–1447. https://doi.org/10.1016/j.ajpath.2012.12.003

Bankhead, P., Loughrey, M. B., Fernández, J. A., Dombrowski, Y., McArt, D. G., Dunne, P. D., McQuaid, S., Gray, R. T., Murray, L. J., Coleman, H. G., James, J. A., Salto-Tellez, M., & Hamilton, P. W. (2017). QuPath: Open source software for digital pathology image analysis. *Scientific Reports*, *7*(1), 16878. https://doi.org/10.1038/s41598-017-17204-5

Barlow, J. T., Bogatyrev, S. R., & Ismagilov, R. F. (2020). A quantitative sequencing framework for absolute abundance measurements of mucosal and lumenal microbial communities. *Nature Communications*, *11*(1), 2590. https://doi.org/10.1038/s41467-020-16224-6

Benahmed, F., Ely, S., & Lu, T. T. (2012). Lymph node vascular-stromal growth and function as a potential target for controlling immunity. *Clinical Immunology*, *144*(2), 109–116. https://doi.org/10.1016/j.clim.2012.05.004

Bernier-Latmani, J., Cisarovsky, C., Demir, C. S., Bruand, M., Jaquet, M., Davanture, S., Ragusa, S., Siegert, S., Dormond, O., Benedito, R., Radtke, F., Luther, S. A., & Petrova, T. V. (2015).

DLL4 promotes continuous adult intestinal lacteal regeneration and dietary fat transport. *Journal of Clinical Investigation*, *125*(12), 4572–4586. https://doi.org/10.1172/JCI82045

Bernier-Latmani, J., & Petrova, T. V. (2017a). Intestinal lymphatic vasculature: Structure, mechanisms and functions. In *Nature Reviews Gastroenterology and Hepatology* (Vol. 14, Issue 9, pp. 510–526). Nature Publishing Group. https://doi.org/10.1038/nrgastro.2017.79

Bernier-Latmani, J., & Petrova, T. V. (2017b). Intestinal lymphatic vasculature: Structure, mechanisms and functions. In *Nature Reviews Gastroenterology and Hepatology* (Vol. 14, Issue 9, pp. 510–526). Nature Publishing Group. https://doi.org/10.1038/nrgastro.2017.79

Beumer, J., & Clevers, H. (2017). How the Gut Feels, Smells, and Talks. In *Cell* (Vol. 170, Issue 1, pp. 10–11). Cell Press. https://doi.org/10.1016/j.cell.2017.06.023

Bogatyrev, S. R., Rolando, J. C., & Ismagilov, R. F. (2020). Self-reinoculation with fecal flora changes microbiota density and composition leading to an altered bile-acid profile in the mouse small intestine. *Microbiome*, *8*(1), 19. https://doi.org/10.1186/s40168-020-0785-4

Cai, R., Kolabas, Z. I., Pan, C., Mai, H., Zhao, S., Kaltenecker, D., Voigt, F. F., Molbay, M., Ohn, T., Vincke, C., Todorov, M. I., Helmchen, F., Van Ginderachter, J. A., & Ertürk, A. (2023). Whole-mouse clearing and imaging at the cellular level with vDISCO. *Nature Protocols*, *18*(4), 1197–1242. https://doi.org/10.1038/s41596-022-00788-2

Card, C. M., Yu, S. S., & Swartz, M. A. (2014). Emerging roles of lymphatic endothelium in regulating adaptive immunity. In *Journal of Clinical Investigation* (Vol. 124, Issue 3, pp. 943–952). https://doi.org/10.1172/JCI73316

Churchill, M. J., du Bois, H., Heim, T. A., Mudianto, T., Steele, M. M., Nolz, J. C., & Lund, A. W. (2022a). Infection-induced lymphatic zippering restricts fluid transport and viral dissemination from skin. *Journal of Experimental Medicine*, *219*(5), e20211830. https://doi.org/10.1084/jem.20211830

Churchill, M. J., du Bois, H., Heim, T. A., Mudianto, T., Steele, M. M., Nolz, J. C., & Lund, A. W. (2022b). Infection-induced lymphatic zippering restricts fluid transport and viral dissemination from skin. *Journal of Experimental Medicine*, *219*(5). https://doi.org/10.1084/jem.20211830

Cifarelli, V., Appak-Baskoy, S., Peche, V. S., Kluzak, A., Shew, T., Narendran, R., Pietka, K. M., Cella, M., Walls, C. W., Czepielewski, R., Ivanov, S., Randolph, G. J., Augustin, H. G., & Abumrad, N. A. (2021). Visceral obesity and insulin resistance associate with CD36 deletion in lymphatic endothelial cells. *Nature Communications*, *12*(1), 3350. https://doi.org/10.1038/s41467-021-23808-3

Colombatti, A., Spessotto, P., Doliana, R., Mongiat, M., Bressan, G. M., & Esposito, G. (2012). The EMILIN/Multimerin Family. *Frontiers in Immunology*, *2*. https://doi.org/10.3389/fimmu.2011.00093

Da Ros, F., Persano, L., Bizzotto, D., Michieli, M., Braghetta, P., Mazzucato, M., & Bonaldo, P. (2022). Emilin-2 is a component of bone marrow extracellular matrix regulating mesenchymal stem cell differentiation and hematopoietic progenitors. *Stem Cell Research & Therapy*, *13*(1), 2. https://doi.org/10.1186/s13287-021-02674-2

Esterházy, D., Canesso, M. C. C., Mesin, L., Muller, P. A., de Castro, T. B. R., Lockhart, A., ElJalby, M., Faria, A. M. C., & Mucida, D. (2019). Compartmentalized gut lymph node

drainage dictates adaptive immune responses. *Nature*, *569*(7754), 126–130. https://doi.org/10.1038/s41586-019-1125-3

Fonseca, D. M. Da, Hand, T. W., Han, S. J., Gerner, M. Y., Zaretsky, A. G., Byrd, A. L., Harrison, O. J., Ortiz, A. M., Quinones, M., Trinchieri, G., Brenchley, J. M., Brodsky, I. E., Germain, R. N., Randolph, G. J., & Belkaid, Y. (2015). Microbiota-Dependent Sequelae of Acute Infection Compromise Tissue-Specific Immunity. *Cell*, *163*(2), 354–366. https://doi.org/10.1016/j.cell.2015.08.030

Förster, R., Braun, A., & Worbs, T. (2012). Lymph node homing of T cells and dendritic cells via afferent lymphatics. In *Trends in Immunology* (Vol. 33, Issue 6, pp. 271–280). https://doi.org/10.1016/j.it.2012.02.007

François, M., Caprini, A., Hosking, B., Orsenigo, F., Wilhelm, D., Browne, C., Paavonen, K., Karnezis, T., Shayan, R., Downes, M., Davidson, T., Tutt, D., Cheah, K. S. E., Stacker, S. A., Muscat, G. E. O., Achen, M. G., Dejana, E., & Koopman, P. (2008). Sox18 induces development of the lymphatic vasculature in mice. *Nature*, *456*(7222), 643–647. https://doi.org/10.1038/nature07391

Fu, S., Wang, Y., Bin, E., Huang, H., Wang, F., & Tang, N. (2023). c-JUN-mediated transcriptional responses in lymphatic endothelial cells are required for lung fluid clearance at birth. *Proceedings of the National Academy of Sciences*, *120*(2). https://doi.org/10.1073/pnas.2215449120

Gale, N. W., Thurston, G., Hackett, S. F., Renard, R., Wang, Q., McClain, J., Martin, C., Witte, C., Witte, M. H., Jackson, D., Suri, C., Campochiaro, P. A., Wiegand, S. J., & Yancopoulos, G. D. (2002). Angiopoietin-2 Is Required for Postnatal Angiogenesis and Lymphatic Patterning,

and Only the Latter Role Is Rescued by Angiopoietin-1. *Developmental Cell*, *3*(3), 411–423. https://doi.org/10.1016/S1534-5807(02)00217-4

Gardenier, J. C., Hespe, G. E., Kataru, R. P., Savetsky, I. L., Torrisi, J. S., García Nores, G. D., Dayan, J. J., Chang, D., Zampell, J., Martínez-Corral, I., Ortega, S., & Mehrara, B. J. (2016). Diphtheria toxin–mediated ablation of lymphatic endothelial cells results in progressive lymphedema. *JCI Insight*, *1*(15). https://doi.org/10.1172/jci.insight.84095

Garnier, L., Pick, R., Montorfani, J., Sun, M., Brighouse, D., Liaudet, N., Kammertoens, T., Blankenstein, T., Page, N., Bernier-Latamani, J., Lan Tran, N., Petrova, T. V, Merkler, D., Scheiermann, C., & Hugues, S. (2022). IFN-γ-dependent tumor-antigen cross-presentation by lymphatic endothelial cells promotes their killing by T cells and inhibits metastasis. In *Sci. Adv* (Vol. 8). https://www.science.org

Gause, W. C., Wynn, T. A., & Allen, J. E. (2013). Type 2 immunity and wound healing: Evolutionary refinement of adaptive immunity by helminths. In *Nature Reviews Immunology* (Vol. 13, Issue 8, pp. 607–614). https://doi.org/10.1038/nri3476

Ge, S. X., Jung, D., & Yao, R. (2020). ShinyGO: a graphical gene-set enrichment tool for animals and plants. *Bioinformatics*, *36*(8), 2628–2629. https://doi.org/10.1093/bioinformatics/btz931

Gieseck, R. L., Wilson, M. S., & Wynn, T. A. (2018). Type 2 immunity in tissue repair and fibrosis. In *Nature Reviews Immunology* (Vol. 18, Issue 1, pp. 62–76). Nature Publishing Group. https://doi.org/10.1038/nri.2017.90

Gkountidi, A. O., Garnier, L., Dubrot, J., Angelillo, J., Harlé, G., Brighouse, D., Wrobel, L. J., Pick, R., Scheiermann, C., Swartz, M. A., & Hugues, S. (2021). MHC Class II antigen presentation by lymphatic endothelial cells in tumors promotes intratumoral regulatory T cell-

suppressive functions. *Cancer Immunology Research*, *9*(7), 748–764. https://doi.org/10.1158/2326-6066.CIR-20-0784

Hammad, H., & Lambrecht, B. N. (2015). Barrier Epithelial Cells and the Control of Type 2 Immunity. *Immunity*, *43*(1), 29–40. https://doi.org/10.1016/j.immuni.2015.07.007

Hampton, H. R., & Chtanova, T. (2019). Lymphatic migration of immune cells. In *Frontiers in Immunology* (Vol. 10, Issue MAY). Frontiers Media S.A. https://doi.org/10.3389/fimmu.2019.01168

Holm, G. H., Pruijssers, A. J., Li, L., Danthi, P., Sherry, B., & Dermody, T. S. (2010). Interferon Regulatory Factor 3 Attenuates Reovirus Myocarditis and Contributes to Viral Clearance. *Journal of Virology*, *84*(14), 6900–6908. https://doi.org/10.1128/JVI.01742-09

Hong, S. P., Yang, M. J., Cho, H., Park, I., Bae, H., Choe, K., Suh, S. H., Adams, R. H., Alitalo, K., Lim, D., & Koh, G. Y. (2020). Distinct fibroblast subsets regulate lacteal integrity through YAP/TAZ-induced VEGF-C in intestinal villi. *Nature Communications*, *11*(1). https://doi.org/10.1038/s41467-020-17886-y

Jalkanen, S., & Salmi, M. (2020). Lymphatic endothelial cells of the lymph node. In *Nature Reviews Immunology* (Vol. 20, Issue 9, pp. 566–578). Nature Research. https://doi.org/10.1038/s41577-020-0281-x

Jannaway, M., Iyer, D., Mastrogiacomo, D. M., Li, K., Sung, D. C., Yang, Y., Kahn, M. L., & Scallan, J. P. (2023). VEGFR3 is required for button junction formation in lymphatic vessels. *Cell Reports*, *42*(7). https://doi.org/10.1016/j.celrep.2023.112777

Kabat, A. M., Hackl, A., Sanin, D. E., Zeis, P., Grzes, K. M., Baixauli, F., Kyle, R., Caputa, G., Edwards-Hicks, J., Villa, M., Rana, N., Curtis, J. D., Castoldi, A., Cupovic, J., Dreesen, L., Sibilia, M., Pospisilik, J. A., Urban, J. F., Grün, D., … Pearce, E. J. (2022). Resident T $_{H}$ 2 cells orchestrate adipose tissue remodeling at a site adjacent to infection. *Science Immunology*, *7*(76). https://doi.org/10.1126/sciimmunol.add3263

Kabat, A. M., Pearce, E. L., & Pearce, E. J. (2023). Metabolism in type 2 immune responses. *Immunity*, *56*(4), 723–741. https://doi.org/10.1016/j.immuni.2023.03.007

Karaman, S., Buschle, D., Luciani, P., Leroux, J.-C., Detmar, M., & Proulx, S. T. (2015). Decline of lymphatic vessel density and function in murine skin during aging. *Angiogenesis*, *18*(4), 489–498. https://doi.org/10.1007/s10456-015-9479-0

Kawagoe, Y., Kawashima, I., Sato, Y., Okamoto, N., Matsubara, K., & Kawamura, K. (2020). CXCL5-CXCR2 signaling is a senescence-associated secretory phenotype in preimplantation embryos. *Aging Cell*, *19*(10). https://doi.org/10.1111/acel.13240

Keenan, A. B., Torre, D., Lachmann, A., Leong, A. K., Wojciechowicz, M. L., Utti, V., Jagodnik, K. M., Kropiwnicki, E., Wang, Z., & Ma'ayan, A. (2019). ChEA3: transcription factor enrichment analysis by orthogonal omics integration. *Nucleic Acids Research*, *47*(W1), W212–W224. https://doi.org/10.1093/nar/gkz446

Kurashima, Y., Kigoshi, T., Murasaki, S., Arai, F., Shimada, K., Seki, N., Kim, Y.-G., Hase, K., Ohno, H., Kawano, K., Ashida, H., Suzuki, T., Morimoto, M., Saito, Y., Sasou, A., Goda, Y., Yuki, Y., Inagaki, Y., Iijima, H., … Kiyono, H. (2021). Pancreatic glycoprotein 2 is a first line of defense for mucosal protection in intestinal inflammation. *Nature Communications*, *12*(1), 1067. https://doi.org/10.1038/s41467-021-21277-2

Li, R., Chen, B., Kubota, A., Hanna, A., Humeres, C., Hernandez, S. C., Liu, Y., Ma, R., Tuleta, I., Huang, S., Venugopal, H., Zhu, F., Su, K., Li, J., Zhang, J., Zheng, D., & Frangogiannis, N. G. (2023). Protective effects of macrophage-specific integrin α5 in myocardial infarction are associated with accentuated angiogenesis. *Nature Communications*, *14*(1), 7555. https://doi.org/10.1038/s41467-023-43369-x

Li, Z.-J. (2013). Insulin-like growth factor-1 induces lymphangiogenesis and facilitates lymphatic metastasis in colorectal cancer. *World Journal of Gastroenterology*, *19*(43), 7788. https://doi.org/10.3748/wjg.v19.i43.7788

Lloyd, C. M., & Snelgrove, R. J. (2018). Type 2 immunity: Expanding our view. In *Sci. Immunol* (Vol. 3). http://immunology.sciencemag.org/

Madisen, L., Zwingman, T. A., Sunkin, S. M., Oh, S. W., Zariwala, H. A., Gu, H., Ng, L. L., Palmiter, R. D., Hawrylycz, M. J., Jones, A. R., Lein, E. S., & Zeng, H. (2010). A robust and high-throughput Cre reporting and characterization system for the whole mouse brain. *Nature Neuroscience*, *13*(1), 133–140. https://doi.org/10.1038/nn.2467

Maeda, Y., Palomares-Rius, J. E., Hino, A., Afrin, T., Mondal, S. I., Nakatake, A., Maruyama, H., & Kikuchi, T. (2019). Secretome analysis of Strongyloides venezuelensis parasitic stages reveals that soluble and insoluble proteins are involved in its parasitism. *Parasites and Vectors*, *12*(1). https://doi.org/10.1186/s13071-018-3266-x

Moest, H., Frei, A. P., Bhattacharya, I., Geiger, M., Wollscheid, B., & Wolfrum, C. (2013). Malfunctioning of adipocytes in obesity is linked to quantitative surfaceome changes. *Biochimica et Biophysica Acta (BBA) - Molecular and Cell Biology of Lipids*, *1831*(7), 1208–1216. https://doi.org/10.1016/j.bbalip.2013.04.001

Odenwald, M. A., Lin, H., Lehmann, C., Dylla, N. P., Cole, C. G., Mostad, J. D., Pappas, T. E., Ramaswamy, R., Moran, A., Hutchison, A. L., Stutz, M. R., Dela Cruz, M., Adler, E., Boissiere, J., Khalid, M., Cantoral, J., Haro, F., Oliveira, R. A., Waligurski, E., … Aronsohn, A. I. (2023). Bifidobacteria metabolize lactulose to optimize gut metabolites and prevent systemic infection in patients with liver disease. *Nature Microbiology*, *8*(11), 2033–2049. https://doi.org/10.1038/s41564-023-01493-w

Oliver, G., Kipnis, J., Randolph, G. J., & Harvey, N. L. (2020a). The Lymphatic Vasculature in the 21st Century: Novel Functional Roles in Homeostasis and Disease. In *Cell* (Vol. 182, Issue 2, pp. 270–296). Cell Press. https://doi.org/10.1016/j.cell.2020.06.039

Oliver, G., Kipnis, J., Randolph, G. J., & Harvey, N. L. (2020b). The Lymphatic Vasculature in the 21st Century: Novel Functional Roles in Homeostasis and Disease. In *Cell* (Vol. 182, Issue 2, pp. 270–296). Cell Press. https://doi.org/10.1016/j.cell.2020.06.039

Olsson, A.-K., Dimberg, A., Kreuger, J., & Claesson-Welsh, L. (2006). VEGF receptor signalling ? in control of vascular function. *Nature Reviews Molecular Cell Biology*, *7*(5), 359–371. https://doi.org/10.1038/nrm1911

Pedicord, V. A., Lockhart, A. A. K., Rangan, K. J., Craig, J. W., Loschko, J., Rogoz, A., Hang, H. C., & Mucida, D. (2016). Exploiting a host-commensal interaction to promote intestinal barrier function and enteric pathogen tolerance. *Science Immunology*, *1*(3). https://doi.org/10.1126/sciimmunol.aai7732

Petrova, T. V., & Koh, G. Y. (2020). Biological functions of lymphatic vessels. *Science*, *369*(6500). https://doi.org/10.1126/science.aax4063

Salzman, N. H., de Jong, H., Paterson, Y., Harmsen, H. J. M., Welling, G. W., & Bos, N. A. (2002). Analysis of 16S libraries of mouse gastrointestinal microflora reveals a large new group of mouse intestinal bacteria b bThe GenBank accession numbers for the clone sequences reported in this paper can be found in Table 1 T1 ; the accession number for isolate MIB-CB3 is AJ418059. *Microbiology*, *148*(11), 3651–3660. https://doi.org/10.1099/00221287-148-11-3651

Schineis, P., Runge, P., & Halin, C. (2019). Cellular traffic through afferent lymphatic vessels. In *Vascular Pharmacology* (Vol. 112, pp. 31–41). Elsevier Inc. https://doi.org/10.1016/j.vph.2018.08.001

Schneider, C. A., Rasband, W. S., & Eliceiri, K. W. (2012). NIH Image to ImageJ: 25 years of image analysis. *Nature Methods*, *9*(7), 671–675. https://doi.org/10.1038/nmeth.2089

Schwager, S., & Detmar, M. (2019). Inflammation and lymphatic function. In *Frontiers in Immunology* (Vol. 10). Frontiers Media S.A. https://doi.org/10.3389/fimmu.2019.00308

Shin, K., Kataru, R. P., Park, H. J., Kwon, B. I., Kim, T. W., Hong, Y. K., & Lee, S. H. (2015). TH2 cells and their cytokines regulate formation and function of lymphatic vessels. *Nature Communications*, *6*. https://doi.org/10.1038/ncomms7196

Simons, M., Gordon, E., & Claesson-Welsh, L. (2016). Mechanisms and regulation of endothelial VEGF receptor signalling. In *Nature Reviews Molecular Cell Biology* (Vol. 17, Issue 10, pp. 611–625). Nature Publishing Group. https://doi.org/10.1038/nrm.2016.87

Su, C. wen, Chen, C.-Y., Li, Y., Long, S. R., Massey, W., Kumar, D. V., Walker, W. A., & Shi, H. N. (2018). Helminth infection protects against high fat diet-induced obesity via induction of

alternatively activated macrophages. *Scientific Reports*, *8*(1), 4607. https://doi.org/10.1038/s41598-018-22920-7

Suh, S. H., Choe, K., Hong, S. P., Jeong, S., Mäkinen, T., Kim, K. S., Alitalo, K., Surh, C. D., Koh, G. Y., & Song, J. (2019). Gut microbiota regulates lacteal integrity by inducing VEGF-C in intestinal villus macrophages. *EMBO Reports*, *20*(4). https://doi.org/10.15252/embr.201846927

Swidsinski, A., Weber, J., Loening-Baucke, V., Hale, L. P., & Lochs, H. (2005). Spatial Organization and Composition of the Mucosal Flora in Patients with Inflammatory Bowel Disease. *Journal of Clinical Microbiology*, *43*(7), 3380–3389. https://doi.org/10.1128/JCM.43.7.3380-3389.2005

Tammela, T., & Alitalo, K. (2010). Lymphangiogenesis: Molecular Mechanisms and Future Promise. *Cell*, *140*(4), 460–476. https://doi.org/10.1016/j.cell.2010.01.045

Tammela, T., Saaristo, A., Holopainen, T., Lyytikkä, J., Kotronen, A., Pitkonen, M., Abo-Ramadan, U., Ylä-Herttuala, S., Petrova, T. V, & Alitalo, K. (2007). Therapeutic differentiation and maturation of lymphatic vessels after lymph node dissection and transplantation. *Nature Medicine*, *13*(12), 1458–1466. https://doi.org/10.1038/nm1689

Turner, S. G., & Barrowman, J. A. (1977). INTESTINAL LYMPH FLOW AND LYMPHATIC TRANSPORT OF PROTEIN DURING FAT ABSORPTION. *Quarterly Journal of Experimental Physiology and Cognate Medical Sciences*, *62*(2), 175–180. https://doi.org/10.1113/expphysiol.1977.sp002387

Xiang, M., Grosso, R. A., Takeda, A., Pan, J., Bekkhus, T., Brulois, K., Dermadi, D., Nordling, S., Vanlandewijck, M., Jalkanen, S., Ulvmar, M. H., & Butcher, E. C. (2020). A Single-Cell

Transcriptional Roadmap of the Mouse and Human Lymph Node Lymphatic Vasculature. *Frontiers in Cardiovascular Medicine*, *7*. https://doi.org/10.3389/fcvm.2020.00052

Yang, X.-M., Han, H.-X., Sui, F., Dai, Y.-M., Chen, M., & Geng, J.-G. (2010). Slit–Robo signaling mediates lymphangiogenesis and promotes tumor lymphatic metastasis. *Biochemical and Biophysical Research Communications*, *396*(2), 571–577. https://doi.org/10.1016/j.bbrc.2010.04.152

Yao, L. C., Baluk, P., Srinivasan, R. S., Oliver, G., & McDonald, D. M. (2012a). Plasticity of button-like junctions in the endothelium of airway lymphatics in development and inflammation. *American Journal of Pathology*, *180*(6), 2561–2575. https://doi.org/10.1016/j.ajpath.2012.02.019

Yao, L. C., Baluk, P., Srinivasan, R. S., Oliver, G., & McDonald, D. M. (2012b). Plasticity of button-like junctions in the endothelium of airway lymphatics in development and inflammation. *American Journal of Pathology*, *180*(6), 2561–2575. https://doi.org/10.1016/j.ajpath.2012.02.019

Yeo, K. P., & Angeli, V. (2017). Bidirectional crosstalk between lymphatic endothelial cell and T cell and its implications in tumor immunity. In *Frontiers in Immunology* (Vol. 8, Issue FEB). Frontiers Media S.A. https://doi.org/10.3389/fimmu.2017.00083

Yue, R., Wei, X., Zhao, J., Zhou, Z., & Zhong, W. (2021). Essential Role of IFN-γ in Regulating Gut Antimicrobial Peptides and Microbiota to Protect Against Alcohol-Induced Bacterial Translocation and Hepatic Inflammation in Mice. *Frontiers in Physiology*, *11*. https://doi.org/10.3389/fphys.2020.629141

Zarkada, G., Chen, X., Zhou, X., Lange, M., Zeng, L., Lv, W., Zhang, X., Li, Y., Zhou, W., Liu, K., Chen, D., Ricard, N., Liao, J., Kim, Y. B., Benedito, R., Claesson-Welsh, L., Alitalo, K., Simons, M., Ju, R., … Zhang, F. (2023). Chylomicrons Regulate Lacteal Permeability and Intestinal Lipid Absorption. *Circulation Research*, *133*(4), 333–349. https://doi.org/10.1161/CIRCRESAHA.123.322607

Zhang, F., Zarkada, G., Han, J., Li, J., Dubrac, A., Ola, R., Genet, G., Boyé, K., Michon, P., Künzel, S. E., Camporez, J. P., Singh, A. K., Fong, G. H., Simons, M., Tso, P., Fernández-Hernando, C., Shulman, G. I., Sessa, W. C., & Eichmann, A. (2018). Lacteal junction zippering protects against diet-induced obesity. *Science*, *361*(6402), 599–603. https://doi.org/10.1126/science.aap9331

Zhang, F., Zarkada, G., Yi, S., & Eichmann, A. (2020). Lymphatic Endothelial Cell Junctions: Molecular Regulation in Physiology and Diseases. In *Frontiers in Physiology* (Vol. 11). Frontiers Media S.A. https://doi.org/10.3389/fphys.2020.00509

Zheng, W., Aspelund, A., & Alitalo, K. (2014a). Lymphangiogenic factors, mechanisms, and applications. *Journal of Clinical Investigation*, *124*(3), 878–887. https://doi.org/10.1172/JCI71603

Zheng, W., Aspelund, A., & Alitalo, K. (2014b). Lymphangiogenic factors, mechanisms, and applications. *Journal of Clinical Investigation*, *124*(3), 878–887. https://doi.org/10.1172/JCI71603

Zuo, L., Kuo, W. T., & Turner, J. R. (2020). Tight Junctions as Targets and Effectors of Mucosal Immune Homeostasis. In *CMGH* (Vol. 10, Issue 2, pp. 327–340). Elsevier Inc. https://doi.org/10.1016/j.jcmgh.2020.04.001